

Aus dem Experimental and Clinical Research Center (ECRC) und  
der Medizinischen Klinik m. S. Nephrologie und Internistische Intensivmedizin  
der Medizinischen Fakultät Charité - Universitätsmedizin Berlin

DISSERTATION

The Role of Angiotensin II Type 1a Receptor and  
Downstream Signaling in Murine Myogenic Vasoconstriction  
(Die Funktion des Angiotensin II Typ 1a-Rezeptors und  
nachfolgender Signalwege bei myogener Vasokonstriktion in  
Mäusen)

zur Erlangung des akademischen Grades  
Doctor medicinae (Dr. med.)

vorgelegt der Medizinischen Fakultät  
Charité - Universitätsmedizin Berlin

von

Frau Yingqiu Cui

aus Shandong, China

Datum der Promotion: 03.03.2023



---

## Table of contents

List of tables .....	iii
List of abbreviations.....	iv
Abstract .....	1
Zusammenfassung .....	2
1 Introduction.....	3
1.1 Myogenic tone and vascular diseases .....	3
1.2 GPCRs signaling pathway and myogenic tone .....	3
1.3 Myogenic tone and aging .....	4
1.4 <i>PDE3A</i> and hypertension .....	4
2 Hypothesis.....	6
3 Materials and Methods.....	7
3.1 Animal models .....	7
3.2 Materials .....	8
3.3 Mesenteric arteries and cerebral arteries isolation.....	8
3.4 Analysis of myogenic tone in isolated perfused kidneys .....	8
3.5 Pressure myography .....	9
3.6 Immunofluorescence .....	9
3.7 Statistic analysis.....	9
4 Results .....	11
4.1 AT1aR is essential for pressure-induced response .....	11
4.2 $G_{q/11}$ signaling pathway is responsible for myogenic tone .....	11
4.3 Age-dependent regulation of myogenic tone by $Ca_v3.2$ channels.....	12
4.4 <i>PDE3A</i> mutations increase peripheral vascular resistance.....	12

---

5	Discussion .....	14
5.1	AT1aRs and downstream signaling to cause vasoconstriction.....	14
5.2	Effects of aging on myogenic tone via Cav3.2-RyR axis.....	15
5.3	PDE3A mutations and myogenic tone.....	16
	Reference list.....	18
	Statutory Declaration .....	22
	Declaration of your own contribution to the publications .....	23
	Excerpt from Journal Summary List .....	25
	Curriculum Vitae .....	81
	Complete list of publications.....	83
	Acknowledgments .....	84



**List of tables**

table 1 Sequences of primers used to genotype genetically modified mice	7
---	---

---

## List of abbreviations

AT1R	angiotensin II type 1 receptor
AT1 <sub>a</sub> R	angiotensin II type 1a receptor
AT1 <sub>b</sub> R	angiotensin II type 1b receptor
<i>Agtr1a</i> <sup>-/-</sup>	AT1a receptor deficiency
<i>Agtr1b</i> <sup>-/-</sup>	AT1b receptor deficiency
BK <sub>Ca</sub>	large-conductance Ca <sup>2+</sup> -activated K <sup>+</sup> channels
CysLT1R	cysteinyl leukotriene 1 receptor
ERK1/2	extracellular signal-regulated kinases
EGFR	epidermal growth factor receptor
GPCRs	G protein coupled receptors
HTNB	hypertension with brachydactyly
MAPK	mitogen-activated protein kinase
PKC	protein kinase C
<i>PDE3A</i>	phosphodiesterase 3A gene
PDGF	platelet-derived growth factor
RyRs	ryanodine receptors
ROS	reactive oxygen species
<i>SM-Agtr1a</i> <sup>-/-</sup>	smooth muscle specific AT1aR deficient
SII	Sar1, Ile4, Ile8 angiotensin II
SR	sarcoplasmic reticulum
VSMCs	vascular smooth muscle cells

## Abstract

**Background:** The myogenic response is autoregulation property of resistance arteries to keep blood flow constant in response to increases in intravascular pressure. Angiotensin II (Ang II) type 1 receptor (AT1R), as a broadly distributed mechanoactivated receptor, has been proposed to transduce myogenic vasoconstriction. However, the AT1R subtype(s) involved and their downstream G protein- and  $\beta$ -arrestin-mediated signaling pathways are still elusive.

**Methods:** *Agtr1a*<sup>-/-</sup>, *Agtr1b*<sup>-/-</sup> and tamoxifen-inducible smooth muscle-specific AT<sub>1a</sub>R knockout mice (SM-*Agtr1a* mice) were used to clarify the function of AT<sub>1a</sub>R and AT<sub>1b</sub>R. FR900359, [Sar1, Ile4, Ile8] Ang II (SII) and TRV120055 were used as selective G<sub>q/11</sub> protein inhibitor and biased agonists to activate non-canonical  $\beta$ -arrestin and G<sub>q/11</sub> signaling of the AT1R. Ca<sub>v</sub>3.2 channel was inhibited by Ni<sup>2+</sup> (50  $\mu$ M).  $\Delta$ 3aa HET rats were used to characterize the role of *PDE3A* in myogenic tone regulation. Forskolin was used to stimulate the adenylyl cyclase/cAMP system.

**Results:** Myogenic and Ang II-induced vasoconstrictions were diminished in several vascular beds of *Agtr1a*<sup>-/-</sup> and SM-*Agtr1a* mice, whereas myogenic tone was normal in arteries from *Agtr1b*<sup>-/-</sup> mice. The G<sub>q/11</sub> blocker FR900359 decreased myogenic tone and Ang II vasoconstrictions while selective biased targeting of AT1R  $\beta$ -arrestin signaling pathways had no effects. Ni<sup>2+</sup> (50  $\mu$ M) blockade increased myogenic tone in young mice but not old mice. The myogenic tone of the vessels was similar in WT and  $\Delta$ 3aa HET rats. However,  $\Delta$ 3aa HET rat mesenteric arteries showed weaker vasodilation in response to forskolin than WT animals. Similar results were observed in aortic rings by myography.

**Conclusion:** Myogenic arterial constriction requires G<sub>q/11</sub>-dependent signaling pathways of mechanoactivated AT<sub>1a</sub>R in the murine peripheral arteries. Inhibition of Cav3.2 had no effect on myogenic constriction in old mice. The mutated *PDE3A* gene drives mechanisms that increase peripheral vascular resistance.

## Zusammenfassung

**Hintergrund:** Die myogene Vasokonstriktion spiegelt die Kontraktionsfähigkeit von glatten Muskelzellen in Widerstandsarterien auf Veränderungen des transmuralen Drucks und der Fließgeschwindigkeit des Blutes wider. Angiotensin-II-Typ-1-Rezeptoren (AT<sub>1</sub>R) aus der Gruppe der G-Protein-gekoppelten Rezeptoren wurden als Mechanosensoren für die myogene Gefäßkonstriktion vermutet. Es ist nicht ausreichend bekannt, ob AT<sub>1a</sub>R und/oder AT<sub>1b</sub>R eine primäre Rolle bei der myogenen Reaktion spielen und ob *biased agonists* die myogene Antwort modulieren und welche Funktion die nachfolgenden G-Protein- und  $\beta$ -Arrestin-vermittelten Signalwege haben.

**Methoden:** *Agtr1a*<sup>-/-</sup>, *Agtr1b*<sup>-/-</sup> und Tamoxifen-induzierbare glattmuskelspezifische AT<sub>1a</sub>R-Knock-out-Mäuse (SM-*Agtr1a*) wurden zur Aufklärung der Funktion von AT<sub>1a</sub>R und AT<sub>1b</sub>R genutzt. FR900359, [Sar<sup>1</sup>, Ile<sup>4</sup>, Ile<sup>8</sup>] Ang II (SII) und TRV120055 wurden als selektive G<sub>q/11</sub>-Protein-Inhibitoren und *biased agonists* genutzt, um zwischen nicht-kanonischen  $\beta$ -Arrestin- und kanonischen G<sub>q/11</sub>-Signalwegen zu unterscheiden. Ca<sub>v</sub>3.2-Kanäle wurden mit Ni<sup>2+</sup> (50  $\mu$ M) inhibiert.  $\Delta$ 3aa HET-Ratten wurden zur Charakterisierung der Rolle von PDE3A bei der Regulation des basalen myogenen Tonus genutzt. Forskolin wurde zur Stimulation des Adenylyl-Cyclase/cAMP-Systems eingesetzt.

**Ergebnisse:** Bei *Agtr1a*<sup>-/-</sup>- und SM-*Agtr1a*-Mäusen waren myogene und Ang II-induzierte Vasokonstriktion in verschiedenen Blutgefäßsystemen verringert, während der myogene Tonus bei Arterien von *Agtr1b*<sup>-/-</sup>-Mäusen normal war. Der G<sub>q/11</sub>-Blocker FR900359 verringerte den myogenen Tonus und Ang II-induzierte Vasokonstriktion, während selektives Ansteuern des AT<sub>1</sub>R- $\beta$ -Arrestin-Signalweges keinen Effekt hatte. Block durch Ni<sup>2+</sup> (50  $\mu$ M) erhöhte den myogenen Tonus bei jungen, aber nicht bei alten Mäusen. Der myogene Gefäßtonus bei Wildtyp- (WT) und  $\Delta$ 3aa HET-Ratten war gleich. Allerdings zeigten  $\Delta$ 3aa HET-Ratten schwächere Forskolin-induzierte Vasodilation als WT-Tiere.

**Schlussfolgerungen:** Die myogene Konstriktion peripherer Arterien der Maus erfordert G<sub>q/11</sub>-abhängige Signalwege mechanoaktivierter AT<sub>1a</sub>Rs. Die Hemmung von Ca<sub>v</sub>3.2 hat keinen Einfluss auf die myogene Konstriktion bei alten Mäusen. Der myogene Tonus wird durch eine Blutdruck steigernde PDE3A-Mutation ( $\Delta$ 3aa) nicht verändert.

---

# 1 Introduction

## 1.1 Myogenic tone and vascular diseases

Myogenic vasoconstriction reflects the ability of resistance arteries to adapt their diameter in response to variations of mechanical stress induced by flow or intraluminal pressure. This response was first described by William Bayliss <sup>1</sup> and it reflects changes to the contractile state of vascular smooth muscle.

Increases in transmural pressure cause vasoconstriction whereas decreases produce the opposing effect. This prototype of autoregulation ability has been observed in various microvascular beds <sup>2</sup> and it is responsible for maintaining constant blood flow at a relatively stable state to prevent organ damage caused by the fluctuation of perfusion pressure.

Many cardiovascular disorders are associated with dysfunctional arterial myogenic response and they include hypertension, chronic heart failure, ischemic stroke, diabetes mellitus <sup>3 4 5 6 7</sup>.

## 1.2 GPCRs signaling pathway and myogenic tone

Myogenic vasoconstriction is mediated by pressure-dependent depolarization of vascular smooth muscle cells, an event that augments  $\text{Ca}^{2+}$  influx through voltage-dependent  $\text{Ca}_v1.2$  channels <sup>8 9 10 11 12 13</sup>.

$\text{G}_{q/11}$ -coupled receptors (GPCRs) are thought to function as the upstream sensor of membrane stretch <sup>14</sup>, with angiotensin II type 1a ( $\text{AT}_{1a}\text{R}$ ), and perhaps  $\text{AT}_{1b}\text{R}$  receptors in concert with cysteinyl leukotriene 1 receptor ( $\text{CysLT}_{1}\text{R}$ ), playing a particularly important role in the mesenteric and renal circulation <sup>15 16 17 18</sup>.

$\text{AT}_{1}\text{R}$ s are known to couple primarily to classical  $\text{G}_{q/11}$  proteins to activate multiple downstream signals, including protein kinase C (PKC), extracellular signal-regulated kinases, Raf kinases, tyrosine kinases, receptor tyrosine kinases (EGFR, PDGF, insulin receptor) and reactive oxygen species (ROS) <sup>19</sup>. The  $\text{AT}_{1}\text{R}$  activation also stimulates G protein-independent signaling pathways such as  $\beta$ -arrestin-mediated mitogen-activated

---

protein kinase (MAPK) activation and Src-Janus kinase signal transducer<sup>19</sup>.

Recently, it has been shown that the activation of intracellular signaling by mechanical stretch of the AT1R does not require the natural ligand angiotensin II (Ang II)<sup>20 21 17</sup> but requires the activation of the transducer  $\beta$ -arrestin<sup>20</sup>. Interestingly, mechanical stretch appears to allosterically stabilize specific  $\beta$ -arrestin-biased active conformations of AT1R to promote noncanonical downstream signaling mediated exclusively by the multifunctional scaffold protein,  $\beta$ -arrestin<sup>22</sup>. Whether this noncanonical  $\beta$ -arrestin effector pathway plays a role in myogenic and ligand-dependent vasoconstriction has yet to be ascertained.

### **1.3 Myogenic tone and aging**

$Ca_v1.2$  channel is required for regulation of peripheral vascular resistance and blood pressure, which is the basis for the use of calcium channel blockers for the treatment of hypertension<sup>13</sup>. Inhibition of L-type  $Ca^{2+}$  channels significantly reduces the myogenic response in most vascular beds indicating a need for  $Ca^{2+}$  entry<sup>9 23 24</sup>. Recently T-type  $Ca_v3.2$  channels have also been implicated in the vasoconstriction autoregulation in several vascular beds.

Genetic deletion or pharmacological inhibition of vascular  $Ca_v3.2$  channels evokes vasoconstriction and enhances the myogenic tone of cerebral and mesenteric arteries<sup>25 26 27</sup>. Besides, while  $Ca_v3.2$  blockade enhanced the myogenic tone in small mesenteric arteries from young mice (2-4 month), no effect on myogenic tone from aged mice (7-13 month) was observed by  $Ca_v3.2$  inhibition<sup>26</sup>. Therefore, how aging effects myogenic tone by  $Ca_v3.2$  signaling needs to be explored.

### **1.4 PDE3A and hypertension**

Hypertension with brachydactyly (HTNB) is an autosomal dominant Mendelian syndrome that is characterized by progressive hypertension, brachydactyly type E and blood vessel hyperplasia and thus resembles essential hypertension<sup>28 29</sup>. It has been suggested that this syndrome is caused by mutations within a 15 bp region of the phosphodiesterase 3A

---

(*PDE3A*) gene<sup>28 30</sup>. However, *in vivo* modeling of the genetic defect to test this hypothesis and the molecular mechanisms underlying the changes in *PDE3A* signaling that lead to HTNB have been lacking.

## 2 Hypothesis

Specifically, the following hypotheses were tested:

### **Project 1**

The specific function of AT1R subtypes in the regulation of myogenic tone and whether downstream signaling pathways are dependent on  $G_{q/11}$  and/or noncanonical alternative signaling pathways.

### **Project 2**

The study investigated the regulation of myogenic tone by  $Ca_v3.2$  channels during aging.

### **Project 3**

Whether basal myogenic tone is affected by mutant *PDE3A* or other changes in *PDE3A* signaling.



### 3 Materials and Methods

#### 3.1 Animal models

SMMHC-Cre-ER<sup>T2</sup> transgenic mouse line expressing Cre recombinase in smooth muscle cells under control of the smooth muscle myosin heavy chain promoter <sup>31</sup> was crossed with a mouse line bearing a floxed allele of the *Agtr1a* gene (*Agtr1a*<sup>flox</sup>), encoding the major murine AT1 receptor isoform (AT1a) to generate SMMHC-Cre+*Agtr1a*<sup>flox/flox</sup> (SMKO) mice <sup>32</sup>. Mice were intraperitoneally injected with tamoxifen (30 µg/mg body weight), dissolved in corn oil, on 5 consecutive days. Isolated arteries were usually obtained 2 to 3 days after tamoxifen treatment. Tamoxifen treatment did not modify myogenic tone or other relevant physiological parameters. Adult male mice with AT1a receptor deficiency (*Agtr1a*<sup>-/-</sup>), and mice with AT1b receptor deficiency (*Agtr1b*<sup>-/-</sup>) were also used. AT1a receptor deficiency mice were backcrossed to the FVB/N genetic background (Charles River, Sulzfeld, Germany) for 8 generations and maintained in the Max Delbrück Center animal facility. Genotyping was performed by polymerase chain reaction analysis of tail or ear biopsy DNA using the following primers <sup>33</sup> :

Table 1: Sequences of primers used to genotype genetically modified mice

SMWT1	TGA CCC CAT CTC TTC ACT CC
SMWT2	AAC TCC ACG ACC ACC TCA TC
phCREAS1	AGT CCC TCA CAT CCT CAG GTT
<i>Agtr1a</i> <sup>flox</sup> PCR	
forward	GCT TTC TCT GTT ATG CAG TCT
reverse	ATC AGC ACA TCC AGG AAT G

12-16 weeks old <sup>34</sup> male mice and littermate controls were used for experiments. We also studied 48-56 weeks old <sup>27</sup> male mice and *PDE3A* transgenic rats. Animal care followed American Physiological Society guidelines, and all protocols were approved by local

---

authority (LAGeSo, Berlin, Germany) and the animal welfare officers of the Max Delbrück Center for Molecular Medicine. Mice were maintained in the Max Delbrück Center animal facility in individually ventilated cages (Tecniplast Deutschland, Hohenpeißenberg, Germany) under standardized conditions with an artificial 12-hour dark-light cycle, with free access to standard chow (0.25% sodium; SSIFF Spezialitäten, Soest, Germany) and drinking water. Animals were euthanized by cervical dislocation and randomly assigned to the experimental procedures.

### **3.2 Materials**

Antibody to  $\alpha$ -smooth muscle actin ( $\alpha$ -SMA, #ab8211) was from Abcam (Cambridge, MA, USA). Anti-AT1R (#PA5-20812) and donkey anti-rabbit IgG (H+L) secondary antibody (A10040) were purchased from Thermo Fisher Scientific (Waltham, MA, USA). 4',6-diamidino-2-phenylindole (DAPI, #D9542) was purchased from Sigma-Aldrich Co. (St. Louis, MO, USA). Ang II (#A9525), SII (#sc-391239A) and tamoxifen (#H7904) were from Sigma-Aldrich Co (82024 Taufkirchen, Germany). TRV120055 (#JT-71995) and TRV120056 (#JT-71996) were from Synpeptide Co., Ltd (Shanghai, China).

### **3.3 Mesenteric arteries and cerebral arteries isolation**

After mice were killed, the mesenteric bed and brain were removed and immediately placed into cold (4°C), gassed (95% O<sub>2</sub>-5% CO<sub>2</sub>) physiological saline solution (PSS) of the following composition (mmol/L): 119 NaCl, 4.7 KCl, 25 NaHCO<sub>3</sub>, 1.2 KH<sub>2</sub>PO<sub>4</sub>, 1.6 CaCl<sub>2</sub>, 1.2 MgSO<sub>4</sub>, 0.03 EDTA, and 11.1 glucose. Third or fourth order mesenteric and middle cerebral arteries or posterior cerebral arteries were dissected and cleaned of adventitial connective tissue<sup>17 35</sup>.

### **3.4 Analysis of myogenic tone in isolated perfused kidneys**

Isolated kidneys were perfused in an organ chamber using a peristaltic pump at constant flow (0.3-1.9 ml/min) of oxygenated (95% O<sub>2</sub> and 5% CO<sub>2</sub>) PSS<sup>17</sup>. Drugs (Ang II or biased agonists) were added to the perfusate. Perfusion pressure was measured by a pressure

---

transducer after an equilibration period of 60-90 min. Data were recorded and analyzed by a Powerlab acquisition system (AD Instruments, Colorado Springs). Ang II-induced pressor effects were normalized to the maximal pressor effect induced by KCl (60 mmol/L)

14 17 35

### 3.5 Pressure myography

Vessel myography was performed as previously described<sup>31 14 17</sup>. Mesenteric or cerebral arteries were mounted on glass cannula and superfused continuously with PSS (95% O<sub>2</sub>-5% CO<sub>2</sub>; pH, 7.4; 37°C). The vessels were stepwise pressurized to 20, 40, 60, 80, or 100 mmHg using a pressure servo control system (Living System Instrumentation, Burlington, VT). We measured the inner diameter of the vessels with a video microscope (Nikon Diaphot, Düsseldorf, Germany) connected to a personal computer for data acquisition and analysis (HaSoTec, Rostock, Germany)<sup>35 36 17</sup>. Arteries were equilibrated for 45 to 60 minutes before starting experiments. To proof maximal contractility, a 60-mmol/L KCl challenge was performed before any other intervention.

### 3.6 Immunofluorescence

*Agtr1a*<sup>+/+</sup> and SM-*Agtr1a*<sup>-/-</sup> mice mesenteric arteries were dissected and further fixed in 4% formaldehyde and embedded in Tissue-Tek O.C.T. compound to be frozen in liquid nitrogen. Tissues were then sectioned and permeabilized in 1% Triton X-100 in PBS. Sections were stained with the primary antibody overnight at 4°C. After washing with PBS for 3 × 5 min, the secondary antibody and DAPI were applied for 2 hours at room temperature. Fluorescence images were captured by use of Olympus FV1000 confocal microscopy and images were analyzed by ImageJ analysis software.

### 3.7 Statistic analysis

Data are presented as means ± SEM. Statistically significant differences in mean values were determined by Student's unpaired t test or one-way analysis of variance (ANOVA).

P values < 0.05 were considered statistically significant.

Citation: **Cui Y**, Kassmann M, Nickel S, Zhang C, Alenina N, Anistan YM, Schleifenbaum J, Bader M, Welsh DG, Huang Y and Gollasch M. Myogenic Vasoconstriction Requires Canonical G<sub>q/11</sub> Signaling of the Angiotensin II Type 1 Receptor. *J Am Heart Assoc.* 2022:e022070.

## 4 Results

### 4.1 AT1aR is essential for pressure-induced response

In mouse renal circulation, the perfusion pressure increased with flow rate in kidneys of wild-type *Agtr1a*<sup>+/+</sup> mice, while kidneys from *Agtr1a*<sup>-/-</sup> mice developed significantly less pressure at the same flow rate (**Figure 1E**). Angiotensin II (Ang II, 10 nmol/L) increased perfusion pressure by 80 mmHg in kidneys of *Agtr1a*<sup>+/+</sup> mice, but had no effect in kidneys of *Agtr1a*<sup>-/-</sup> mice (**Figure 1C**). SM-*Agtr1a*<sup>-/-</sup> kidneys showed largely reduced myogenic vasoconstriction as assessed by exposure of the kidneys to Ca<sup>2+</sup> free PSS, whereas wild-type kidneys showed strong myogenic vasoconstrictions (**Figure 1D**). Of note, there was no difference in myogenic tone and Ang II vasoconstrictions between *Agtr1b*<sup>-/-</sup> versus *Agtr1b*<sup>+/+</sup> kidneys.

Increases in intraluminal pressure generated active tension that counteracted further dilation of the vessels at 60 to 80 mmHg in mesenteric arteries from *Agtr1a*<sup>+/+</sup> mice. In contrast, mesenteric arteries from SM-*Agtr1a*<sup>-/-</sup> mice only produced ~35% of the constriction observed in wild-type arteries (**Figure 2C**). Ang II strongly constricted mesenteric and cerebral arteries from *Agtr1a*<sup>+/+</sup> mice but had no effect on arteries from SM-*Agtr1a*<sup>-/-</sup> mice (**Figure 2D**). A marked reduction in AT1aR expression in the media of SM-*Agtr1a*<sup>-/-</sup> mesenteric arteries was observed compared to wild-type.

### 4.2 G<sub>q/11</sub> signaling pathway is responsible for myogenic tone

To explore the role of G<sub>q/11</sub> and β-arrestin signaling pathways downstream of AT1R, the biased agonists TRV120055 and SII were used to activate G<sub>q/11</sub> and β-arrestin signaling pathways respectively. TRV120055 increased vascular tone in mesenteric arteries, whereas SII had no effect. Similarly, TRV120055 and TRV120056 (another biased G<sub>q/11</sub> coupled AT1R agonist) enhanced dose-dependent perfusion pressure in isolated kidneys, whereas SII had no effect. FR900359, a selective G<sub>q/11</sub>-protein inhibitor, abolished both myogenic and Ang II-dependent constrictions in renal arterioles and mesenteric arteries.

### 4.3 Age-dependent regulation of myogenic tone by Ca<sub>v</sub>3.2 channels

In young wild-type mesenteric arteries, the Ca<sub>v</sub>3.2 channel blocker Ni<sup>2+</sup> (50 μM) increased myogenic tone from 9.2% ± 1.2% to 13.04% ± 0.8% at 60 mmHg, 11.6% ± 1.2% to 19.7% ± 0.5% at 80 mmHg, and 17.7% ± 2% to 27.8% ± 1.3% at 100 mmHg, whereas a similar constriction was absent in old vessels. Despite these differences, 60 mM K<sup>+</sup>-induced vasoconstrictions were similar between young (54.2% ± 1.2%) and old (60.7% ± 2.1%) pressurized arteries.

### 4.4 PDE3A mutations increase peripheral vascular resistance

The rat model exhibits a 9 bp deletion within the hotspot that leads to the loss of 3 amino acids (the Δ3aa deletion) was generated to prove that mutations in the mutational hotspot of the *PDE3A* gene cause HTNB.

Myogenic tone was assessed over a range of intraluminal pressures from 20 to 100 mmHg. The myogenic tone of the vessels was similar at all pressures between wild-type and heterozygous Δ3aa (Δ3aa HET) mesenteric arteries. However, the pressurized (100 mmHg) vessels from Δ3aa HET rats showed weaker vasodilation in response to forskolin than those from wild-type animals.

Citations:

**Cui Y**, Kassmann M, Nickel S, Zhang C, Alenina N, Anistan YM, Schleifenbaum J, Bader M, Welsh DG, Huang Y and Gollasch M. Myogenic Vasoconstriction Requires Canonical G<sub>q/11</sub> Signaling of the Angiotensin II Type 1 Receptor. *J Am Heart Assoc.* 2022:e022070.

Fan G, Kaßmann M, **Cui Y**, Matthaeus C, Kunz S, Zhong C, Zhu S, Xie Y, Tsvetkov D, Daumke O, Huang Y and Gollasch M. Age attenuates the T-type Ca 3.2-RyR axis in vascular smooth muscle. *Aging Cell.* 2020;19:e13134.

Ercu M, Markó L, Schächterle C, Tsvetkov D, **Cui Y**, Maghsodi S, Bartolomaeus TUP, Maass PG, Zühlke K, Gregersen N, Hübner N, Hodge R, Mühl A, Pohl B, Illas RM, Geelhaar A, Walter S,

Napieczynska H, Schelenz S, Taube M, Heuser A, Anistan Y-M, Qadri F, Todiras M, Plehm R, Popova E, Langanki R, Eichhorst J, Lehmann M, Wiesner B, Russwurm M, Forslund SK, Kamer I, Müller DN, Gollasch M, Aydin A, Bähring S, Bader M, Luft FC and Klusmann E. Phosphodiesterase 3A and Arterial Hypertension. *Circulation*. 2020;142:133-149.

## 5 Discussion

A loss of myogenic autoregulation in the renal circulation of *Agtr1a*<sup>-/-</sup> mice was observed, an effect which was normal in *Agtr1b*<sup>-/-</sup> mice. Similarly, myogenic tone was strongly reduced in mesenteric and cerebral arteries from smooth muscle specific AT1aR-deficient (SM-*Agtr1a*<sup>-/-</sup>) mice compared to wild-type. Using the pharmacological G<sub>q/11</sub> inhibitor FR900359 and several GPCR biased agonists, the data showed that AT1Rs cause vasoconstriction *via* canonical G<sub>q/11</sub>-mediated signaling but not anticipated alternative G protein signaling downstream of the AT1R.

### 5.1 AT1aRs and downstream signaling to cause vasoconstriction

Multiple GPCRs have been proposed to act as mechanosensors to regulate myogenic tone in resistance arteries<sup>37 38 39</sup>, the AT1R remains one of the best characterized mechanosensors in the vasculature<sup>18 21</sup>. Using *Agtr1a*<sup>-/-</sup> mice and inverse AT1R agonist, previous data suggested that ligand independent AT1aR activation is required for myogenic response in resistance mesenteric arteries and renal arterioles<sup>17</sup>. However, two recent studies reported that myogenic tone was diminished in *Agtr1b*<sup>-/-</sup> mesenteric and cerebral arteries, which implies a possible role of AT1bRs in mechanosensation<sup>40 15</sup>. To overcome these potential limitations, the tamoxifen-inducible SM-*Agtr1a* (SMMHC-Cre+*Agtr1a*<sup>fllox/fllox</sup>) mice provided firm evidence that AT1aRs play a key role as mechanosensors mediating myogenic constriction in the murine vasculature.

In cell culture, osmotic cell stretch has been found to increase the binding affinity and potency of the  $\beta$ -arrestin-biased agonist TRV120023 with no effect on the balanced agonist Ang II through AT1R to induce a conformation change of  $\beta$ -arrestin 2, similar to that induced by  $\beta$ -arrestin-biased agonists<sup>22</sup>. Similarly, hypo-osmotic stretch induced  $\beta$ -arrestin-biased signaling of AT1Rs in the absence of G protein activation<sup>20</sup>. We failed to observe  $\beta$ -arrestin mediated enhancement of myogenic vasoconstriction with the  $\beta$ -arrestin biased agonist SII in intact arteries. The discrepancy might be caused by differences between the hypo-osmotic cell swelling and tensile stretch on the smooth



muscle cell layer in intact arteries to cause mechanoactivation of AT1aRs *in situ*. Instead, the vasoconstrictor responses were strongly increased by the G<sub>q/11</sub> AT1R biased agonists TRV120055 in mesenteric and renal arterioles. Moreover, the G<sub>q/11</sub> blocker FR900359 inhibited both myogenic tone and Ang II induced constrictions in similar vascular beds. The data imply that myogenic vasoconstriction requires canonical G<sub>q/11</sub> signaling of the AT1aR. Finally, the conclusions are supported by findings indicating that another G<sub>q/11</sub>-protein inhibitor YM 254890 profoundly reduced myogenic tone in mesenteric arteries<sup>18</sup>. Of note, this data contradict with recent findings, which proposed that G<sub>12/13</sub>- and Rho/Rho kinase-mediated signaling is required in myogenic vasoconstriction by inhibition of myosin phosphatase<sup>34</sup>. The reason may depend on which vessel order was utilized, i.e. 3<sup>rd</sup> or 4<sup>th</sup> order mesenteric versus 1<sup>st</sup> or 2<sup>nd</sup> order mesenteric arteries. Moreover, the myogenic response was only reduced by 50% in G<sub>12/13</sub>-deficient cerebral arteries<sup>34</sup>, which may indicate that this pathway may play a role in some but not all vessels. Thus, it is possible that the relevance to the two signaling pathways differs between various vascular beds and artery branches. This study provides firm evidence that AT<sub>1a</sub>Rs coupled to G<sub>q/11</sub> signaling is an essential component of dynamic mechanochemical signaling in arterial vascular smooth muscle cells causing myogenic tone.

Signaling of most GPCRs *via* G proteins is terminated by the phosphorylation of active receptor by specific kinases (GPCR kinases, or GRKs) and subsequent binding of  $\beta$ -arrestins that selectively recognize active phosphorylated receptors. Although, GRKs and  $\beta$ -arrestins play also a role in multiple noncanonical signaling pathways in the cell, both GPCR-initiated and receptor-independent<sup>41 42</sup>, our study failed to demonstrate that this pathway plays an important role in the myogenic response. Thus, it is unlikely that blood pressure lowering effects of  $\beta$ -arrestin biased AT1R agonists, e.g. Trevena 120027<sup>43</sup>, are caused by direct effects of this GPCR in the arterial smooth muscle cells.

## 5.2 Effects of aging on myogenic tone via Cav3.2-RyR axis

Ca<sub>v</sub>3.2-mediated Ca<sup>2+</sup> influx stimulates the cytosolic domain of ryanodine receptors (RyRs) to release Ca<sup>2+</sup> from the sarcoplasmic reticulum<sup>44</sup> in the form of Ca<sup>2+</sup> sparks<sup>27</sup>.

The latter are crucial for the activation of  $\text{Ca}^{2+}$ -activated, large-conductance  $\text{Ca}^{2+}$ -activated  $\text{K}^+$  ( $\text{BK}_{\text{Ca}}$ ) channels leading to  $\text{K}^+$  efflux and hyperpolarization. This negative feedback mechanisms, that are intrinsic to VSMCs, help attenuate arterial tone and limit excessive vasoconstriction.

Inhibition of vascular  $\text{Ca}_v3.2$  channels evokes vasoconstriction and enhances the myogenic tone of cerebral and mesenteric arteries has been reported <sup>45</sup>. Age-dependent changes in the expression and function of T-type  $\text{Ca}^{2+}$  channels such as functional downregulation in cardiomyocytes from several species also have been reported <sup>46 47</sup>. This study further explored how aging affects myogenic tone with  $\text{Ca}_v3.2$ -RyR- $\text{BK}_{\text{Ca}}$  signaling in VSMCs. Experiments with pressurized arteries confirmed that pharmacological  $\text{Ca}_v3.2$  inhibition had no effect in old mice, consistent with the loss of function of  $\text{Ca}_v3.2$ /RyR/ $\text{BK}_{\text{Ca}}$  signaling with aging.

### 5.3 PDE3A mutations and myogenic tone

HTNB patients usually develop decade-long hypertension and die from stroke by the age 50 years if left untreated. Prior study has shown that gain of function mutations in a mutational hotspot of the gene encoding phosphodiesterase 3A (*PDE3A*) cause HTNB <sup>28</sup>. *PDEs* comprise 11 enzyme families degrading cAMP and cyclic guanosine monophosphate. Some enzymes degrade both, cAMP and cGMP, such as *PDE3A* <sup>48</sup>. *PDE3A* is a cGMP-inhibited cAMP-hydrolyzing *PDE* <sup>49</sup>. It appears that the mutated *PDE3A* gene drives mechanisms that increase peripheral vascular resistance causing hypertension. The data indicate that the basal myogenic tone is not affected by mutant *PDE3A*, but that, upon stimulation of the adenylyl cyclase/cAMP system, the hyperactivity of *PDE3A* limits the ability of small arteries to dilate. This study explored the molecular mechanisms underlying HTNB and could lead to the identification of new therapeutic strategies targeting *PDE3A*-directed signaling compartments for the treatment of HTNB.

Citations:

**Cui Y**, Kassmann M, Nickel S, Zhang C, Alenina N, Anistan YM, Schleifenbaum J, Bader M, Welsh DG, Huang Y and Gollasch M. Myogenic Vasoconstriction Requires Canonical  $\text{G}_{q/11}$

---

Signaling of the Angiotensin II Type 1 Receptor. *J Am Heart Assoc.* 2022:e022070.

Fan G, Kaßmann M, **Cui Y**, Matthaeus C, Kunz S, Zhong C, Zhu S, Xie Y, Tsvetkov D, Daumke O, Huang Y and Gollasch M. Age attenuates the T-type Ca 3.2-RyR axis in vascular smooth muscle. *Aging Cell.* 2020;19:e13134.

Ercu M, Markó L, Schächterle C, Tsvetkov D, **Cui Y**, Maghsodi S, Bartolomaeus TUP, Maass PG, Zühlke K, Gregersen N, Hübner N, Hodge R, Mühl A, Pohl B, Illas RM, Geelhaar A, Walter S, Napieczynska H, Schelenz S, Taube M, Heuser A, Anistan Y-M, Qadri F, Todiras M, Plehm R, Popova E, Langanki R, Eichhorst J, Lehmann M, Wiesner B, Russwurm M, Forslund SK, Kamer I, Müller DN, Gollasch M, Aydin A, Bähring S, Bader M, Luft FC and Klusmann E. Phosphodiesterase 3A and Arterial Hypertension. *Circulation.* 2020;142:133-149.

## Reference list

- 1 W. M. Bayliss, "On the local reactions of the arterial wall to changes of internal pressure," *The Journal of physiology* **28** (3), 220-231 (1902).
- 2 M. J. Davis, "Perspective: physiological role(s) of the vascular myogenic response," *Microcirculation* (New York, N.Y. : 1994) **19** (2), 99-114 (2012).
- 3 Marilyn J. Cipolla and Amy B. Curry, "Middle cerebral artery function after stroke: the threshold duration of reperfusion for myogenic activity," *Stroke* **33** (8), 2094-2099 (2002).
- 4 S. Gschwend, R. H. Henning, Y. M. Pinto, D. de Zeeuw, W. H. van Gilst, and H. Buikema, "Myogenic constriction is increased in mesenteric resistance arteries from rats with chronic heart failure: instantaneous counteraction by acute AT1 receptor blockade," *British journal of pharmacology* **139** (7), 1317-1325 (2003).
- 5 J. Ledoux, D. M. Gee, and N. Leblanc, "Increased peripheral resistance in heart failure: new evidence suggests an alteration in vascular smooth muscle function," *British journal of pharmacology* **139** (7), 1245-1248 (2003).
- 6 P. W. Pires, W. F. Jackson, and A. M. Dorrance, "Regulation of myogenic tone and structure of parenchymal arterioles by hypertension and the mineralocorticoid receptor," *Am J Physiol Heart Circ Physiol* **309** (1), H127-136 (2015).
- 7 Meghan Sauv , Sonya K. Hui, Danny D. Dinh, Warren D. Foltz, Abdul Momen, Sergei A. Nedospasov, Stefan Offermanns, Mansoor Husain, Jeffrey T. Kroetsch, Darcy Lidington, and Steffen-Sebastian Bolz, "Tumor Necrosis Factor/Sphingosine-1-Phosphate Signaling Augments Resistance Artery Myogenic Tone in Diabetes," *Diabetes* **65** (7), 1916-1928 (2016).
- 8 M. T. Nelson, J. B. Patlak, J. F. Worley, and N. B. Standen, "Calcium channels, potassium channels, and voltage dependence of arterial smooth muscle tone," *Am J Physiol* **259** (1 Pt 1), C3-18 (1990).
- 9 P. Coats, F. Johnston, J. MacDonald, J. J. McMurray, and C. Hillier, "Signalling mechanisms underlying the myogenic response in human subcutaneous resistance arteries," *Cardiovascular research* **49** (4), 828-837 (2001).
- 10 M. J. Davis and M. A. Hill, "Signaling mechanisms underlying the vascular myogenic response," *Physiol Rev* **79** (2), 387-423 (1999).
- 11 P. B. Hansen, B. L. Jensen, D. Andreasen, and O. Sk tt, "Differential expression of T- and L-type voltage-dependent calcium channels in renal resistance vessels," *Circulation research* **89** (7), 630-638 (2001).
- 12 D. R. Harder, "Pressure-dependent membrane depolarization in cat middle cerebral artery," *Circulation research* **55** (2), 197-202 (1984).
- 13 S. Moosmang, V. Schulla, A. Welling, R. Feil, S. Feil, J. W. Wegener, F. Hofmann, and N. Klugbauer, "Dominant role of smooth muscle L-type calcium channel Cav1.2 for blood pressure regulation," *Embo j.* **22** (22), 6027-6034 (2003).
- 14 M. Mederos y Schnitzler, U. Storch, S. Meibers, P. Nurwakagari, A. Breit, K. Essin, M. Gollasch, and T. Gudermann, "Gq-coupled receptors as mechanosensors mediating myogenic vasoconstriction," *Embo j.* **27** (23), 3092-3103 (2008).
- 15 S. Blodow, H. Schneider, U. Storch, R. Wizemann, A. L. Forst, T. Gudermann, and M. Mederos y Schnitzler, "Novel role of mechanosensitive AT1B receptors in myogenic vasoconstriction," *Pflugers Archiv : European journal of physiology* **466** (7), 1343-1353 (2014).

- 
- 16 M. I. Oliverio, H. S. Kim, M. Ito, T. Le, L. Audoly, C. F. Best, S. Hiller, K. Kluckman, N. Maeda, O. Smithies, and T. M. Coffman, "Reduced growth, abnormal kidney structure, and type 2 (AT<sub>2</sub>) angiotensin receptor-mediated blood pressure regulation in mice lacking both AT<sub>1A</sub> and AT<sub>1B</sub> receptors for angiotensin II," *Proceedings of the National Academy of Sciences of the United States of America* **95** (26), 15496-15501 (1998).
- 17 J. Schleifenbaum, M. Kassmann, I. A. Szijarto, H. C. Hercule, J. Y. Tano, S. Weinert, M. Heidenreich, A. R. Pathan, Y. M. Anistan, N. Alenina, N. J. Rusch, M. Bader, T. J. Jentsch, and M. Gollasch, "Stretch-activation of angiotensin II type 1a receptors contributes to the myogenic response of mouse mesenteric and renal arteries," *Circ Res* **115** (2), 263-272 (2014).
- 18 Ursula Storch, Stephanie Blodow, Thomas Gudermann, and Michael Mederos Y Schnitzler, "Cysteinyl leukotriene 1 receptors as novel mechanosensors mediating myogenic tone together with angiotensin II type 1 receptors-brief report," *Arteriosclerosis, thrombosis, and vascular biology* **35** (1), 121-126 (2015).
- 19 P. Balakumar and G. Jagadeesh, "A century old renin-angiotensin system still grows with endless possibilities: AT<sub>1</sub> receptor signaling cascades in cardiovascular physiopathology," *Cell Signal* **26** (10), 2147-2160 (2014).
- 20 K. Rakesh, B. Yoo, I. M. Kim, N. Salazar, K. S. Kim, and H. A. Rockman, "beta-Arrestin-biased agonism of the angiotensin receptor induced by mechanical stress," *Sci Signal* **3** (125), ra46 (2010).
- 21 Yunzeng Zou, Hiroshi Akazawa, Yingjie Qin, Masanori Sano, Hiroyuki Takano, Tohru Minamino, Noriko Makita, Koji Iwanaga, Weidong Zhu, Sumiyo Kudoh, Haruhiro Toko, Koichi Tamura, Minoru Kihara, Toshio Nagai, Akiyoshi Fukamizu, Satoshi Umemura, Taroh Iiri, Toshiro Fujita, and Issei Komuro, "Mechanical stress activates angiotensin II type 1 receptor without the involvement of angiotensin II," *Nat Cell Biol* **6** (6), 499-506 (2004).
- 22 Wei Tang, Ryan T. Strachan, Robert J. Lefkowitz, and Howard A. Rockman, "Allosteric Modulation of  $\beta$ -Arrestin-biased Angiotensin II Type 1 Receptor Signaling by Membrane Stretch," *Journal of Biological Chemistry* **289** (41), 28271-28283 (2014).
- 23 P. J. Mace, T. J. Stallard, and W. A. Littler, "The effect of felodipine on forearm haemodynamics and the myogenic response of the forearm resistance vessels in normal man," *Br J Clin Pharmacol* **20** (4), 383-386 (1985).
- 24 E. VanBavel, J. P. Wesselman, and J. A. Spaan, "Myogenic activation and calcium sensitivity of cannulated rat mesenteric small arteries," *Circulation research* **82** (2), 210-220 (1998).
- 25 Osama F. Harraz, Suzanne E. Brett, Anil Zechariah, Monica Romero, Jose L. Puglisi, Sean M. Wilson, and Donald G. Welsh, "Genetic ablation of Ca<sub>v</sub>3.2 channels enhances the arterial myogenic response by modulating the RyR-BKCa axis," *Arteriosclerosis, thrombosis, and vascular biology* **35** (8), 1843-1851 (2015).
- 26 M. F. Mikkelsen, K. Björling, and L. J. Jensen, "Age-dependent impact of Ca<sub>v</sub>3.2 T-type calcium channel deletion on myogenic tone and flow-mediated vasodilatation in small arteries," *J. Physiol. (Lond.)* **594** (20), 5881-5898 (2016).
- 27 Osama F. Harraz, Frank Visser, Suzanne E. Brett, Daniel Goldman, Anil Zechariah, Ahmed M. Hashad, Bijoy K. Menon, Tim Watson, Yves Starreveld, and Donald G. Welsh, "Ca<sub>v</sub>1.2/Ca<sub>v</sub>3.x channels mediate divergent vasomotor responses in human cerebral arteries," *The Journal of general physiology* **145** (5), 405-418 (2015).
- 28 Philipp G. Maass, Atakan Aydin, Friedrich C. Luft, Carolin Schächterle, Anja Weise, Sigmar Stricker, Carsten Lindschau, Martin Vaegler, Fatimunnisa Qadri, Hakan R. Toka, Herbert Schulz, Peter M. Krawitz,

- Dmitri Parkhomchuk, Jochen Hecht, Irene Hollfinger, Yvette Wefeld-Neuenfeld, Eireen Bartels-Klein, Astrid Mühl, Martin Kann, Herbert Schuster, David Chitayat, Martin G. Bialer, Thomas F. Wienker, Jürg Ott, Katharina Rittscher, Thomas Liehr, Jens Jordan, Ghislaine Plessis, Jens Tank, Knut Mai, Ramin Naraghi, Russell Hodge, Maxwell Hopp, Lars O. Hattenbach, Andreas Busjahn, Anita Rauch, Fabrice Vandeput, Maolian Gong, Franz Rüschen-dorf, Norbert Hübner, Hermann Haller, Stefan Mundlos, Nihat Bilginturan, Matthew A. Movsesian, Enno Klussmann, Okan Toka, and Sylvia Bähring, "PDE3A mutations cause autosomal dominant hypertension with brachydactyly," *Nat Genet* **47** (6), 647-653 (2015).
- 29 Okan Toka, Jens Tank, Carolin Schächterle, Atakan Aydin, Philipp G. Maass, Saban Elitok, Eireen Bartels-Klein, Irene Hollfinger, Carsten Lindschau, Knut Mai, Michael Boschmann, Gabriele Rahn, Matthew A. Movsesian, Thomas Müller, Andrea Doescher, Simone Gnoth, Astrid Mühl, Hakan R. Toka, Yvette Wefeld-Neuenfeld, Wolfgang Utz, Agnieszka Töpfer, Jens Jordan, Jeanette Schulz-Menger, Enno Klussmann, Sylvia Bähring, and Friedrich C. Luft, "Clinical effects of phosphodiesterase 3A mutations in inherited hypertension with brachydactyly," *Hypertension (Dallas, Tex. : 1979)* **66** (4), 800-808 (2015).
- 30 Bert-Jan H. van den Born, Louise C. Oskam, Majida Zidane, Carolin Schächterle, Enno Klussmann, Sylvia Bähring, and Friedrich C. Luft, "The Case| A handful of hypertension," *Kidney Int* **90** (4), 911-913 (2016).
- 31 Mario Kaßmann, István András Szijártó, Concha F. García-Prieto, Gang Fan, Johanna Schleifenbaum, Yoland-Marie Anistan, Christoph Tabeling, Yu Shi, Ferdinand le Noble, Martin Witzzenrath, Yu Huang, Lajos Markó, Mark T. Nelson, and Maik Gollasch, "Role of Ryanodine Type 2 Receptors in Elementary Ca Signaling in Arteries and Vascular Adaptive Responses," *J Am Heart Assoc* **8** (9), e010090 (2019).
- 32 Matthew A. Sparks, Kelly K. Parsons, Johannes Stegbauer, Susan B. Gurley, Anuradha Vivekanandan-Giri, Christopher N. Fortner, Jay Snouwaert, Eric W. Raasch, Robert C. Griffiths, Timothy A. J. Haystead, Thu H. Le, Subramaniam Pennathur, Beverly Koller, and Thomas M. Coffman, "Angiotensin II type 1A receptors in vascular smooth muscle cells do not influence aortic remodeling in hypertension," *Hypertension (Dallas, Tex. : 1979)* **57** (3), 577-585 (2011).
- 33 Dieter Groneberg, Peter König, Angela Wirth, Stefan Offermanns, Doris Koesling, and Andreas Friebe, "Smooth muscle-specific deletion of nitric oxide-sensitive guanylyl cyclase is sufficient to induce hypertension in mice," *Circulation* **121** (3), 401-409 (2010).
- 34 Ramesh Chennupati, Angela Wirth, Julie Favre, Rui Li, Rémy Bonnavion, Young-June Jin, Astrid Wietelmann, Frank Schweda, Nina Wettschureck, Daniel Henrion, and Stefan Offermanns, "Myogenic vasoconstriction requires G/G and LARG to maintain local and systemic vascular resistance," *Elife* **8** (2019).
- 35 C. Heinze, A. Seniuk, M. V. Sokolov, A. K. Huebner, A. E. Klementowicz, I. A. Szijarto, J. Schleifenbaum, H. Vitzthum, M. Gollasch, H. Ehmke, B. C. Schroeder, and C. A. Hubner, "Disruption of vascular Ca<sup>2+</sup>-activated chloride currents lowers blood pressure," *J Clin Invest* **124** (2), 675-686 (2014).
- 36 H. C. Hercule, J. Tank, R. Plehm, M. Wellner, A. C. da Costa Goncalves, M. Gollasch, A. Diedrich, J. Jordan, F. C. Luft, and V. Gross, "Regulator of G protein signalling 2 ameliorates angiotensin II-induced hypertension in mice," *Exp Physiol* **92** (6), 1014-1022 (2007).
- 37 Gilles Kauffenstein, Ismail Laher, Khalid Matrougui, Nathalie C. Guérineau, and Daniel Henrion, "Emerging role of G protein-coupled receptors in microvascular myogenic tone," *Cardiovascular research* **95** (2), 223-232 (2012).
- 38 Gilles Kauffenstein, Sophie Tamareille, Fabrice Prunier, Charlotte Roy, Audrey Ayer, Bertrand Toutain,

- 
- Marie Billaud, Brant E. Isakson, Linda Grimaud, Laurent Loufrani, Pascal Rousseau, Pierre Abraham, Vincent Procaccio, Hannah Monyer, Cor de Wit, Jean-Marie Boeynaems, Bernard Robaye, Brenda R. Kwak, and Daniel Henrion, "Central Role of P2Y<sub>6</sub> UDP Receptor in Arteriolar Myogenic Tone," *Arteriosclerosis, thrombosis, and vascular biology* **36** (8), 1598-1606 (2016).
- 39 Jeffrey T. Kroetsch and Steffen-Sebastian Bolz, "The TNF- $\alpha$ /sphingosine-1-phosphate signaling axis drives myogenic responsiveness in heart failure," *Journal of vascular research* **50** (3), 177-185 (2013).
- 40 P. W. Pires, E. A. Ko, H. A. T. Pritchard, M. Rudokas, E. Yamasaki, and S. Earley, "The angiotensin II receptor type 1b is the primary sensor of intraluminal pressure in cerebral artery smooth muscle cells," *J. Physiol. (Lond.)* **595** (14), 4735-4753 (2017).
- 41 R. J. Lefkowitz, "A brief history of G-protein coupled receptors (Nobel Lecture)," *Angew Chem Int Ed Engl* **52** (25), 6366-6378 (2013).
- 42 V. V. Gurevich and E. V. Gurevich, "GPCR Signaling Regulation: The Role of GRKs and Arrestins," *Front Pharmacol* **10**, 125 (2019).
- 43 G. Boerrigter, M. W. Lark, E. J. Whalen, D. G. Soergel, J. D. Violin, and J. C. Burnett, Jr., "Cardiorenal actions of TRV120027, a novel ss-arrestin-biased ligand at the angiotensin II type I receptor, in healthy and heart failure canines: a novel therapeutic strategy for acute heart failure," *Circ Heart Fail* **4** (6), 770-778 (2011).
- 44 Joseph T. Reed, Tanya Pareek, Srinivas Sriramula, and Mallikarjuna R. Pabbidi, "Aging influences cerebrovascular myogenic reactivity and BK channel function in a sex-specific manner," *Cardiovascular research* **116** (7), 1372-1385 (2020).
- 45 Osama F. Harraz, Rasha R. Abd El-Rahman, Kamran Bigdely-Shamloo, Sean M. Wilson, Suzanne E. Brett, Monica Romero, Albert L. Gonzales, Scott Earley, Edward J. Vigmond, Anders Nygren, Bijoy K. Menon, Rania E. Mufti, Tim Watson, Yves Starreveld, Tobias Furstenhaupt, Philip R. Muellerleile, David T. Kurjiaka, Barry D. Kyle, Andrew P. Braun, and Donald G. Welsh, "Ca(V)<sub>3.2</sub> channels and the induction of negative feedback in cerebral arteries," *Circulation research* **115** (7), 650-661 (2014).
- 46 Kyoichi Ono and Toshihiko Iijima, "Cardiac T-type Ca<sup>2+</sup> channels in the heart," *Journal of molecular and cellular cardiology* **48** (1), 65-70 (2010).
- 47 Guy Vassort, Karel Talavera, and Julio L. Alvarez, "Role of T-type Ca<sup>2+</sup> channels in the heart," *Cell Calcium* **40** (2), 205-220 (2006).
- 48 Maria Ercu and Enno Klussmann, "Roles of A-Kinase Anchoring Proteins and Phosphodiesterases in the Cardiovascular System," *J Cardiovasc Dev Dis* **5** (1) (2018).
- 49 J. A. Beavo, "Cyclic nucleotide phosphodiesterases: functional implications of multiple isoforms," *Physiol Rev* **75** (4), 725-748 (1995).

---

## Statutory Declaration

I, Yingqiu Cui, by personally signing this document in lieu of an oath, hereby affirm that I prepared the submitted dissertation on the topic The Role of Angiotensin II Type 1a Receptor and Downstream Signaling in Murine Myogenic Vasoconstriction (Die Funktion des Angiotensin II Typ 1a-Rezeptors und nachfolgender Signalwege bei myogener Vasokonstriktion in Mäusen), independently and without the support of third parties, and that I used no other sources and aids than those stated.

All parts which are based on the publications or presentations of other authors, either in letter or in spirit, are specified as such in accordance with the citing guidelines. The sections on methodology (in particular regarding practical work, laboratory regulations, statistical processing) and results (in particular regarding figures, charts and tables) are exclusively my responsibility.

Furthermore, I declare that I have correctly marked all of the data, the analyses, and the conclusions generated from data obtained in collaboration with other persons, and that I have correctly marked my own contribution and the contributions of other persons (cf. declaration of contribution). I have correctly marked all texts or parts of texts that were generated in collaboration with other persons.

My contributions to any publications to this dissertation correspond to those stated in the below joint declaration made together with the supervisor. All publications created within the scope of the dissertation comply with the guidelines of the ICMJE (International Committee of Medical Journal Editors; [www.icmje.org](http://www.icmje.org)) on authorship. In addition, I declare that I shall comply with the regulations of Charité-Universitätsmedizin Berlin on ensuring good scientific practice.

I declare that I have not yet submitted this dissertation in identical or similar form to another Faculty.

The significance of this statutory declaration and the consequences of a false statutory declaration under criminal law (Sections 156, 161 of the German Criminal Code) are known to me.”

Date

Signature



---

## Declaration of your own contribution to the publications

Yingqiu Cui contributed the following to the below listed publications:

### Publication 1:

**Cui Y**, Kassmann M, Nickel S, Zhang C, Alenina N, Anistan YM, Schleifenbaum J, Bader M, Welsh DG, Huang Y and Gollasch M. Myogenic Vasoconstriction Requires Canonical G<sub>q/11</sub> Signaling of the Angiotensin II Type 1 Receptor. *J Am Heart Assoc.* 2022:e022070. Contribution: Design of experimental protocols, preparation of vessels, vessel diameter measurements in mouse arteries, analysis and interpretation of data, literature searches, preparation of the manuscript draft. Figure 1A, 2, 3, 4, 5, 6 7, 8 were created based on the results I recorded.

### Publication 2:

Fan G, Kaßmann M, **Cui Y**, Matthaues C, Kunz S, Zhong C, Zhu S, Xie Y, Tsvetkov D, Daumke O, Huang Y and Gollasch M. Age attenuates the T-type Ca 3.2-RyR axis in vascular smooth muscle. *Aging Cell.* 2020;19:e13134. Contribution: Design of experimental protocols, preparation of vessels, vessel diameter measurements in mouse arteries, analysis and interpretation of data. Figure 6 was created based on the results I recorded.

### Publication 3:

Ercu M, Markó L, Schächterle C, Tsvetkov D, **Cui Y**, Maghsodi S, Bartolomaeus TUP, Maass PG, Zühlke K, Gregersen N, Hübner N, Hodge R, Mühl A, Pohl B, Illas RM, Geelhaar A, Walter S, Napieczynska H, Schelenz S, Taube M, Heuser A, Anistan Y-M, Qadri F, Todiras M, Plehm R, Popova E, Langanke R, Eichhorst J, Lehmann M, Wiesner B, Russwurm M, Forslund SK, Kamer I, Müller DN, Gollasch M, Aydin A, Bähring S, Bader M, Luft FC and Klusmann E. Phosphodiesterase 3A and Arterial Hypertension. *Circulation.* 2020;142:133-149.

Contribution: Design of experimental protocols, preparation of vessels, vessel diameter measurements in mouse arteries, analysis and interpretation of data. Figure 4I was created based on the results I recorded.

---

Signature, date and stamp of first supervising university professor / lecturer

---

Signature of doctoral candidate

## Excerpt from Journal Summary List

### Publication #1:

#### **Myogenic Vasoconstriction Requires Canonical G<sub>q/11</sub> Signaling of the Angiotensin II Type 1 Receptor.**

Cui Y, Kassmann M, Nickel S, Zhang C, Alenina N, Anistan YM, Schleifenbaum J, Bader M, Welsh DG, Huang Y and Gollasch M. Myogenic Vasoconstriction Requires Canonical G<sub>q/11</sub> Signaling of the Angiotensin II Type 1 Receptor. *J Am Heart Assoc.* 2022:e022070.

Received: 2021 Apr 14; Accepted: 2021 Nov 11; Published online: 2022 Feb 08.





Journal Data Filtered By: **Selected JCR Year: 2019** Selected Editions: SCIE,SSCI  
 Selected Categories: **"CARDIAC and CARDIOVASCULAR SYSTEMS"** Selected  
 Category Scheme: WoS  
**Gesamtanzahl: 138 Journale**

Rank	Full Journal Title	Total Cites	Journal Impact Factor	Eigenfactor Score
1	CIRCULATION	158,218	23.603	0.205020
2	EUROPEAN HEART JOURNAL	59,968	22.673	0.140620
3	JOURNAL OF THE AMERICAN COLLEGE OF CARDIOLOGY	101,927	20.589	0.190280
4	Nature Reviews Cardiology	7,100	20.260	0.021130
5	CIRCULATION RESEARCH	51,539	14.467	0.071470
6	JAMA Cardiology	4,740	12.794	0.030110
7	JACC-Cardiovascular Imaging	10,110	12.740	0.027550
8	BASIC RESEARCH IN CARDIOLOGY	4,704	11.981	0.006380
9	EUROPEAN JOURNAL OF HEART FAILURE	12,784	11.627	0.028700
10	JACC-Heart Failure	4,117	8.750	0.019180
11	JACC-Cardiovascular Interventions	11,371	8.432	0.037330
12	CARDIOVASCULAR RESEARCH	21,526	8.168	0.019950
13	JOURNAL OF HEART AND LUNG TRANSPLANTATION	12,465	7.865	0.028140
14	Cardiovascular Diabetology	6,179	7.332	0.011390
15	PROGRESS IN CARDIOVASCULAR DISEASES	4,193	6.763	0.008340
16	European Heart Journal- Cardiovascular Pharmacotherapy	521	6.696	0.001640
17	Circulation-Heart Failure	6,773	6.033	0.018490
18	European Journal of Preventive Cardiology	5,589	5.864	0.015370
19	HEART RHYTHM	12,246	5.731	0.028620
20	Circulation- Cardiovascular Imaging	5,574	5.691	0.016320

Rank	Full Journal Title	Total Cites	Journal Impact Factor	Eigenfactor Score
21	JOURNAL OF THE AMERICAN SOCIETY OF ECHOCARDIOGRAPHY	11,347	5.508	0.018230
22	Circulation-Cardiovascular Interventions	5,012	5.493	0.018140
23	JOURNAL OF CARDIOVASCULAR MAGNETIC RESONANCE	5,205	5.361	0.011120
24	Clinical Research in Cardiology	3,321	5.268	0.007280
25	HEART	18,108	5.213	0.030140
26	Circulation-Cardiovascular Quality and Outcomes	4,728	5.071	0.014350
27	CANADIAN JOURNAL OF CARDIOLOGY	6,980	5.000	0.017630
28	European Heart Journal-Cardiovascular Imaging	6,359	4.841	0.023110
29	TRENDS IN CARDIOVASCULAR MEDICINE	2,695	4.755	0.003920
30	REVISTA ESPANOLA DE CARDIOLOGIA	3,672	4.642	0.004610
31	Journal of the American Heart Association	17,149	4.605	0.070620
32	Circulation-Cardiovascular Genetics	3,090	4.534	0.008600
33	JOURNAL OF THORACIC AND CARDIOVASCULAR SURGERY	28,491	4.451	0.034300
34	Circulation-Arrhythmia and Electrophysiology	6,344	4.393	0.016630
35	AMERICAN HEART JOURNAL	19,814	4.153	0.026810
36	JOURNAL OF MOLECULAR AND CELLULAR CARDIOLOGY	14,031	4.133	0.017960
37	CARDIOVASCULAR DRUGS AND THERAPY	2,114	4.069	0.003340
38	Circulation-Genomic and Precision Medicine	375	4.063	0.002220
39	Hellenic Journal of Cardiology	987	4.047	0.001000
40	EUROPACE	9,973	4.045	0.024750

## ORIGINAL RESEARCH

Myogenic Vasoconstriction Requires Canonical  $G_{q/11}$  Signaling of the Angiotensin II Type 1 Receptor

Yingqiu Cui, MS; Mario Kassmann , PhD; Sophie Nickel, MS; Chenglin Zhang, PhD; Natalia Alenina , PhD; Yolande Marie Anistan, BA; Johanna Schleifenbaum, PhD; Michael Bader, PhD; Donald G. Welsh, PhD; Yu Huang , PhD; Maik Gollasch , MD, PhD

**BACKGROUND:** Blood pressure and tissue perfusion are controlled in part by the level of intrinsic (myogenic) arterial tone. However, many of the molecular determinants of this response are unknown. We previously found that mice with targeted disruption of the gene encoding the angiotensin II type 1a receptor (AT1AR) (*Agtr1a*), the major murine angiotensin II type 1 receptor (AT1R) isoform, showed reduced myogenic tone; however, uncontrolled genetic events (in this case, gene ablation) can lead to phenotypes that are difficult or impossible to interpret.

**METHODS AND RESULTS:** We tested the mechanosensitive function of AT1R using tamoxifen-inducible smooth muscle-specific AT1aR knockout (smooth muscle-*Agtr1a*<sup>-/-</sup>) mice and studied downstream signaling cascades mediated by  $G_{q/11}$  and/or  $\beta$ -arrestins. FR900359, Sar11e4lle8-angiotensin II (SII), TRV120027 and TRV120055 were used as selective  $G_{q/11}$  inhibitor and biased agonists to activate noncanonical  $\beta$ -arrestin and canonical  $G_{q/11}$  signaling of the AT1R, respectively. Myogenic and Ang II-induced constrictions were diminished in the perfused renal vasculature, mesenteric and cerebral arteries of smooth muscle-*Agtr1a*<sup>-/-</sup> mice. Similar effects were observed in arteries of global mutant *Agtr1a*<sup>-/-</sup> but not *Agtr1b*<sup>-/-</sup> mice. FR900359 decreased myogenic tone and angiotensin II-induced constrictions whereas selective biased targeting of AT1R- $\beta$ -arrestin signaling pathways had no effects.

**CONCLUSIONS:** This study demonstrates that myogenic arterial constriction requires  $G_{q/11}$ -dependent signaling pathways of mechanoactivated AT1R but not G protein-independent, noncanonical pathways in smooth muscle cells.

**Key Words:** angiotensin II type 1a receptor ■ arterial smooth muscle ■ biased ligands ■ myogenic vasoconstriction

## See Editorial by Chen and Sonkusare

Elevation of intravascular pressure causes constriction (myogenic tone) of small arteries and arterioles, and this response is a key element in regulating blood flow. This response was first described by Bayliss<sup>1</sup> and has been observed in various microvascular beds.<sup>2</sup> Many cardiovascular disorders are associated with dysfunctional arterial myogenic response and they include hypertension, chronic heart failure, ischemic stroke, and

diabetes.<sup>3-7</sup> Despite the functional importance of the myogenic response, the nature of sensing intraluminal pressure that causes this response has remained elusive.

Myogenic vasoconstriction is mediated by pressure-dependent depolarization of vascular smooth muscle (SM) cells, an event that augments  $Ca^{2+}$  influx through voltage-dependent  $Ca_v1.2$  channels.<sup>8-13</sup>  $G_{q/11}$ -coupled receptors (GPCRs) are thought to function as the upstream

Correspondence to: Maik Gollasch, MD, PhD, Department of Internal Medicine and Geriatrics, University Medicine, Greifswald, Germany, and Experimental and Clinical Research Center (ECRC), 13125 Berlin, Germany. E-mail: maik.gollasch@charite.demaik.gollasch@med.uni-greifswald.de

Preprint posted on BioRxiv September 11, 2020. <https://doi.org/10.1101/2020.09.09.289280>.

Supplemental Material for this article is available at <https://www.ahajournals.org/doi/suppl/10.1161/JAHA.121.022070>

For Sources of Funding and Disclosures, see page 14.

© 2022 The Authors. Published on behalf of the American Heart Association, Inc., by Wiley. This is an open access article under the terms of the Creative Commons Attribution-NonCommercial License, which permits use, distribution and reproduction in any medium, provided the original work is properly cited and is not used for commercial purposes.

JAHA is available at: [www.ahajournals.org/journal/jaha](http://www.ahajournals.org/journal/jaha)

## CLINICAL PERSPECTIVE

### What Is New?

- Our study using novel tamoxifen-inducible smooth muscle-specific angiotensin II receptor type 1a knockout mice (smooth muscle-*Agtr1a*<sup>-/-</sup>) demonstrates that myogenic arterial constriction requires canonical G<sub>q/11</sub>-dependent signaling pathways of mechanoactivated AT1R but not G protein-independent, noncanonical pathways in smooth muscle cells.

### What Are the Clinical Implications?

- Our study will foster understanding and development of new diagnostic and therapeutic options for hypertension.
- Our study also will provide valuable new insights for researchers working on blood pressure control-related signaling mechanisms and for clinicians treating patients with hypertension.

## Nonstandard Abbreviations and Acronyms

<b>AT1R/AT1aR/AT1bR</b>	angiotensin II type 1/1a/1b receptor
<b>GRK</b>	G protein-coupled receptor kinase
<b>MA</b>	mesenteric arteries
<b>SM</b>	smooth muscle
<b>SMMHC</b>	smooth muscle myosin heavy chain

sensor of membrane stretch.<sup>14</sup> We previously found that mice with targeted disruption of the gene encoding the angiotensin II (Ang II) type 1a receptor (*Agtr1a*), the major murine AT1 receptor isoform, showed reduced myogenic tone.<sup>15</sup> However, uncontrolled genetic events (in this case, global gene ablation) can lead to phenotypes that are difficult or impossible to interpret in terms of cardiovascular function. This is particularly relevant for mouse models of the renin-angiotensin system. For example, mice with body-wide elimination of angiotensin-converting enzyme have systolic blood pressures that average 35 mm Hg below that of wild-type mice. Surprisingly, renal arterioles and small arteries were thickened, a paradoxical finding given the very low systolic blood pressure that could have been caused by developmental processes and/or mouse strains. The renal changes in angiotensin-converting enzyme knockout mice were completely unanticipated but have also been noted in angiotensinogen and Ang II receptor knockout mice.<sup>16</sup> AT1Rs are known to couple primarily to classical G<sub>q/11</sub> proteins to activate multiple downstream

signals, including protein kinase C, extracellular signal-regulated kinases, Raf kinases, tyrosine kinases, receptor tyrosine kinases (epidermal growth factor receptor, platelet-derived growth factor, insulin receptor) and reactive oxygen species.<sup>17</sup> The AT1R activation also stimulates G protein-independent signaling pathways such as  $\beta$ -arrestin-mediated mitogen-activated protein kinase activation and Src-Janus kinase-signal transducer and activator of transcription.<sup>17</sup> Recently, it has been shown that the activation of intracellular signaling by mechanical stretch of the AT1R does not require the natural ligand Ang II<sup>15,18,19</sup> but requires the activation of the transducer  $\beta$ -arrestin.<sup>18</sup> Interestingly, mechanical stretch appears to allosterically stabilize specific  $\beta$ -arrestin-biased active conformations of AT1R to promote noncanonical downstream signaling mediated exclusively by the multifunctional scaffold protein,  $\beta$ -arrestin.<sup>20</sup> Whether this noncanonical  $\beta$ -arrestin effector pathway plays a role in myogenic and ligand-dependent vasoconstriction has yet to be ascertained.

This study explored the specific function of AT1R in the regulation of myogenic tone and whether downstream signaling pathways are dependent on canonical G<sub>q/11</sub> and/or noncanonical alternative signaling pathways. In this regard, we generated mice with cell specific deletion of SM AT1a receptors (SM-*Agtr1a* mice) and studied the effects of biased GPCR agonists and G<sub>q/11</sub> protein inhibition on tone development in 3 distinct vascular beds (renal, cerebral, and mesenteric circulation). We found that the SM AT1aR coupled toward the canonical G<sub>q/11</sub> signaling pathway is required for the myogenic response in all 3 vascular beds. Our data argue against involvement of noncanonical G protein-independent alternative signaling downstream of the AT1R to cause myogenic vasoconstriction.

## METHODS

Data and analytic methods will be made available to other researchers upon reasonable request to the corresponding author.

### Mouse Model

We used the SM myosin heavy chain (SMMHC)-Cre-ER<sup>T2</sup> transgenic mouse line expressing Cre recombinase in SM cells under control of the SMMHC promoter<sup>21</sup> and a mouse line bearing a floxed allele of the *Agtr1a* gene (*Agtr1a*<sup>fllox</sup>), encoding the major murine AT1 receptor isoform (AT1aR)<sup>22</sup> to generate SMMHC-Cre+*Agtr1a*<sup>fllox/fllox</sup> (SM-*Agtr1a*<sup>fl/fl</sup>) mice (Figure S1A). Genotyping was performed by polymerase chain reaction analysis of tail DNA as described previously.<sup>21</sup> Amplification of the SMMHC-Cre gene was performed in a multiplex polymerase chain reaction with the primers TGA CCC CAT CTC TTC ACT CC (SMWT1), AAC TCC ACG ACC ACC TCA TC (SMWT2), and AGT CCC TCA CAT CCT CAG GTT (phCREAS1).<sup>23</sup> The following primers (5'-3') were

used to identify *Agtr1a*<sup>fl<sup>ox</sup></sup> alleles: forward GCT TTC TCT GTT ATG CAG TCT and reverse ATC AGC ACA TCC AGG AAT G. Knockout (SM-*Agtr1a*<sup>-/-</sup>) was induced in adult (12–16 weeks) SM-*Agtr1a*<sup>fl<sup>ox</sup></sup> male mice by intraperitoneal injection with tamoxifen (30 µg/mg body weight) on 5 consecutive days. Isolated arteries were usually obtained after 2 to 3 days after tamoxifen treatment. Tamoxifen treatment of mice did not influence myogenic tone (SM-*Agtr1a*<sup>+/+</sup> cerebral arteries without tamoxifen: 12.35±2.16%, n=6 vessels, each from individual mice; SM-*Agtr1a*<sup>+/+</sup> cerebral arteries with tamoxifen: 13.23±1.07%, n=4 vessels, each from individual mice). Figure S1B shows reduction of AT1aR expression in vascular SM cells of SM-*Agtr1a*<sup>-/-</sup> arteries. The same antibody did not detect AT1R expression across the vessel wall from global *Agtr1a*<sup>-/-</sup> mice<sup>15</sup> (Figure S1C). We also studied adult (12–16 weeks) male mice with global AT1a receptor deficiency (*Agtr1a*<sup>-/-</sup>),<sup>15,24,25</sup> and with global AT1b receptor deficiency (*Agtr1b*<sup>-/-</sup>).<sup>26</sup> Age-matched male mice were used as controls in the experiments. Animal care followed American Physiological Society guidelines, and all protocols were approved by local authority (LAGeSo, Berlin, Germany) and the animal welfare officers of the Max Delbrück Center for Molecular Medicine (approval reference number X 9011/16). All procedures conformed to the guidelines from Directive 2010/63/EU of the European Parliament on the protection of animals used for scientific purposes or the National Institutes of Health *Guide for the Care and Use of Laboratory Animals*. Mice were maintained in the Max Delbrück Center animal facility in individually ventilated cages (Tecniplast Deutschland, Hohenpeißenberg, Germany) under standardized conditions with an artificial 12-hour dark-light cycle, with free access to standard chow (0.25% sodium; SSNIFF Spezialitäten, Soest, Germany) and drinking water. Animals were euthanized by cervical dislocation and randomly assigned to the experimental procedures.

## Materials

Antibody to  $\alpha$ -SM actin ( $\alpha$ -SMA, #ab8211) was from Abcam (Cambridge, MA). Anti-AT1R (#PA5-20812) and donkey anti-rabbit IgG (H+L) secondary antibody (A10040) were purchased from Thermo Fisher Scientific (Waltham, MA). 4',6-diamidino-2-phenylindole (DAPI, #D9542) was purchased from Sigma-Aldrich Co. (St. Louis, MO). Ang II (#A9525), SII (#sc-391239A), and tamoxifen (#H7904) were from Sigma-Aldrich Co (82024 Taufkirchen, Germany). TRV120055 (#JT-71995) and TRV120056 (#JT-71996) were from Synpeptide Co., Ltd (Shanghai, China). TRV120027 (#HY-P2141A) was from MedChemExpress (Monmouth Junction, NJ).

## Mesenteric and Cerebral Arteries

After mice were killed, the mesenteric bed and brain were removed and placed into cold (4 °C), gassed

(95% O<sub>2</sub>-5% CO<sub>2</sub>) physiological saline solution (PSS) of the following composition (mmol/L): 119 NaCl, 4.7 KCl, 25 NaHCO<sub>3</sub>, 1.2 KH<sub>2</sub>PO<sub>4</sub>, 1.6 CaCl<sub>2</sub>, 1.2 MgSO<sub>4</sub>, 0.03 EDTA, and 11.1 glucose. Third- or fourth-order mesenteric arteries (MA) and middle cerebral arteries or posterior cerebral arteries were dissected and cleaned of adventitial connective tissue.<sup>15,27–29</sup>

## Pressure Myography

Vessel myography was performed as previously described.<sup>14,15,21,28</sup> MA or cerebral arteries were mounted on glass cannula and superfused continuously with PSS (95% O<sub>2</sub>-5% CO<sub>2</sub>; pH, 7.4; 37 °C). The vessels were stepwise pressurized to 20, 40, 60, 80, or 100 mm Hg using a pressure servo control system (Living System Instrumentation, Burlington, VT). We measured the inner diameter of the vessels with a video microscope (Nikon Diaphot, Düsseldorf, Germany) connected to a personal computer for data acquisition and analysis (HaSoTec, Rostock, Germany).<sup>15,27–30</sup> Arteries were equilibrated for 45 to 60 minutes before starting experiments. A 60-mmol/L KCl challenge was performed before any other intervention.

## Isolated Perfused Kidneys

Isolated kidneys were perfused in an organ chamber using a peristaltic pump at constant flow (0.3–1.9 mL/min) of oxygenated (95% O<sub>2</sub> and 5% CO<sub>2</sub>) PSS.<sup>15</sup> Drugs (Ang II or biased agonists) were added to the perfusate. Perfusion pressure was measured by a pressure transducer after an equilibration period of 60 to 90 minutes. Data were recorded and analyzed by a Powerlab acquisition system (AD Instruments, Colorado Springs, CO). Ang II-induced pressor effects were normalized to the maximal pressor effect induced by KCl (60 mmol/L).<sup>14,15,27</sup>

## Immunofluorescence

SM-*Agtr1a*<sup>+/+</sup> and SM-*Agtr1a*<sup>-/-</sup> mice MA were dissected and further fixed in 4% formaldehyde and embedded in Tissue-Tek O.C.T. compound to be frozen in liquid nitrogen. Tissues were then sectioned and permeabilized in 1% Triton X-100 in PBS. Sections were stained with the primary antibody overnight at 4 °C. After washing with PBS for 3×5 minutes, the secondary antibody and DAPI were applied for 2 hours at room temperature. Fluorescence images were captured by use of Olympus FV1000 confocal microscopy and images were analyzed by ImageJ analysis software.

## Statistical Analysis

Data are presented as means±SEM. Statistically significant differences in mean values were determined by



Student unpaired *t* test or 1-way analysis of variance.  $P < 0.05$  were considered statistically significant.

## RESULTS

### AT1aR Is Essential for Pressure-Induced Response in the Renal Circulation

We evaluated myogenic tone in mouse renal circulation, a highly myogenic bed regulating blood flow to

the kidneys and consequently sodium excretion and systemic blood pressure. Renal vascular resistance of isolated perfused kidneys was determined by measuring perfusion pressure at fixed levels of flow. The perfusion pressure increased with flow rate in kidneys of wild-type *Agtr1a*<sup>+/+</sup> mice, reaching a value of about 160 mm Hg at a flow rate of 1.9 mL/min, which is in the physiological range (between 1.5 and 3.5 mL/min pulsatile flow)<sup>31</sup> (Figure 1A). Kidneys from *Agtr1a*<sup>-/-</sup> mice developed significantly less pressure at the same

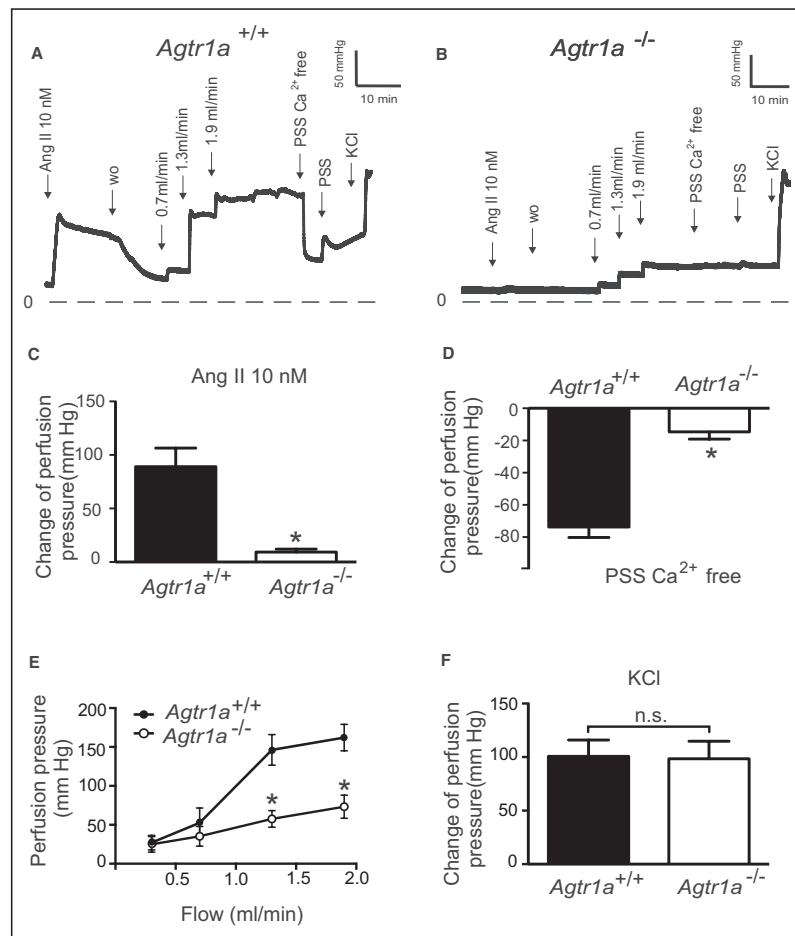


**Figure 1. Vasoregulation in isolated perfused kidneys of *Agtr1a*<sup>-/-</sup> mice.**

**A and B.** Original recordings of perfusion pressure in kidneys of *Agtr1a*<sup>+/+</sup> (**A**) and *Agtr1a*<sup>-/-</sup> mice (**B**). **C.** Increase in the perfusion pressure induced by 10 nmol/L Ang II. **D.** Myogenic tone assessed by exposure to Ca<sup>2+</sup> free PSS. **E.** Perfusion pressure at flow rates of 0.3, 0.7, 1.3, and 1.9 mL/min. **F.** Increase in the perfusion pressure induced by 60 mmol/L KCl.  $n = 6$  *Agtr1a*<sup>+/+</sup> kidneys from 6 mice and  $n = 7$  *Agtr1a*<sup>-/-</sup> kidneys from 7 mice for all panels. Ang II indicates angiotensin II; n.s., not significant; PSS, physiological saline solution; and wo, wash-out.

flow rate (Figure 1B and 1E). 60 mmol/L KCl-induced increases in perfusion pressure were not altered in *Agtr1a*<sup>-/-</sup> kidneys (Figure 1F). At a flow rate of 1.9 mL/min, pressure in *Agtr1a*<sup>-/-</sup> kidneys was ≈100 mm Hg lower than in *Agtr1a*<sup>+/+</sup> kidneys. Ang II (10 nmol/L) increased perfusion pressure by ≈80 mm Hg in kidneys of *Agtr1a*<sup>+/+</sup> mice but had no effect in kidneys of *Agtr1a*<sup>-/-</sup> mice (Figure 1C); this is indicative of AT1aRs mediating Ang II-dependent vasoconstriction. Removal of

external Ca<sup>2+</sup> nearly abolished flow-induced myogenic constriction in perfused kidneys of *Agtr1a*<sup>+/+</sup> mice but had no effect in kidneys of *Agtr1a*<sup>-/-</sup> mice (Figure 1D), indicating AT1aRs mediate also myogenic constriction of mouse renal arterioles. Of note, there was no difference in myogenic tone and Ang II vasoconstrictions between *Agtr1b*<sup>-/-</sup> versus *Agtr1b*<sup>+/+</sup> kidneys (Figure 2). Next, we focused on kidneys from SM-*Agtr1a*<sup>-/-</sup> mice (Figure 3). At a flow rate of 1.9 mL/min, pressure

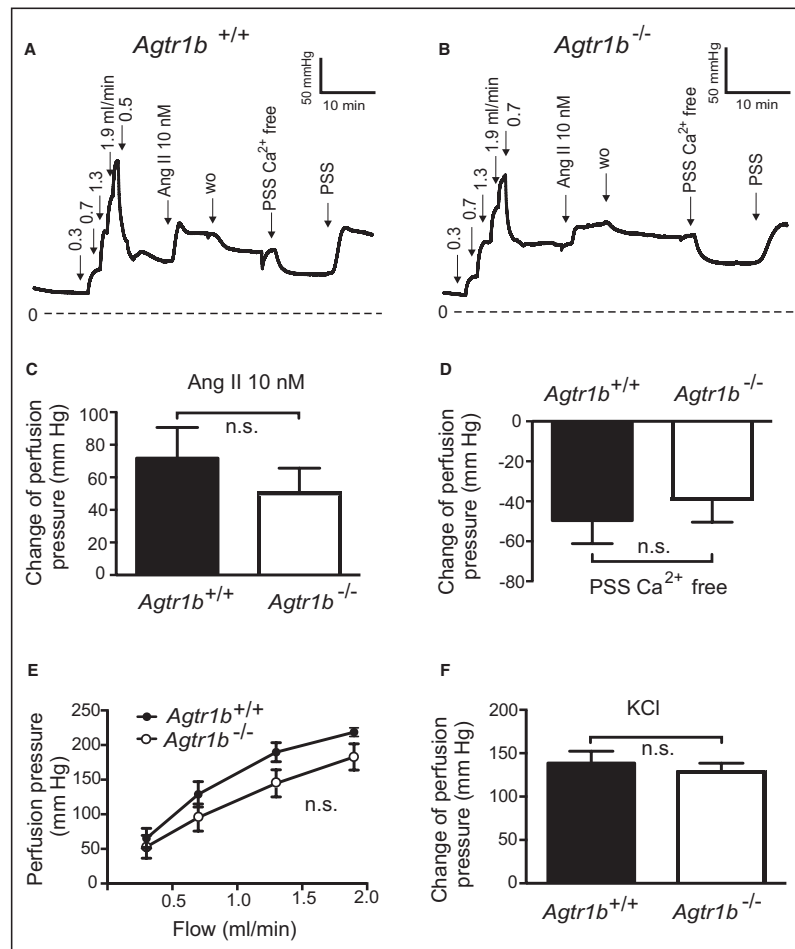


**Figure 2. Vasoregulation in isolated perfused kidneys of *Agtr1b*<sup>-/-</sup> mice.**

**A** and **B**, Original recordings of the perfusion pressure in kidneys of *Agtr1b*<sup>+/+</sup> (**A**) and *Agtr1b*<sup>-/-</sup> mice (**B**). **C**, Increase in perfusion pressure induced by 10 nmol/L Ang II. **D**, Change of pressure assessed by exposure to Ca<sup>2+</sup> free PSS. **E**, Perfusion pressure at flow rates of 0.3, 0.7, 1.3, and 1.9 mL/min. **F**, Increase in perfusion pressure induced by 60 mmol/L KCl. n=6 *Agtr1b*<sup>+/+</sup> kidneys from 5 mice and n=6 *Agtr1b*<sup>-/-</sup> kidneys from 3 mice for all panels. Ang II indicates angiotensin II; n.s., not significant; PSS, physiological saline solution; and w.o., washout.

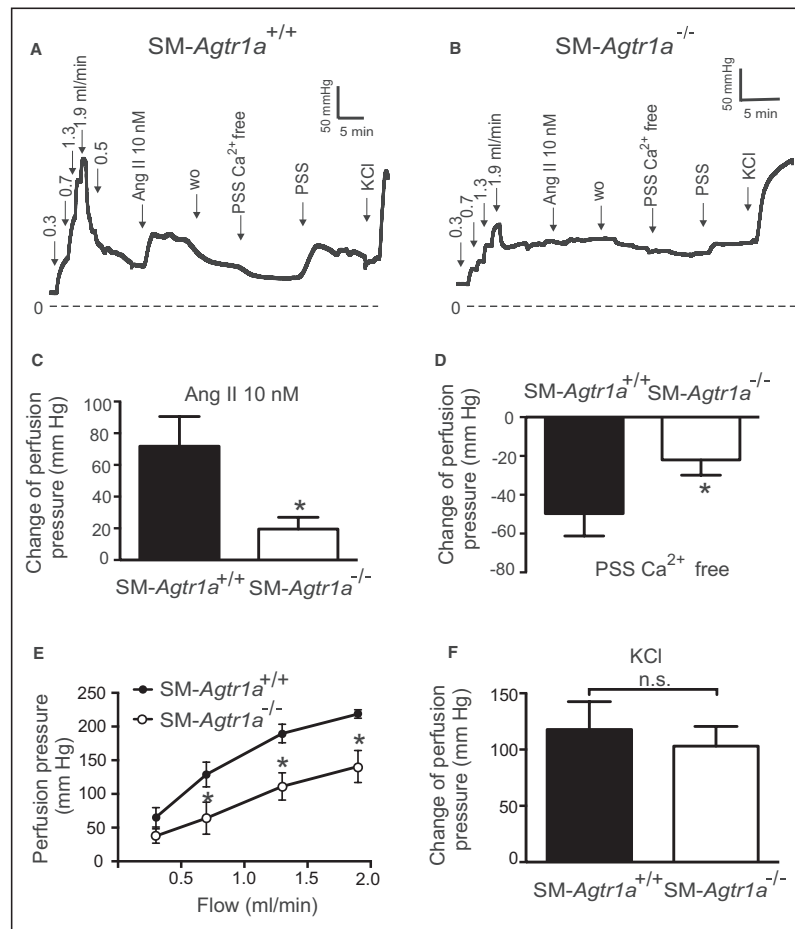


**Figure 3. Vasoregulation in isolated perfused kidneys of SM-Agtr1a<sup>-/-</sup> mice.** **A** and **B**, Original recordings of the perfusion pressure in kidneys of SM-Agtr1a<sup>+/+</sup> (**A**) and SM-Agtr1a<sup>-/-</sup> mice (**B**). **C**, Increase in perfusion pressure induced by 10 nmol/L Ang II. **D**, Change of pressure assessed by exposure to Ca<sup>2+</sup> free PSS. **E**, Perfusion pressure at flow rates of 0.3, 0.7, 1.3, and 1.9 mL/min. **F**, Increase in perfusion pressure induced by 60 mmol/L KCl. n=6 SM-Agtr1a<sup>+/+</sup> kidneys from 5 mice and n=6 SM-Agtr1a<sup>-/-</sup> kidneys from 6 mice for all panels. \*P<0.05. Ang II indicates angiotensin II; n.s., not significant; PSS, physiological saline solution; SM, smooth muscle; and w.o., washout.

in SM-Agtr1a<sup>-/-</sup> kidneys was ~90 mm Hg lower than in SM-Agtr1a<sup>+/+</sup> kidneys (Figure 3A, 3B, and 3E). SM-Agtr1a<sup>-/-</sup> kidneys showed largely reduced myogenic vasoconstriction as assessed by exposure of the kidneys to Ca<sup>2+</sup> free PSS (Figure 3B and 3D), whereas wild-type kidneys showed strong myogenic vasoconstrictions (Figure 3A and 3D). Sixty mmol/L KCl-induced increases in perfusion pressure were normal in SM-Agtr1a<sup>-/-</sup> kidneys (Figure 3F). Ang II (10 nmol/L) induced weaker increases in perfusion pressure in kidneys of SM-Agtr1a<sup>-/-</sup> mice compared with controls

(Figure 3C). Together, these results reveal a key role of AT1aR but not AT1bR in the flow-induced myogenic response and Ang II-evoked constriction of the mouse renal vasculature.

### AT1aR Contributes to Myogenic Constriction in Mesenteric and Cerebral Arteries

We first monitored myogenic constriction in resistance-sized MA using videomicroscopy. MA were exposed to

stepwise (20 mm Hg) increases in intraluminal pressure (20–100 mm Hg) in the presence and absence of external  $\text{Ca}^{2+}$  (1.6 mmol/L) to determine active and passive vessel diameters, respectively. Figure 4 shows representative recordings of MA from SM-*Agtr1a*<sup>+/+</sup> mice (Figure 4A) and SM-*Agtr1a*<sup>-/-</sup> mice (Figure 4B) and myogenic vasoconstriction was defined as the diameter difference in the presence and absence of external  $\text{Ca}^{2+}$  (1.6 mmol/L) at each pressure step.<sup>15</sup> Increases in intraluminal pressure generated active tension that counteracted further dilation of the vessels at 60 to 80 mm Hg in MA from SM-*Agtr1a*<sup>+/+</sup> mice, reaching peak constrictions of ~50  $\mu\text{m}$  at 80 to 100 mm Hg

(Figure 4A). In contrast, MA from SM-*Agtr1a*<sup>-/-</sup> mice produced only ~35% of the constriction observed in wild-type arteries (Figure 4B and 4C). Ang II strongly constricted arteries from SM-*Agtr1a*<sup>+/+</sup> mice but had no effect on arteries from SM-*Agtr1a*<sup>-/-</sup> mice (Figure 4D); the latter did constrict in response to 60 mmol/L KCl (Figure 4E). This study observed a marked reduction in AT1aR expression in the media of SM-*Agtr1a*<sup>-/-</sup> MA compared with wild-type (Figure S1B), in keeping with this receptor mediating myogenic constriction in MA. Next, we studied the function of AT1aRs in cerebral arteries. Vessels were equilibrated at 15 mm Hg (30 minutes) and following an assessment of KCl-induced

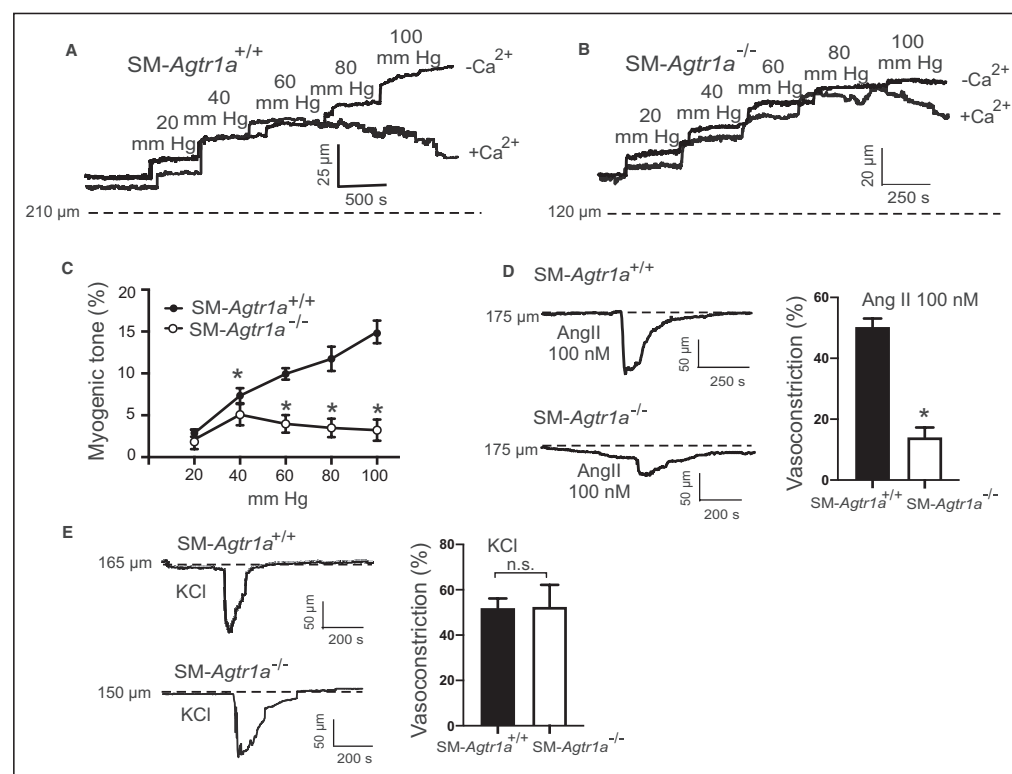


**Figure 4. Myogenic tone in mesenteric arteries.**

**A and B.** Representative recordings of MA diameter during a series of pressure steps from 20 to 100 mm Hg in 20 mm Hg increments in control conditions (+ $\text{Ca}^{2+}$ ) and in  $\text{Ca}^{2+}$  free solution ( $-\text{Ca}^{2+}$ ). Arteries were isolated from SM-*Agtr1a*<sup>+/+</sup> (A) and SM-*Agtr1a*<sup>-/-</sup> mice (B). Note the increase in active constriction over the entire pressure range from 60 to 100 mm Hg in vessels from SM-*Agtr1a*<sup>+/+</sup>, but not from SM-*Agtr1a*<sup>-/-</sup> mice. Vasodilation in  $\text{Ca}^{2+}$ -free solution was observed in SM-*Agtr1a*<sup>+/+</sup> but not in SM-*Agtr1a*<sup>-/-</sup> arteries ( $P < 0.05$ ). **C.** Average myogenic tone of mesenteric arteries in PSS expressed as dilation of vessels induced by external  $\text{Ca}^{2+}$  free solution (0  $\text{Ca}/\text{EGTA}$ ; SM-*Agtr1a*<sup>+/+</sup>,  $n = 9$ , and SM-*Agtr1a*<sup>-/-</sup>,  $n = 6$  vessels, each from individual mice for both groups). **D.** Response to Ang II and **(E)** response to 60 mmol/L KCl in MA of SM-*Agtr1a*<sup>+/+</sup> and SM-*Agtr1a*<sup>-/-</sup> mice. MAs were pressurized to 80 mm Hg. Responses are expressed as relative changes in vessel inner diameter. SM-*Agtr1a*<sup>+/+</sup>,  $n = 5$  vessels, and SM-*Agtr1a*<sup>-/-</sup>,  $n = 4$  vessels, from 5 and 4 mice, respectively. \* $P < 0.05$ . Ang II indicates angiotensin II; MA, mesenteric arteries; PSS, physiological saline solution; and SM, smooth muscle.

constriction, arteries were pressurized to 80 mm Hg (Figure S2A). Ang II constrictions and myogenic constriction was significantly decreased in SM-*Agtr1a*<sup>-/-</sup> arteries compared with wild-type (Figure S2A through S2D). Both wild-type and SM-*Agtr1a*<sup>-/-</sup> arteries produced similar constrictions when exposed to 60 mmol/L KCl (Figure S2E). The results demonstrate a key role of AT1aR in the myogenic response of mouse cerebral arteries.

### G<sub>q/11</sub> Protein Dependent Signaling Pathway Is Responsible for Myogenic Tone

To explore the role of G<sub>q/11</sub> and β-arrestin signaling pathways downstream of AT1R, we used the biased agonists TRV120055, SII, and TRV120027 to activate G<sub>q/11</sub> and β-arrestin signaling pathways, respectively.<sup>32-36</sup> We found that TRV120055 increased vascular tone in MA (Figure 5A and 5B), whereas SII and TRV120027 had no effect (Figure 5C through 5F). Similarly, TRV120055 and TRV120056 (another biased G<sub>q/11</sub> coupled AT1R agonist) enhanced dose-dependent perfusion pressure in isolated kidneys (Figure 6A and 6C), whereas SII had no effect (Figure 6B and 6C). The removal of external Ca<sup>2+</sup> abolished agonist-induced vasoconstrictions in perfused kidneys (Figure 6D), indicating AT1aRs mediate vasoconstriction via canonical G<sub>q/11</sub> but not noncanonical β-arrestin pathways. The biased G<sub>q/11</sub> coupled AT1R agonist TRV120055 and TRV120056 equally modified perfusion pressure (Figure 6E). Viability of the isolated perfused kidneys was assessed by 60 mmol/L KCl (Figure 6F). To confirm the results, we next examined the effects of FR900359, a selective G<sub>q/11</sub>-protein inhibitor.<sup>37-39</sup> FR900359 abolished both myogenic and Ang II-dependent constrictions in renal arterioles (Figure 7), MA (Figure 5G and 5H) and cerebral arteries (Figure S2F). These results indicate that myogenic vasoconstriction is mediated through the mechanosensitive AT1aR and the canonical G<sub>q/11</sub> signaling pathway.

## DISCUSSION

### AT1Rs Are Primary Mechanosensors in Intact Arteries

Multiple GPCRs have been proposed to act as mechanosensors to regulate myogenic tone in resistance

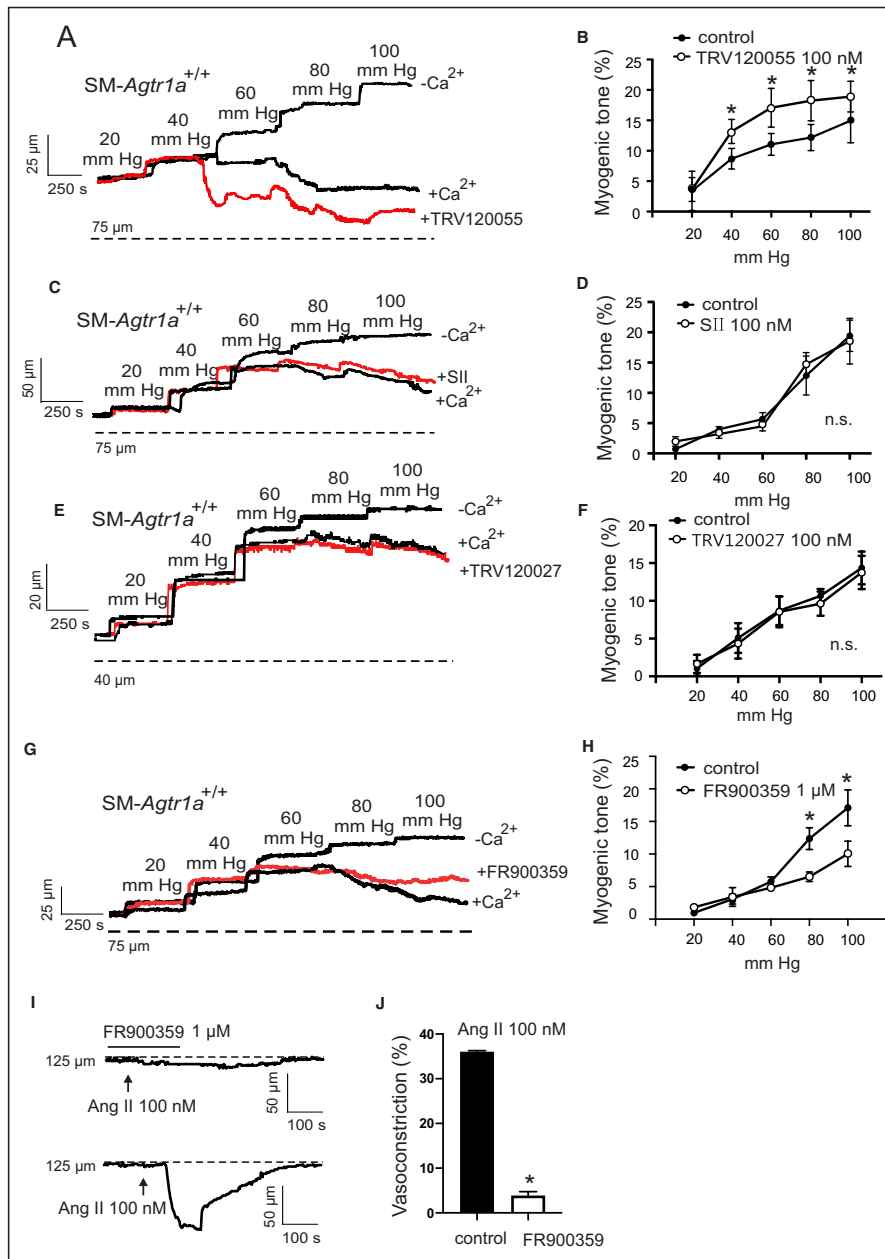
arteries. Although stretch induces activation of purinergic P2Y6 UDP receptors, thromboxane A2 receptors and sphingosine-1-phosphate receptors in certain vascular beds,<sup>40-42</sup> the AT1R remains one of the best characterized mechanosensors in the vasculature.<sup>19,43</sup> Humans express a single type of AT1R, whereas 2 isoforms (AT1aR and AT1bR) are present in rodents.<sup>44,45</sup> Using *Agtr1a*<sup>-/-</sup> mice and inverse AT1R agonist, our previous data suggested that ligand-independent AT1aR activation is required for myogenic response in resistance MA and renal arterioles.<sup>15</sup> Two recent studies reported also a possible role of AT1bRs in myogenic constriction in certain vessels.<sup>46,47</sup> We found that Ang II and myogenic constrictions were normal in *Agtr1b*<sup>-/-</sup> perfused kidneys, which is consistent with AT1A receptor being the major murine AT1 receptor isoform in the renal circulation.<sup>48</sup> All data were, however, obtained in global mutant mice, which often display compensatory mechanisms for the lack of AT1Rs and can lead to phenotypes that are difficult or impossible to interpret in terms of cardiovascular function. For example, AT1aR and AT1bR are expressed at similar levels in cerebral parenchymal arterioles and genetic knockout of AT1aR (but not AT1bR) blunted the ability of these vessels to generate myogenic tone.<sup>49</sup> The latter effect is opposite to cerebral arteries where genetic knockout of AT1bR blunted the ability to develop myogenic tone.<sup>46</sup> To overcome these potential limitations, we generated tamoxifen-inducible SM-*Agtr1a* (SMMHC-Cre+*Agtr1a*<sup>fllox/fllox</sup>) mice for careful phenotypic investigation. We found that myogenic constriction was impaired in cerebral, mesenteric, and renal arteries isolated from SM AT1aR-deficient mice. Our data provide firm evidence that AT1Rs play a key role as mechanosensors mediating myogenic constriction in the murine vasculature.

### AT1Rs Downstream Signaling to Cause Vasoconstriction

We next explored downstream signaling pathways mediated by G<sub>q/11</sub> and/or β-arrestin of AT1R in the vascular response. In cell culture, osmotic cell stretch has been found to increase the binding affinity and potency of the β-arrestin-biased agonist TRV120023 with no effect on the balanced agonist Ang II through AT1R to induce a conformation change of β-arrestin 2, similar to that induced by β-arrestin-biased agonists.<sup>20</sup>

#### Figure 5. Enhancement of the vascular tone by TRV120055.

**A, C, E, and G.** Representative recordings of mesenteric artery diameter during a series of pressure steps from 20 to 100 mm Hg in 20 mm Hg increments in control conditions (+Ca<sup>2+</sup>), TRV120055 100 nmol/L (**A**), SII 100 nmol/L (**C**), TRV120027 100 nmol/L (**E**), FR900359 1 μmol/L (**G**) and in Ca<sup>2+</sup>-free solution. **B, D, F, and H.** Average myogenic constriction of mesenteric arteries in drug-free physiological saline solution and in PSS containing 100 nmol/L TRV120055 (**B**), 100 nmol/L SII (**D**), TRV120027 100 nmol/L (**F**) and 1 μmol/L FR900359 (**H**) (n=6, 4, 5 and 4, respectively, each from individual mice). **I and J.** Response to Ang II in MA in drug-free PSS and PSS in presence of FR900359 at 80 mm Hg (n=6 each from individual mice). \*P<0.05. Ang II indicates angiotensin II; n.s. indicates not significant; and SII, Sar11le4lle8-angiotensin.



Similarly, hypo-osmotic stretch induced  $\beta$ -arrestin-biased signaling of AT1Rs in the absence of G protein activation.<sup>18</sup> We failed to observe  $\beta$ -arrestin-mediated

enhancement of myogenic constriction with the  $\beta$ -arrestin biased agonists SII and TRV120027 in intact arteries (mesenteric and renal arteries: Figure 8). The

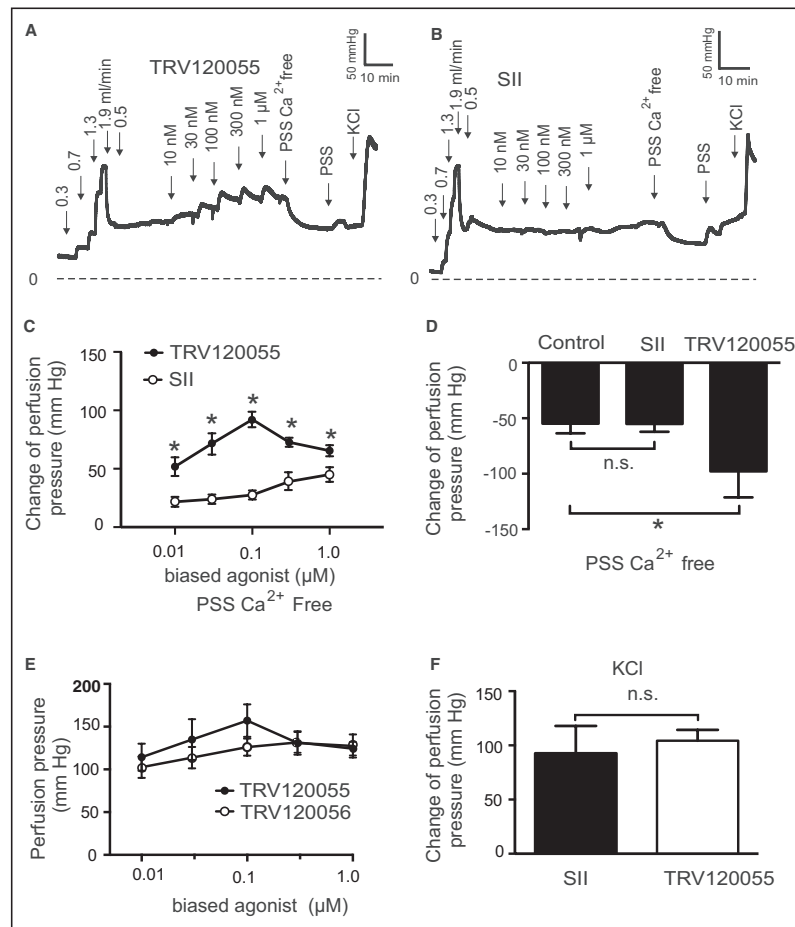


**Figure 6.** Function of biased AT1R agonists to vasoregulation in isolated perfused kidneys from SM-Agr1a<sup>+/+</sup> mice.

**A and B.** Original recordings of perfusion pressure in response to various flow rates (in mL/min), TRV120055 (A) or Sar1le4Ile8-SII (B), Ca<sup>2+</sup> free perfusion solution (PSS Ca<sup>2+</sup> free) and reexposure of the kidneys to PSS. **C.** Increase in perfusion pressure induced by TRV120055 and SII in various concentrations (10 nmol/L to 1 μmol/L). **D.** Change of perfusion pressure assessed by exposure of the kidneys to Ca<sup>2+</sup> free PSS at the presence of TRV120055 or Sar-Ile II at the concentration of 100 nmol/L. **E.** Dose-response relationships for TRV120055 and TRV120056. **F.** Increase in perfusion pressure induced by 60 mmol/L KCl. TRV120055, TRV120056, SII. n=6 kidneys from 5 mice in each group; n=6 kidneys from 5 mice in the control group. \*P<0.05. AT1R, angiotensin II type 1 receptor; Control, SM-Agr1a<sup>+/+</sup> without biased ligand; n.s., not significant; PSS, physiological saline solution; and SM, smooth muscle.

discrepancy might be caused by differences between hypo-osmotic cell swelling and tensile stretch on the SM cell layer in intact arteries to cause mechanoactivation of AT1Rs in situ. AT1R is one of the best characterized GPCR enabling biased receptor signaling. It can be activated in either a canonical G protein-dependent signaling mode<sup>14,50</sup> or noncanonical β-arrestin-mediated

signaling mode.<sup>18,20</sup> In line, we found that the natural biased agonist Ang II was able to increase G protein signaling of mechanoactivated AT1R receptors to enhance the vasoconstrictor response. A recent study reported that GPCRs, including AT1R, can promote a direct interaction between Gai protein subtype family members and β-arrestins, regardless of their canonical

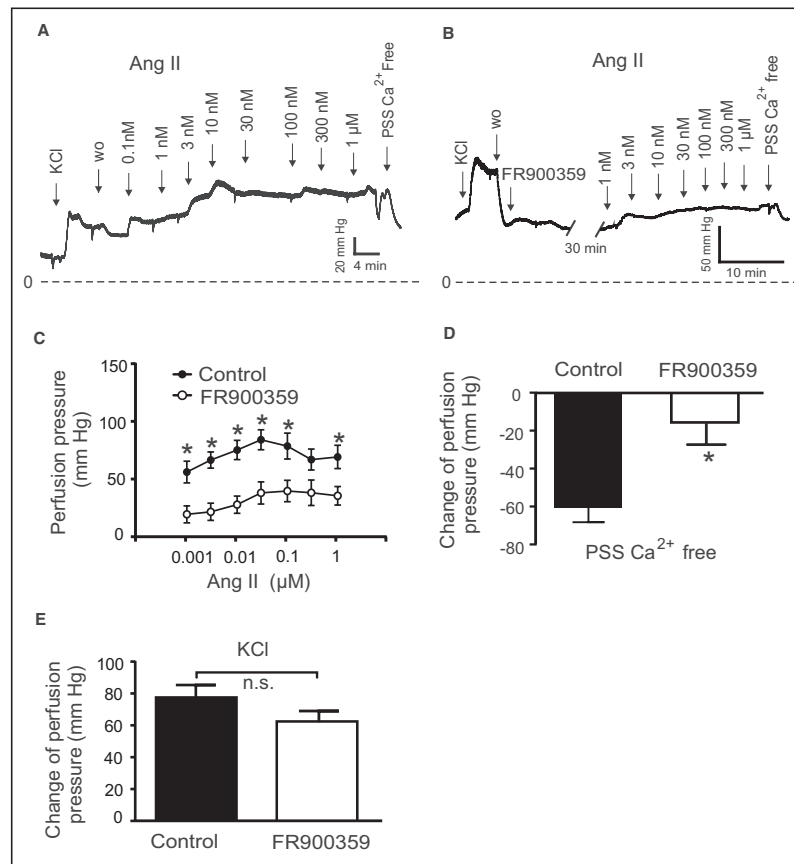


**Figure 7. Vasoregulation in isolated perfused kidneys of SM-*Agtr1a*<sup>+/+</sup> mice pretreated with 300 nmol/L G<sub>q/11</sub> blocker FR900359.**

**A.** Original recordings of perfusion pressure in kidneys of *Agtr1a*<sup>+/+</sup> mice in response to various concentrations of Ang II (**B**) same as (**A**) but pretreated with 300 nmol/L FR900359 for 30 minutes. **C.** Increases in perfusion pressure induced by Ang II (1 nmol/L to 1 μmol/L). **D.** Myogenic tone assessed by exposure of the kidneys to Ca<sup>2+</sup>-free PSS. **E.** Increase in perfusion pressure induced by 60 mmol/L KCl. n=15 SM-*Agtr1a*<sup>+/+</sup> kidneys from 12 mice and n=6 SM-*Agtr1a*<sup>+/+</sup> kidneys from 4 mice pretreated with FR900359 for all panels. \*P<0.05. Ang II indicates angiotensin II; n.s., not significant; PSS, physiological saline solution; SM, smooth muscle; and w.o., wash-out.

G protein subtype coupling, that might be prerequisite for certain β-arrestin signaling pathways.<sup>51</sup>

We hypothesized that G<sub>q/11</sub> signaling contributes to myogenic tone in MA and renal arteries and consistent with this idea, we found that the vasoconstrictor responses were strongly increased by the G<sub>q/11</sub> AT1R biased agonists TRV120055 and TRV20056 (Figure 8). Moreover, we found that the G<sub>q/11</sub> blocker FR900359 inhibited both myogenic tone and Ang II-induced constrictions in MA and renal arterioles (Figure 8). The data imply that myogenic vasoconstriction requires

canonical G<sub>q/11</sub> signaling of the AT1R. Consistently, myogenic tone is increased in the absence of regulator of G-protein signaling 2, which is an endogenous terminator of Gα<sub>q/11</sub> (Gα<sub>q/11</sub>) signaling.<sup>14,30</sup> The data align with findings indicating that mechanically activated AT1Rs generate diacylglycerol, which in turn activates protein kinase C to induce the actin cytoskeleton reorganization necessary for pressure-induced vasoconstriction.<sup>52</sup> Finally, our conclusions are supported by findings indicating that another G<sub>q/11</sub>-protein inhibitor YM 254890 profoundly reduced myogenic tone in MA<sup>43</sup> (but see



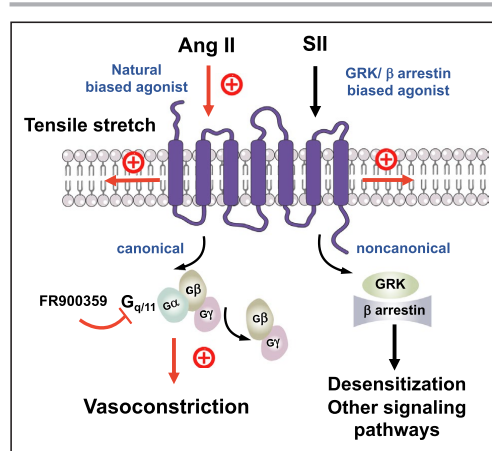


**Figure 8.** Schematic illustration of angiotensin II type 1a receptor (AT1R) biased signaling cascade regulating myogenic arterial tone.

Canonical  $G_{q/11}$  signaling pathway of the AT1R (purple blue) causes myogenic vasoconstriction whereas noncanonical  $\beta$ -arrestin-biased signaling is not involved in this process.  $G_{q/11}$  proteins are heterotrimeric G proteins, which are made up of alpha ( $\alpha$ ), beta ( $\beta$ ), and gamma ( $\gamma$ ) subunits. The alpha subunit is attached to either a guanosine triphosphate (GTP) or guanosine diphosphate (GDP), which serves as an on-off switch for the activation of the G-protein. Upon activation of the AT1R by either ligand-independent mechanical stretch or the natural-biased ligand Ang II, the  $G\beta\gamma$  complex is released from the  $G\alpha$  subunit after its GDP-GTP exchange for canonical G protein signaling to cause myogenic and/or humoral (Ang II-mediated) vasoconstriction. This pathway is inhibited by the  $G_{q/11}$  inhibitor FR900359. Although, GRKs and arrestins play a role in multiple noncanonical signaling pathways in cells, this pathway is unlikely engaged by mechanoactivated AT1Rs in response to tensile stretch or their natural ligand angiotensin II to cause vasoconstriction. Ang II indicates angiotensin II; GRK, G protein-coupled receptor kinase; and SII, Sar11le41le8-angiotensin.

Ref. 50). Our study provides firm evidence that AT1Rs coupled to  $G_{q/11}$  signaling is an essential component of dynamic mechanochemical signaling in arterial vascular SM cells causing myogenic tone (Figure 8).

Signaling of most GPCRs via G proteins is terminated (desensitization) by the phosphorylation of active receptor by specific kinases (GPCR kinases) and subsequent binding of  $\beta$ -arrestins that selectively recognize active phosphorylated receptors. Although, GPCR kinases and  $\beta$ -arrestins also play a role in multiple non-canonical signaling pathways in the cell, both GPCR initiated and receptor independent,<sup>53,54</sup> our study demonstrates that this pathway is not involved in the myogenic response (Figure 8). Thus, blood pressure-lowering effects of  $\beta$ -arrestin biased AT1R agonists, for example, Trevena 120027,<sup>55</sup> are unlikely caused by direct effects of this GPCR in arterial SM cells.

## CONCLUSIONS

In summary, we provide new and firm evidence for a mechanosensitive function of AT1R in myogenic constriction in mesenteric, renal, and cerebral arteries, that is, in 3 different highly myogenic vascular beds. Our study clearly shows that mechanical stress activates AT1R in arterial SM cells, which subsequently triggers canonical  $G_{q/11}$  signaling, irrespective of GPCR kinases/ $\beta$ -arrestin signaling, to cause myogenic vasoconstriction. Our results argue against the idea of multiple mechanosensors coupled to noncanonical  $\beta$ -arrestin pathways generating myogenic arterial tone. These findings lay ground for future studies to characterize the molecular mechanisms of mechanoactivated AT1R coupled to  $G_{q/11}$  signaling in intact arteries, which may reveal new molecular targets for drug development to alleviate increased or dysregulated arterial tone in hypertension and other cardiovascular diseases.

## ARTICLE INFORMATION

Received April 14, 2021; accepted November 11, 2021.

### Affiliations

Experimental and Clinical Research Center (ECRC), a joint cooperation between the Charité Medical Faculty and the Max Delbrück Center for Molecular Medicine (MDC), Charité - Universitätsmedizin Berlin, Berlin, Germany (Y.C., M.K., S.N., Y.M.A., J.S., M.G.); Department of Internal Medicine and Geriatrics, University Medicine, Greifswald, Germany (M.K., Y.M.A., M.G.); Heart and Vascular Institute and School of Biomedical Sciences, Chinese University of Hong Kong, China (C.Z., Y.H.); Max Delbrück Center for Molecular Medicine, Berlin, Germany (N.A., M.B.); DZHK (German Center for Cardiovascular Research), Partner Site Berlin, Berlin, Germany (N.A., M.B.); Charité - Universitätsmedizin Berlin, Berlin, Germany (M.B.); Institute for Biology, University of Lübeck, Germany (M.B.); Department of Physiology and Pharmacology, Robarts, Research Institute, Western University, London, Ontario, Canada (D.G.W.); Department of Biomedical Sciences (Y.H.) and Medical Clinic for Nephrology and Internal Intensive Care, Campus Virchow, Charité - Universitätsmedizin Berlin, Berlin, Germany (M.G.).

### Acknowledgments

We thank Thomas Coffman for providing *Agtr1a*<sup>-/-</sup>, *Agtr1b*<sup>-/-</sup> and *Agtr1a*<sup>lox</sup> mice. We thank Gabriele M. König and Evi Kostenis for FR900359.

Author contributions: Conceptualization: Gollasch, Huang; Pressure microscopy: Cui; Perfused kidneys: Cui, Nickel, Immunohistochemistry: Zhang; Formal analysis: Cui, Nickel, Zhang, Kassmann, Gollasch; Funding acquisition: Gollasch; Investigation: Cui, Nickel, Zhang; Methodology: Cui, Zhang, Alenina; Visualization: Cui, Zhang; Writing—original draft: Cui, Gollasch; Writing—review and editing: Cui, Kassmann, Schleifenbaum, Bader, Welsh, Huang.

### Sources of Funding

The Deutsche Forschungsgemeinschaft (DFG, GO766/12-3, GO766/15-2, GO766/18-2, SFB1365) (Gollasch, Schleifenbaum, Alenina, and Bader), Germany/Hong Kong Joint Research Scheme (G-CUHK408/18 and Deutscher Akademischer Austauschdienst [DAAD]) (Gollasch, Huang), and Hong Kong Research Grants Council (SRFS2021-4S0) (Huang) supported our study.

### Disclosures

None.

### Supplemental Material

Figures S1–S2

## REFERENCES

- Bayliss WM. On the local reactions of the arterial wall to changes of internal pressure. *J Physiol.* 1902;28:220–231. doi: 10.1113/jphysiol.1902.sp000911
- Davis MJ. Perspective: physiological role(s) of the vascular myogenic response. *Microcirculation.* 2012;19:99–114. doi: 10.1111/j.1549-8719.2011.00131.x
- Cipolla MJ, Curry AB. Middle cerebral artery function after stroke: the threshold duration of reperfusion for myogenic activity. *Stroke.* 2002;33:2094–2099. doi: 10.1161/01.STR.0000020712.84444.8D
- Gschwend S, Henning RH, Pinto YM, de Zeeuw D, van Gilst WH, Buikema H. Myogenic constriction is increased in mesenteric resistance arteries from rats with chronic heart failure: instantaneous counteraction by acute AT1 receptor blockade. *Br J Pharmacol.* 2003;139:1317–1325.
- Ledoux J, Gee DM, Leblanc N. Increased peripheral resistance in heart failure: new evidence suggests an alteration in vascular smooth muscle function. *Br J Pharmacol.* 2003;139:1245–1248. doi: 10.1038/sj.bjp.0705366
- Pires PW, Jackson WF, Dorrance AM. Regulation of myogenic tone and structure of parenchymal arterioles by hypertension and the mineralocorticoid receptor. *Am J Physiol Heart Circ Physiol.* 2015;309:H127–H136. doi: 10.1152/ajpheart.00168.2015
- Sauvé M, Hui SK, Dinh DD, Foltz WD, Momen A, Nedospasov SA, Offermanns S, Husain M, Kroetsch JT, Lidington D, et al. Tumor necrosis factor/sphingosine-1-phosphate signaling augments resistance artery myogenic tone in diabetes. *Diabetes.* 2016;65:1916–1928. doi: 10.2337/db15-1450
- Nelson MT, Patlak JB, Worley JF, Standen NB. Calcium channels, potassium channels, and voltage dependence of arterial smooth muscle tone. *Am J Physiol.* 1990;259:C3–C18. doi: 10.1152/ajpcell.1990.259.1.C3
- Coats P, Johnston F, MacDonald J, McMurray JJ, Hillier C. Signalling mechanisms underlying the myogenic response in human subcutaneous resistance arteries. *Cardiovasc Res.* 2001;49:828–837. doi: 10.1016/S0008-6363(00)00314-X
- Davis MJ, Hill MA. Signaling mechanisms underlying the vascular myogenic response. *Physiol Rev.* 1999;79:387–423. doi: 10.1152/physrev.1999.79.2.387
- Hansen PB, Jensen BL, Andreassen D, Skøtt O. Differential expression of T- and L-type voltage-dependent calcium channels in renal resistance vessels. *Circ Res.* 2001;89:630–638. doi: 10.1161/hh1901.097126
- Harder DR. Pressure-dependent membrane depolarization in cat middle cerebral artery. *Circ Res.* 1984;55:197–202. doi: 10.1161/01.RES.55.2.197
- Moosmang S, Schulla V, Welling A, Feil R, Feil S, Wegener JW, Hofmann F, Klugbauer N. Dominant role of smooth muscle L-type calcium channel Cav1.2 for blood pressure regulation. *EMBO J.* 2003;22:6027–6034. doi: 10.1093/emboj/cdg583
- Mederos y Schnitzler MM, Storch U, Meibers S, Nurwakagari P, Breit A, Essin K, Gollasch M, Gudermann T. Gq-coupled receptors as mechanosensors mediating myogenic vasoconstriction. *EMBO J.* 2008;27:3092–3103. doi: 10.1038/emboj.2008.233
- Schleifenbaum J, Kassmann M, Szijarto IA, Hercule HC, Tano JY, Weinert S, Heidenreich M, Pathan AR, Anistan YM, Alenina N, et al. Stretch-activation of angiotensin II type 1a receptors contributes to the myogenic response of mouse mesenteric and renal arteries. *Circ Res.* 2014;115:263–272. doi: 10.1161/CIRCRESAHA.115.302882
- Xiao HD, Fuchs S, Frenzel K, Cole JM, Bernstein KE. Newer approaches to genetic modeling in mice: tissue-specific protein expression as studied using angiotensin-converting enzyme (ACE). *Am J Pathol.* 2003;163:807–817. doi: 10.1016/S0002-9440(10)63441-4
- Balakumar P, Jagadeesh G. A century old renin-angiotensin system still grows with endless possibilities: AT1 receptor signaling cascades in cardiovascular pathophysiology. *Cell Signal.* 2014;26:2147–2160. doi: 10.1016/j.cellsig.2014.06.011
- Rakesh K, Yoo B, Kim IM, Salazar N, Kim KS, Rockman HA. Beta-arrestin-biased agonism of the angiotensin receptor induced by mechanical stress. *Sci Signal.* 2010;3:ra46.
- Zou Y, Akazawa H, Qin Y, Sano M, Takano H, Minamoto T, Makita N, Iwanaga K, Zhu W, Kudoh S, et al. Mechanical stress activates angiotensin II type 1 receptor without the involvement of angiotensin II. *Nat Cell Biol.* 2004;6:499–506. doi: 10.1038/ncb1137
- Tang W, Strachan RT, Lefkowitz RJ, Rockman HA. Allosteric modulation of  $\beta$ -arrestin-biased angiotensin II type 1 receptor signaling by membrane stretch. *J Biol Chem.* 2014;289:28271–28283. doi: 10.1074/jbc.M114.585067
- Kaßmann M, Szijártó IA, García-Prieto CF, Fan G, Schleifenbaum J, Anistan Y-M, Tabeling C, Shi Y, le Noble F, Witzennath M, et al. Role of ryanodine type 2 receptors in elementary Ca signaling in arteries and vascular adaptive responses. *J Am Heart Assoc.* 2019;8:e010090. doi: 10.1161/JAHA.118.010090
- Sparks MA, Parsons KK, Stegbauer J, Gurley SB, Vivekanandan-Giri A, Fortner CN, Snouwaert J, Raasch EW, Griffiths RC, Haystead TAJ, et al. Angiotensin II type 1A receptors in vascular smooth muscle cells do not influence aortic remodeling in hypertension. *Hypertension.* 2011;57:577–585. doi: 10.1161/HYPERTENSIONAHA.110.165274
- Groneberg D, König P, Wirth A, Offermanns S, Koesling D, Friebe A. Smooth muscle-specific deletion of nitric oxide-sensitive guanylyl cyclase is sufficient to induce hypertension in mice. *Circulation.* 2010;121:401–409. doi: 10.1161/CIRCULATIONAHA.109.890962
- Ito M, Oliverio MI, Mannon PJ, Best CF, Maeda N, Smithies O, Coffman TM. Regulation of blood pressure by the type 1A angiotensin II receptor gene. *Proc Natl Acad Sci USA.* 1995;92:3521–3525. doi: 10.1073/pnas.92.8.3521
- Jarve A, Todiras M, Lian X, Filippelli-Silva R, Qadri F, Martin RP, Gollasch M, Bader M. Distinct roles of angiotensin receptors in autonomic dysreflexia following high-level spinal cord injury in mice. *Exp Neurol.* 2019;311:173–181. doi: 10.1016/j.expneurol.2018.10.003
- Oliverio MI, Kim H-S, Ito M, Le T, Audoly L, Best CF, Hiller S, Kluckman K, Maeda N, Smithies O, et al. Reduced growth, abnormal kidney structure, and type 2 (AT2) angiotensin receptor-mediated blood pressure regulation in mice lacking both AT1A and AT1B receptors for angiotensin II. *Proc Natl Acad Sci USA.* 1998;95:15496–15501. doi: 10.1073/pnas.95.26.15496
- Heinze C, Seniuk A, Sokolov MV, Huebner AK, Klementowicz AE, Szijártó IA, Schleifenbaum J, Vitzthum H, Gollasch M, Ehmke H, et al. Disruption of vascular  $Ca^{2+}$ -activated chloride currents lowers blood pressure. *J Clin Invest.* 2014;124:675–686. doi: 10.1172/JCI70025
- Ercu M, Markó L, Schächterle C, Tsvetkov D, Cui Y, Maghsodi S, Bartolomaeus TUP, Maass PG, Zühlke K, Gregersen N, et al. Phosphodiesterase 3A and arterial hypertension. *Circulation.* 2020;142:133–149. doi: 10.1161/CIRCULATIONAHA.119.043061
- Fan G, Kassmann M, Cui Y, Mattheaus C, Kunz S, Zhong C, Zhu S, Xie Y, Tsvetkov D, Daumke O, et al. Age attenuates the T-type Cav 3.2-RyR axis in vascular smooth muscle. *Aging Cell.* 2020;19:e13134. doi: 10.1111/acel.13134
- Hercule HC, Tank J, Plehm R, Wellner M, da Costa Goncalves AC, Gollasch M, Diedrich A, Jordan J, Luft FC, Gross V. Regulator of G protein signalling 2 ameliorates angiotensin II-induced hypertension in mice. *Exp Physiol.* 2007;92:1014–1022. doi: 10.1111/expphysiol.2007.038240
- Janssen BJA, Smits JFM. Autonomic control of blood pressure in mice: basic physiology and effects of genetic modification. *Am J Physiol Regul Integr Comp Physiol.* 2002;282:R1545–R1564. doi: 10.1152/ajpregu.00714.2001
- Kendall RT, Strungs EG, Rachidi SM, Lee M-H, El-Shewy HM, Luttrell DK, Janach MG, Luttrell LM. The beta-arrestin pathway-selective type 1A angiotensin receptor (AT1A) agonist [Sar1, Ile4, Ile8] angiotensin II regulates a robust G protein-independent signaling network. *J Biol Chem.* 2011;286:19880–19891. doi: 10.1074/jbc.M111.233080
- Li W, Xu J, Kou X, Zhao R, Zhou W, Fang X. Single-molecule force spectroscopy study of interactions between angiotensin II type 1 receptor and different biased ligands in living cells. *Anal Bioanal Chem.* 2018;410:3275–3284. doi: 10.1007/s00216-018-0956-3
- Wei H, Ahn S, Shenoy SK, Karnik SS, Hunyady L, Luttrell LM, Lefkowitz RJ. Independent beta-arrestin 2 and G protein-mediated pathways for angiotensin II activation of extracellular signal-regulated kinases 1 and 2. *Proc Natl Acad Sci USA.* 2003;100:10782–10787.
- Liu C-H, Gong Z, Liang Z-L, Liu Z-X, Yang F, Sun Y-J, Ma M-L, Wang Y-J, Ji C-R, Wang Y-H, et al. Arrestin-biased AT1R agonism induces acute catecholamine secretion through TRPC3 coupling. *Nat Commun.* 2017;8:14335. doi: 10.1038/ncomms14335
- Santos GA, Duarte DA, Parreiras-E-Silva LT, Teixeira FR, Silva-Rocha R, Oliveira EB, Bouvier M, Costa-Neto CM. Comparative analyses of downstream signal transduction targets modulated after activation of the AT1 receptor by two  $\beta$ -arrestin-biased agonists. *Front Pharmacol.* 2015;6:131. doi: 10.3389/fphar.2015.00131

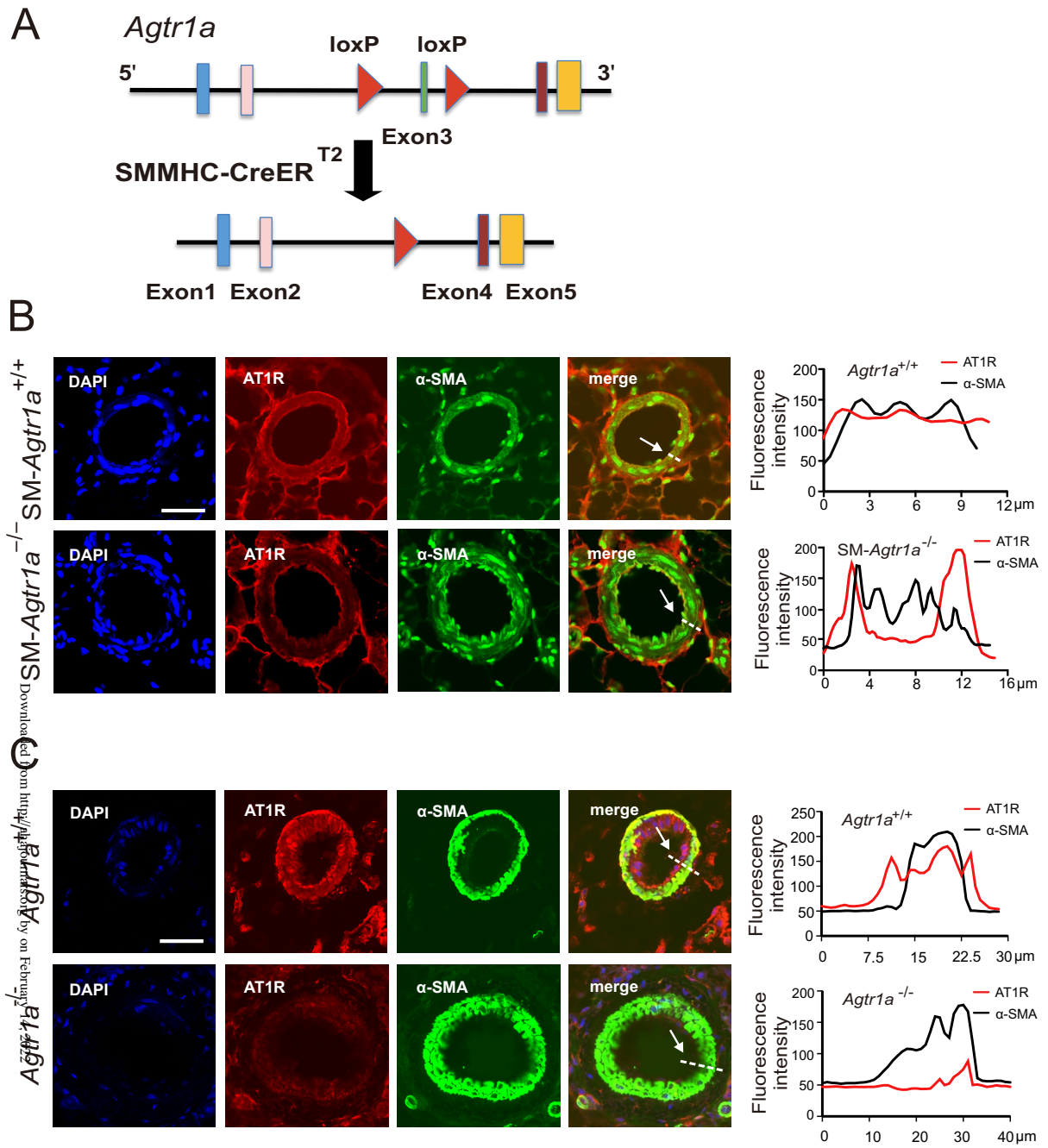
37. Inamdar V, Patel A, Manne BK, Dangelmaier C, Kunapuli SP. Characterization of UBO-QIC as a Galphaq inhibitor in platelets. *Platelets*. 2015;26:771–778. doi: 10.3109/09537104.2014.998993
38. Schrage R, Schmitz A-L, Gaffal E, Annala S, Kehraus S, Wenzel D, Büllsbach KM, Bald T, Inoue A, Shinjo Y, et al. The experimental power of FR900359 to study Gq-regulated biological processes. *Nat Commun*. 2015;6:10156. doi: 10.1038/ncomms10156
39. Lian X, Beer-Hammer S, König GM, Kostenis E, Nurnberg B, Gollasch M. RXFP1 receptor activation by relaxin-2 induces vascular relaxation in mice via a Galphai2-protein/PI3K $\beta$ /gamma/nitric oxide-coupled pathway. *Front Physiol*. 2018;9:1234. doi: 10.3389/fphys.2018.01234
40. Kauffenstein G, Laher I, Matrougui K, Guérineau NC, Henrion D. Emerging role of G protein-coupled receptors in microvascular myogenic tone. *Cardiovasc Res*. 2012;95:223–232. doi: 10.1093/cvr/cvs152
41. Kauffenstein G, Tamarelle S, Prunier F, Roy C, Ayer A, Toutain B, Billaud M, Isakson BE, Grimaud L, Loufrani L, et al. Central role of P2y6 UDP receptor in arteriolar myogenic tone. *Arterioscler Thromb Vasc Biol*. 2016;36:1598–1606. doi: 10.1161/ATVBAHA.116.307739
42. Kroetsch JT, Bolz S-S. The TNF- $\alpha$ /sphingosine-1-phosphate signaling axis drives myogenic responsiveness in heart failure. *J Vasc Res*. 2013;50:177–185. doi: 10.1159/000350528
43. Storch U, Blodow S, Gudermann T, Mederos Y, Schnitzler M. Cysteinyl leukotriene 1 receptors as novel mechanosensors mediating myogenic tone together with angiotensin II type 1 receptors—brief report. *Arterioscler Thromb Vasc Biol*. 2015;35:121–126. doi: 10.1161/ATVBAHA.114.304844
44. Madhun ZT, Ernsberger P, Ke FC, Zhou J, Hoptler U, Douglas JG. Signal transduction mediated by angiotensin II receptor subtypes expressed in rat renal mesangial cells. *Regul Pept*. 1993;44:149–157. doi: 10.1016/0167-0115(93)90238-4
45. Zhou J, Ernsberger P, Douglas JG. A novel angiotensin receptor subtype in rat mesangium. Coupling to adenylyl cyclase. *Hypertension*. 1993;21:1035–1038.
46. Pires PW, Ko EA, Pritchard HAT, Rudokas M, Yamasaki E, Earley S. The angiotensin II receptor type 1b is the primary sensor of intraluminal pressure in cerebral artery smooth muscle cells. *J Physiol*. 2017;595:4735–4753. doi: 10.1113/JP274310
47. Blodow S, Schneider H, Storch U, Wizemann R, Forst AL, Gudermann T, Mederos Y, Schnitzler M. Novel role of mechanosensitive AT1B receptors in myogenic vasoconstriction. *Pflügers Arch*. 2014;466:1343–1353. doi: 10.1007/s00424-013-1372-3
48. Le TH, Fogo AB, Salzler HR, Vinogradova T, Oliverio MI, Marchuk DA, Coffman TM. Modifier locus on mouse chromosome 3 for renal vascular pathology in AT1A receptor-deficiency. *Hypertension*. 2004;43:445–451. doi: 10.1161/01.HYP.0000112423.28987.00
49. Yamasaki E, Thakore P, Krishnan V, Earley S. Differential expression of angiotensin II type 1 receptor subtypes within the cerebral microvasculature. *Am J Physiol Heart Circ Physiol*. 2020;318:H461–H469. doi: 10.1152/ajpheart.00582.2019
50. Chennupati R, Wirth A, Favre J, Li R, Bonnavaion R, Jin Y-J, Wietelmann A, Schweda F, Wettschureck N, Henrion D, et al. Myogenic vasoconstriction requires G/G and LARG to maintain local and systemic vascular resistance. *Elife*. 2019;8:e49374. doi: 10.7554/eLife.49374
51. Smith JS, Pack TF, Inoue A, Lee C, Zheng K, Choi I, Eiger DS, Warman A, Xiong X, Ma Z, et al. Noncanonical scaffolding of G and  $\beta$ -arrestin by G protein-coupled receptors. *Science*. 2021;371:eaay1833.
52. Hong K, Zhao G, Hong Z, Sun Z, Yang Y, Clifford PS, Davis MJ, Meininger GA, Hill MA. Mechanical activation of angiotensin II type 1 receptors causes actin remodelling and myogenic responsiveness in skeletal muscle arterioles. *J Physiol*. 2016;594:7027–7047. doi: 10.1113/JP272834
53. Lefkowitz RJ. A brief history of G-protein coupled receptors (Nobel Lecture). *Angew Chem Int Ed Engl*. 2013;52:6366–6378. doi: 10.1002/anie.201301924
54. Gurevich VV, Gurevich EV. GPCR signaling regulation: the role of GRKs and arrestins. *Front Pharmacol*. 2019;10:125. doi: 10.3389/fphar.2019.00125
55. Boerrigter G, Lark MW, Whalen EJ, Soergel DG, Violin JD, Burnett JC Jr. Cardiorenal actions of TRV120027, a novel  $\beta$ -arrestin-biased ligand at the angiotensin II type I receptor, in healthy and heart failure canines: a novel therapeutic strategy for acute heart failure. *Circ Heart Fail*. 2011;4:770–778. doi: 10.1161/CIRCHEARTFAILURE.111.962571

# SUPPLEMENTAL MATERIAL

### Supplemental Figures

**Figure S1. Conditional deletion of AT1a receptors in vascular smooth muscle cells of arteries.** **A:** Schematic representation of the mouse allele containing loxP sequences, and the floxed allele after the action of Cre recombinase. **B:** Immunofluorescence staining results show that AT1R (red) is highly expressed in the mesenteric artery of SM-*Agtr1a*<sup>+/+</sup> mice. In SM-*Agtr1a*<sup>-/-</sup> mouse mesenteric artery, the expression of AT1R is specifically reduced in smooth muscle cells. **C:** Expression of AT1R is completely reduced in the mesenteric artery of global *Agtr1a*<sup>-/-</sup> mice. DAPI (4',6-diamino-2-phenylindole) nuclear staining, alpha-SMA (alpha smooth muscle actin), Scale bar: 40  $\mu$ m.

**Figure S2. Myogenic tone in cerebral arteries.** **A, B:** Representative recordings of middle/posterior cerebral arteries diameter at the pressure of 80 mmHg in control conditions (WT), Ang II 100 nmol/L, and in Ca<sup>2+</sup> free solution. **C:** Myogenic tone (at 80 mmHg) expressed as dilation of vessels induced by external Ca<sup>2+</sup> free solution. **D, E:** Response to Ang II (**D**) and 60 mM KCl (**E**) in middle/posterior cerebral arteries of SM-*Agtr1a*<sup>+/+</sup> and SM-*Agtr1a*<sup>-/-</sup> mice. SM-*Agtr1a*<sup>+/+</sup>, n=6 vessels from 6 mice, and SM-*Agtr1a*<sup>-/-</sup>, n=6 vessels from 6 mice. **F:** Average myogenic constriction of cerebral arteries in physiological salt solution (PSS) in the absence and presence of 1  $\mu$ mol/L FR900359 (n=6 each, from 6 mice each). **G:** Response to Ang II in the absence and presence of 1  $\mu$ mol/L FR900359 at 80 mmHg (n=6 each, from 6 mice each). \*p<0.05; n.s., not significant.



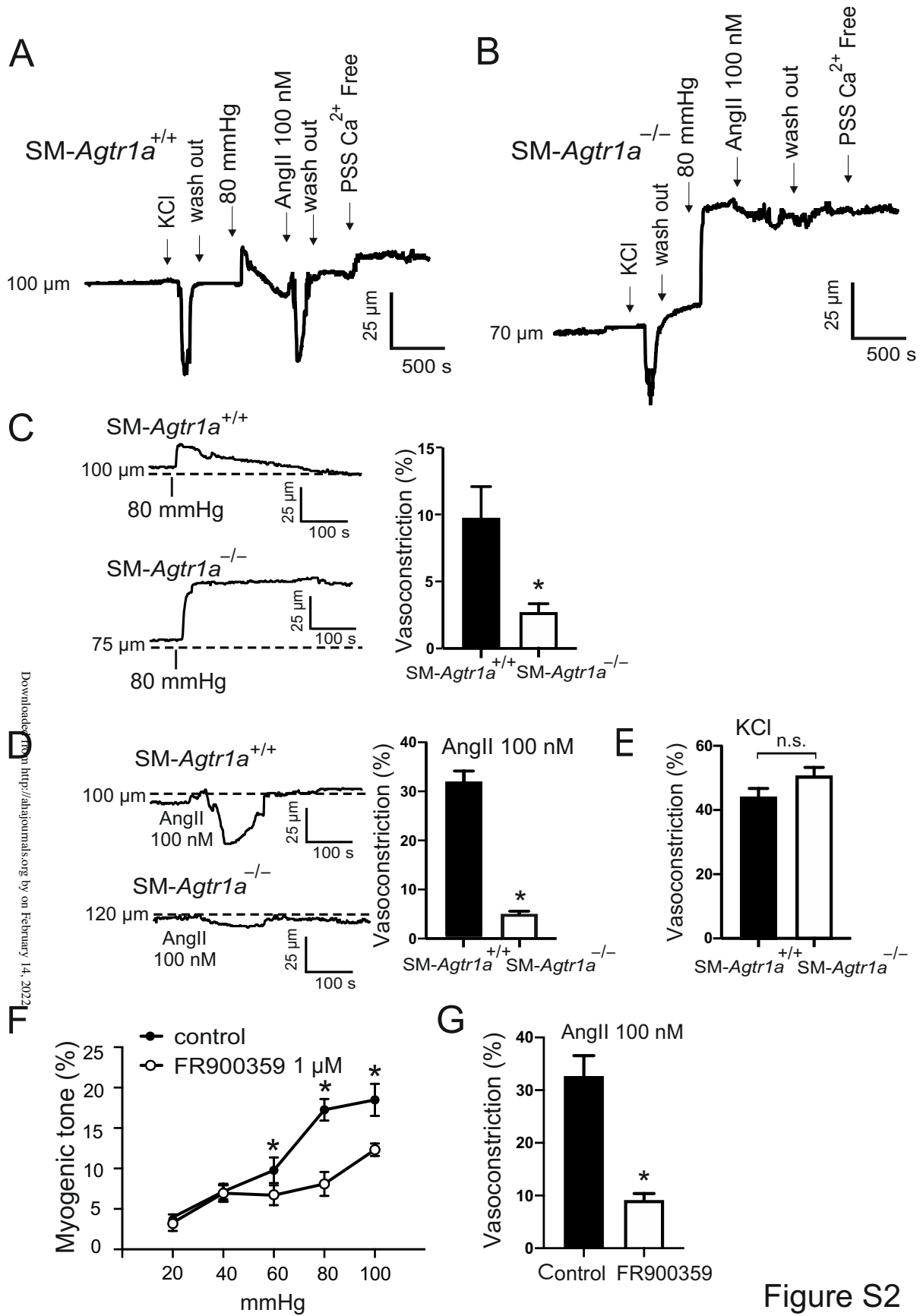


Figure S2

**Publication #2:****Age attenuates the T-type Ca 3.2-RyR axis in vascular smooth muscle**

Fan G, Kaßmann M, Cui Y, Matthaeus C, Kunz S, Zhong C, Zhu S, Xie Y, Tsvetkov D, Daumke O, Huang Y and Gollasch M. Age attenuates the T-type Ca 3.2-RyR axis in vascular smooth muscle. *Aging Cell*. 2020;19:e13134.

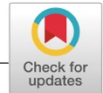
Received: 2019 May 23; Revised: 2020 Jan 28; Accepted: 2020 Feb 16.



Journal Data Filtered By: **Selected JCR Year: 2017** Selected Editions: SCIE,SSCI  
 Selected Categories: **“GERIATRICS and GERONTOLOGY”** Selected Category  
 Scheme: WoS

**Gesamtanzahl: 53 Journale**

Rank	Full Journal Title	Total Cites	Journal Impact Factor	Eigenfactor Score
1	Journal of Cachexia Sarcopenia and Muscle	2,207	12.511	0.005180
2	AGEING RESEARCH REVIEWS	5,297	8.973	0.012030
3	AGING CELL	8,067	7.627	0.018910
4	Journal of the American Medical Directors Association	6,905	5.325	0.018230
5	Aging-US	4,410	5.179	0.010910
6	Aging and Disease	1,386	5.058	0.003230
7	JOURNALS OF GERONTOLOGY SERIES A-BIOLOGICAL SCIENCES AND MEDICAL SCIENCES	17,809	4.902	0.023940
8	NEUROBIOLOGY OF AGING	21,914	4.454	0.044830
9	JOURNAL OF THE AMERICAN GERIATRICS SOCIETY	29,943	4.155	0.036360
10	Immunity & Ageing	749	4.019	0.001580
11	AGE AND AGEING	10,751	4.013	0.014720
12	MECHANISMS OF AGEING AND DEVELOPMENT	5,523	3.739	0.004380
13	BIOGERONTOLOGY	2,135	3.702	0.003510
14	Frontiers in Aging Neuroscience	4,995	3.582	0.016550
15	GERONTOLOGY	3,763	3.532	0.005820
16	AMERICAN JOURNAL OF GERIATRIC PSYCHIATRY	6,363	3.480	0.010470
17	Journal of Geriatric Oncology	895	3.359	0.003320
18	MATURITAS	6,290	3.315	0.011100
19	EXPERIMENTAL GERONTOLOGY	8,691	3.224	0.012520
20	REJUVENATION RESEARCH	1,669	3.220	0.002080
21	European Review of Aging and Physical Activity	309	3.091	0.000710



## Age attenuates the T-type $\text{Ca}_v3.2$ -RyR axis in vascular smooth muscle

Gang Fan<sup>1,2</sup> | Mario Kaßmann<sup>1</sup> | Yingqiu Cui<sup>1</sup> | Claudia Matthaeus<sup>3</sup> |  
 Séverine Kunz<sup>4</sup> | Cheng Zhong<sup>1</sup> | Shuai Zhu<sup>2</sup> | Yu Xie<sup>2</sup> | Dmitry Tsvetkov<sup>1</sup> |  
 Oliver Daumke<sup>3,5</sup> | Yu Huang<sup>6</sup> | Maik Gollasch<sup>1,7,8</sup>

<sup>1</sup>Experimental and Clinical Research Center (ECRC), a joint cooperation between the Charité Medical Faculty and the Max Delbrück Center for Molecular Medicine (MDC), Charité – Universitätsmedizin Berlin, Berlin, Germany

<sup>2</sup>Hunan Cancer Hospital, The Affiliated Cancer Hospital of Xiangya School of Medicine, Central South University, Changsha, China

<sup>3</sup>Crystallography, Max-Delbrück-Center for Molecular Medicine, Berlin, Germany

<sup>4</sup>Electron Microscopy Facility, Max Delbrück Center for Molecular Medicine (MDC), Berlin, Germany

<sup>5</sup>Institute of Chemistry and Biochemistry, Freie Universität Berlin, Berlin, Germany

<sup>6</sup>Institute of Vascular Medicine and School of Biomedical Sciences, Chinese University of Hong Kong, Hong Kong, China

<sup>7</sup>Medical Clinic for Nephrology and Internal Intensive Care, Charité – Universitätsmedizin Berlin, Berlin, Germany

<sup>8</sup>Department of Geriatrics, University Medicine Greifswald, Greifswald, Germany

### Correspondence

Maik Gollasch, Experimental and Clinical Research Center (ECRC), Charité Campus Virchow, Berlin 13125, Germany.  
 Email: maik.gollasch@charite.de

### Funding information

Deutsche Forschungsgemeinschaft; Deutscher Akademischer Austauschdienst; China Scholarship Council

### Abstract

Caveolae position  $\text{Ca}_v3.2$  (T-type  $\text{Ca}^{2+}$  channel encoded by the  $\alpha$ -3.2 subunit) sufficiently close to RyR (ryanodine receptors) for extracellular  $\text{Ca}^{2+}$  influx to trigger  $\text{Ca}^{2+}$  sparks and large-conductance  $\text{Ca}^{2+}$ -activated  $\text{K}^+$  channel feedback in vascular smooth muscle. We hypothesize that this mechanism of  $\text{Ca}^{2+}$  spark generation is affected by age. Using smooth muscle cells (VSMCs) from mouse mesenteric arteries, we found that both  $\text{Ca}_v3.2$  channel inhibition by  $\text{Ni}^{2+}$  (50  $\mu\text{M}$ ) and caveolae disruption by methyl- $\beta$ -cyclodextrin or genetic abolition of Eps15 homology domain-containing protein (EHD2) inhibited  $\text{Ca}^{2+}$  sparks in cells from young (4 months) but not old (12 months) mice. In accordance, expression of  $\text{Ca}_v3.2$  channel was higher in mesenteric arteries from young than old mice. Similar effects were observed for caveolae density. Using SMAKO  $\text{Ca}_v1.2^{-/-}$  mice, caffeine (RyR activator) and thapsigargin ( $\text{Ca}^{2+}$  transport ATPase inhibitor), we found that sufficient SR  $\text{Ca}^{2+}$  load is a prerequisite for the  $\text{Ca}_v3.2$ -RyR axis to generate  $\text{Ca}^{2+}$  sparks. We identified a fraction of  $\text{Ca}^{2+}$  sparks in aged VSMCs, which is sensitive to the TRP channel blocker  $\text{Gd}^{3+}$  (100  $\mu\text{M}$ ), but insensitive to  $\text{Ca}_v1.2$  and  $\text{Ca}_v3.2$  channel blockade. Our data demonstrate that the VSMC  $\text{Ca}_v3.2$ -RyR axis is down-regulated by aging. This defective  $\text{Ca}_v3.2$ -RyR coupling is counterbalanced by a  $\text{Gd}^{3+}$  sensitive  $\text{Ca}^{2+}$  pathway providing compensatory  $\text{Ca}^{2+}$  influx for triggering  $\text{Ca}^{2+}$  sparks in aged VSMCs.

### KEYWORDS

aging, calcium sparks, caveolae, ryanodine receptors, T-type calcium channels, vascular smooth muscle

Gang Fan and Mario Kaßmann contributed equally to this work.

This is an open access article under the terms of the Creative Commons Attribution License, which permits use, distribution and reproduction in any medium, provided the original work is properly cited.

© 2020 The Authors. *Aging Cell* published by the Anatomical Society and John Wiley & Sons Ltd

## 1 | INTRODUCTION

In resistance arteries, voltage-dependent  $\text{Ca}^{2+}$  channels activate ryanodine receptors (RyRs) to cause elementary  $\text{Ca}^{2+}$  release events ( $\text{Ca}^{2+}$  sparks) from the sarcoplasmic reticulum (SR) (Essin et al., 2007; Jaggar et al., 1998; Nelson et al., 1995; Wang et al., 2004).  $\text{Ca}^{2+}$  release from the SR in the form of  $\text{Ca}^{2+}$  sparks opens numerous large-conductance  $\text{Ca}^{2+}$ -sensitive  $\text{K}^+$  ( $\text{BK}_{\text{Ca}}$ ) channels, causing spontaneous transient outward  $\text{K}^+$  currents (STOCs) (Knot, Standen, & Nelson, 1998; Nelson et al., 1995). As a result,  $\text{Ca}^{2+}$  spark- $\text{BK}_{\text{Ca}}$  channel coupling induces vascular smooth muscle cell (VSMCs) hyperpolarization and attenuation of arterial constriction (Brenner et al., 2000; Löhn et al., 2001; Pérez, Bonev, Patlak, & Nelson, 1999). In previous studies, we demonstrated that L-type  $\text{Ca}_v1.2$  channels play the predominant role (~75%) in  $\text{Ca}^{2+}$  sparks generation in mesenteric arterial VSMCs, and T-type  $\text{Ca}_v3.2$  channels, localized in caveolae, represent an additional source (~25%) (Fan, Kaßmann, Hashad, Welsh, & Gollasch, 2018; Hashad et al., 2018). In the latter pathway, caveolae position  $\text{Ca}_v3.2$  channels sufficiently close to RyRs (<40 nm) of the sarcoplasmic reticulum (SR) for extracellular  $\text{Ca}^{2+}$  influx to trigger  $\text{Ca}^{2+}$  sparks and large-conductance  $\text{Ca}^{2+}$ -activated  $\text{K}^+$  channel feedback in vascular smooth muscle (Fan et al., 2018; Harraz et al., 2014; Hashad et al., 2018; Löhn et al., 2000). These conclusions were mainly derived from experiments using  $\text{Ca}_v3.2$  channel (*Cacna1h*<sup>-/-</sup>) and caveolin-1 (*Cav1*<sup>-/-</sup>) knockout mice. Although genetic caveolin-1 deletion leads to a complete lack of caveolae from the VSMC plasma membrane, data interpretation is limited because *Cav1* deletion may affect SR  $\text{Ca}^{2+}$  load and is known to increase the density of  $\text{BK}_{\text{Ca}}$  channels in VSMCs (Cheng & Jaggar, 2006). Caveolins affect also trafficking of other  $\text{K}^+$  channels ( $\text{K}_{\text{v}}1.5$ ) to cholesterol-rich membrane microdomains (McEwen, Li, Jackson, Jenkins, & Martens, 2008).

Little is known about the effects of aging on the T-type  $\text{Ca}_v3.2$ -RyR axis to generate  $\text{Ca}^{2+}$  sparks. While L-type  $\text{Ca}^{2+}$  current densities are preserved in VSMCs, aging has been reported to cause decrements in  $\text{Ca}^{2+}$  signaling in response to either ryanodine receptor stimulation by caffeine or inositol trisphosphate ( $\text{InsP}_3$ ) receptor activation with phenylephrine in mesenteric arteries of mice (del Corso et al., 2006). Loss of  $\text{Ca}_v3.2$  channels attenuates a protective function to excess myogenic tone in response to intravascular pressure (Mikkelsen, Björling, & Jensen, 2016). Advanced age can also alter the composition of lipid rafts and caveolae, which could affect a variety of signaling molecules (Bergdahl & Sward, 2004; Parton & Simons, 2007) to contribute to the pathophysiology of Alzheimer's, Parkinson's, diabetes, and cardiovascular diseases (Boersma et al., 2001; Headrick et al., 2003; Ohno-Iwashita, Shimada, Hayashi, & Inomata, 2010; Simons & Ehehalt, 2002). Aging has been also found to alter the number and morphology of caveolae in smooth muscle cells (Bakircioglu et al., 2001; Lowalekar, Cristofaro, Radisavljevic, Yalla, & Sullivan, 2012; Ratajczak et al., 2003). We hypothesize that aging affects the T-type  $\text{Ca}_v3.2$ -RyR axis to generate  $\text{Ca}^{2+}$  sparks in vascular smooth muscle. To test this hypothesis, we used methyl- $\beta$ -cyclodextrin, smooth muscle-specific (SMAKO)  $\text{Ca}_v1.2$ <sup>-/-</sup> mice

and a novel Eps15 homology domain-containing protein (*EHD2*) knockout mouse model, which leads to destabilization of caveolae at the plasma membrane (Lian, Matthaues, Kassmann, Daumke, & Gollasch, 2019). We also evaluated the role of luminal SR calcium on T-type  $\text{Ca}_v3.2$ -RyR coupling. Clarification of this hypothesis is important for understanding age-dependent effects in cardiovascular disease and may provide new therapeutic avenues in the elderly.

## 2 | RESULTS

### 2.1 | Age effects on T-type $\text{Ca}_v3.2$ -RyR axis

The T-type  $\text{Ca}_v3.2$  channel blocker  $\text{Ni}^{2+}$  decreased  $\text{Ca}^{2+}$  spark frequency and fraction of cells with sparks in young VSMCs (see also (Fan et al., 2018; Hashad et al., 2018)), while it failed to decrease  $\text{Ca}^{2+}$  spark events in old VSMCs (Figure 1). These data suggest that  $\text{Ca}_v3.2$  channels contribute to generation of  $\text{Ca}^{2+}$  sparks in young but not in old VSMC. To address whether the reduced function of T-type  $\text{Ca}_v3.2$  channels in generating  $\text{Ca}^{2+}$  sparks in old VSMCs could rely on reduced protein expression, we analyzed  $\text{Ca}_v3.2$  protein expression in mesenteric arteries from young mice versus old mice. In Western blot analyses, we found that  $\text{Ca}_v3.2$  expression decreased with age (Figure 1g,h).

### 2.2 | Role of luminal SR calcium on T-type $\text{Ca}_v3.2$ -RyR axis

Thapsigargin inhibits the SR  $\text{Ca}^{2+}$  transport ATPase (SERCA) and thereby reduces SR  $[\text{Ca}^{2+}]_{\text{SR}}$  load (Janczewski & Lakatta, 1993; Sagara & Inesi, 1991; Thastrup, 1990). We studied the effects of thapsigargin on  $[\text{Ca}^{2+}]_{\text{SR}}$  load and its role on T-type  $\text{Ca}_v3.2$ -RyR axis. Caffeine (10 mM)-induced peak fluorescence was measured to monitor maximal RyR  $\text{Ca}^{2+}$  release from SR stores. Our data showed that thapsigargin decreased concentration-dependently caffeine-induced cytosolic  $[\text{Ca}^{2+}]$  peaks (Figure S1a-d). The results confirm that thapsigargin causes luminal SR calcium depletion. We next studied the individual contributions of  $\text{Ca}_v1.2$  versus  $\text{Ca}_v3.2$  channels to generate  $\text{Ca}^{2+}$  sparks under these different  $[\text{Ca}^{2+}]_{\text{SR}}$  loads. We found that  $[\text{Ca}^{2+}]_{\text{SR}}$  depletion by thapsigargin reduced  $\text{Ca}^{2+}$  spark frequency and the percentage of cells firing  $\text{Ca}^{2+}$  sparks in  $\text{Ca}_v1.2$ <sup>+/+</sup> VSMCs (Figure 2a,c) (see also (Essin et al., 2007)). In contrast, thapsigargin had no or little effects on  $\text{Ca}^{2+}$  spark frequency and the percentage of cells firing  $\text{Ca}^{2+}$  sparks in  $\text{Ca}_v1.2$ <sup>-/-</sup> (SMAKO) VSMCs (Figure 2b,c). These data are consistent with the idea that L-type  $\text{Ca}_v1.2$  channels couple indirectly to RyRs, that is, by influencing luminal SR calcium load to generate  $\text{Ca}^{2+}$  sparks (Essin et al., 2007). The data also show that SR  $\text{Ca}^{2+}$  load is controlled by SERCA (Nelson et al., 1995). We next studied how  $\text{Ca}_v1.2$  channel ablation and reduced  $[\text{Ca}^{2+}]_{\text{SR}}$  load affect the  $\text{Ca}_v3.2$ -RyR axis, that is, direct coupling between  $\text{Ca}_v3.2$  channels and RyRs to generate  $\text{Ca}^{2+}$  sparks (Fan et al., 2018; Hashad et al., 2018; Löhn et al., 2000). Consistent with our previous results



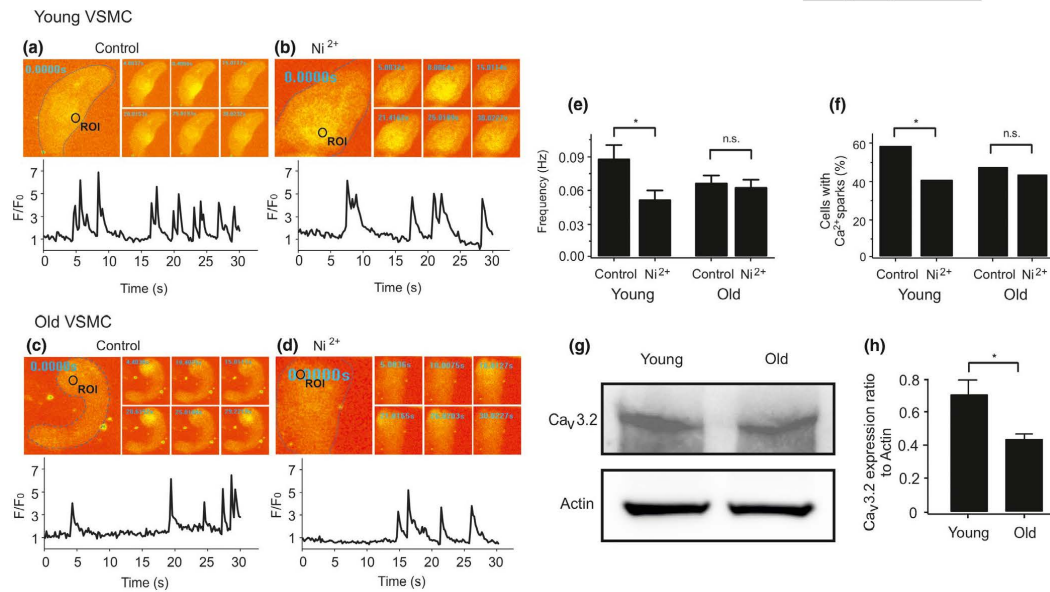


**FIGURE 1** Age attenuates the role of  $\text{Ca}_v3.2$  channels in  $\text{Ca}^{2+}$  spark generation and decreases  $\text{Ca}_v3.2$  protein expression in VSMC. (a),  $\text{Ca}^{2+}$  fluorescence images of a Fluo-4-AM-loaded VSMC from a young mouse and time course of  $\text{Ca}^{2+}$  fluorescence changes in the cellular ROI (upper panel). Cell boundary is marked with dashed line. (b), same as (a) but in the presence of  $\text{Ni}^{2+}$  (50  $\mu\text{M}$ ). (c), same as (a) but in a VSMC from an old mouse. (d), same as (c) but in the presence of  $\text{Ni}^{2+}$  (50  $\mu\text{M}$ ). (e, f), summary of the results.  $\text{Ca}^{2+}$  spark frequency (e) and fraction of cells producing  $\text{Ca}^{2+}$  sparks (f) in VSMCs from young mice ( $n = 102$ ), in VSMCs from young mice cells incubated with  $\text{Ni}^{2+}$  ( $n = 85$ ), in VSMCs from aged mice ( $n = 129$ ), and in VSMCs from aged mice cells incubated with  $\text{Ni}^{2+}$  ( $n = 127$ ). Cells were isolated from 4 mice in each group; 25–40 cells were recorded and analyzed from each mouse. VSMC, vascular smooth muscle cell. (g), Western blot analysis of  $\text{Ca}_v3.2$  proteins in mesenteric arteries of young versus old mice. (h), quantification of Western blot results. Mesenteric arteries were taken from 9 mice in each group. \*,  $p < .05$ . n.s., not significant

(Essin et al., 2007), we found that  $[\text{Ca}^{2+}]_{\text{SR}}$  was lower in  $\text{Ca}_v1.2^{-/-}$  (SMAKO) VSMCs compared to  $\text{Ca}_v1.2^{+/+}$  control cells. As illustrated in Figure 2d–f, caffeine-induced cytosolic  $[\text{Ca}^{2+}]$  peaks were larger in  $\text{Ca}_v1.2^{+/+}$  cells compared to SMAKO  $\text{Ca}_v1.2^{-/-}$  VSMCs, consistent with the idea that L-type  $\text{Ca}_v1.2$  channels are critical for SR  $\text{Ca}^{2+}$  load and peak  $[\text{Ca}^{2+}]$  release. We compared the role of  $\text{Ca}^{2+}$  uptake into SR in these cells. 15 min after the first caffeine pulse, subsequent application of caffeine induced a strong  $[\text{Ca}^{2+}]$  peak in  $\text{Ca}_v1.2^{+/+}$  control compared to  $\text{Ca}_v1.2^{-/-}$  (SMAKO) cells (Figure 2d–f). We also compared the effects of caffeine on mesenteric arteries in the absence and presence of  $\text{Ni}^{2+}$ .  $\text{Ni}^{2+}$  did not alter caffeine-induced constrictions (Figure S1i–k). These data indicate that SR  $\text{Ca}^{2+}$  load mainly depends on  $\text{Ca}^{2+}$  influx through L-type  $\text{Ca}_v1.2$  channels (see also (Essin et al., 2007)). We confirmed these results by measuring  $\text{BK}_{\text{Ca}}$  channel currents activated by  $\text{Ca}^{2+}$  sparks (STOCs) in VSMCs (Figure S1e–h). STOCs were measured in presence of  $\text{Cd}^{2+}$  and/or  $\text{Ni}^{2+}$  after depletion of the  $[\text{Ca}^{2+}]_{\text{SR}}$  by thapsigargin. The holding potential was set to  $-40$  mV, a physiological membrane potential that should drive T-type  $\text{Ca}^{2+}$  channel-mediated  $\text{Ca}^{2+}$  sparks, enabling the activation of  $\text{BK}_{\text{Ca}}$  channels (Fan et al., 2018; Harraz et al., 2014; Hashad et al., 2018). Figure S1 shows that thapsigargin removed  $\sim 60\%$  of STOCs in VSMCs (Figure S1e–g). The  $\text{Ca}_v1.2$  channel blocker  $\text{Cd}^{2+}$  blocked

all STOCs in thapsigargin-treated cells (Figure S1f), while  $\text{Ni}^{2+}$  had no effects (Figure S1e,h). Together, the results indicate that (a)  $\text{Ca}^{2+}$  influx through L-type  $\text{Ca}_v1.2$  channels is the main source of filling the SR with  $\text{Ca}^{2+}$  and (b) proper function of the T-type  $\text{Ca}_v3.2$ -RyR axis requires sufficient high  $[\text{Ca}^{2+}]_{\text{SR}}$  load.

### 2.3 | Aging and alterations of VSMC caveolae

Defective  $\text{Ca}_v3.2$ -RyR axis in old VSMCs could result from alterations in the ultrastructure of caveolae, where  $\text{Ca}_v3.2$  channels reside to drive RyR-mediated  $\text{Ca}^{2+}$  sparks (Fan et al., 2018; Harraz et al., 2014; Hashad et al., 2018). We first explored the contribution of caveolae to  $\text{Ca}^{2+}$  spark generation in VSMCs using methyl- $\beta$ -cyclodextrin (10 mM), a cholesterol-depleting drug, which is known to disturb caveolae and inhibit a significant fraction of  $\text{Ca}^{2+}$  sparks in VSMCs (Löhn et al., 2000). In accordance with our previous data (Fan et al., 2018; Löhn et al., 2000), we found that methyl- $\beta$ -cyclodextrin decreased the frequency of  $\text{Ca}^{2+}$  spark and the fraction of cells with sparks by  $\sim 30\%$  in young VSMCs. However, methyl- $\beta$ -cyclodextrin did not alter  $\text{Ca}^{2+}$  spark generation in old VSMCs (Figure 3a–f).  $\text{Ni}^{2+}$  (50  $\mu\text{M}$ ) did not further reduce  $\text{Ca}^{2+}$  sparks in methyl- $\beta$ -cyclodextrin

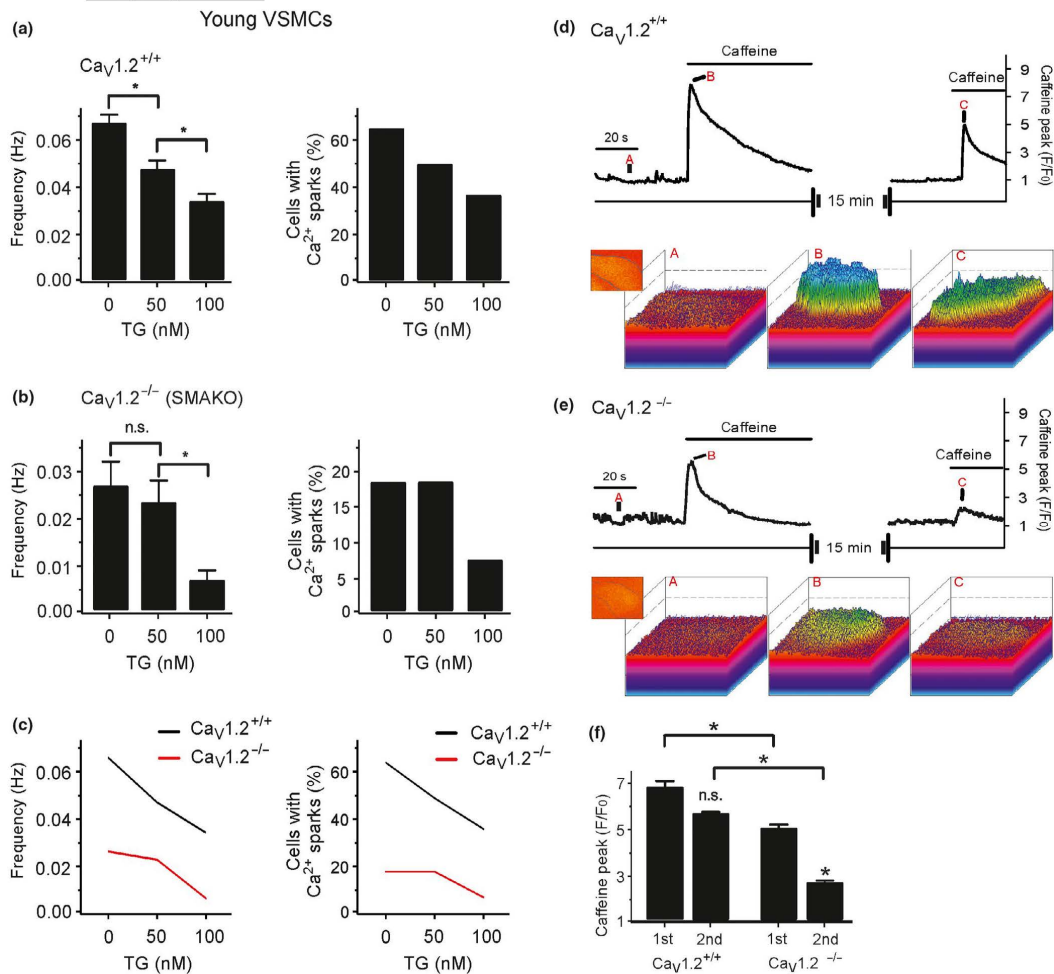


**FIGURE 2** Role of luminal SR calcium on T-type  $Ca_v3.2$ -RyR axis. Effects of different concentrations of thapsigargin on  $Ca^{2+}$  spark frequency (a, left) and fraction of cells producing  $Ca^{2+}$  sparks (a, right) in  $Ca_v1.2^{+/+}$  VSMCs from young mice. Effects of different concentrations of thapsigargin on  $Ca^{2+}$  spark frequency (b, left) and fraction of cells producing  $Ca^{2+}$  sparks (b, right) in VSMCs from  $Ca_v1.2^{-/-}$  (SMAKO) mice. (c), overlay of the data for  $Ca^{2+}$  spark frequency (left) and fraction of cells producing  $Ca^{2+}$  sparks (right). Cells were isolated from 4 mice in each group; 30–35 cells were recorded and analyzed from each mouse. (d), time course of  $Ca^{2+}$  fluorescence changes in the cellular ROI in a wild-type ( $Ca_v1.2^{+/+}$ ) Fluo-4-AM-loaded VSMC induced by 10 mM caffeine (upper panel) and  $Ca^{2+}$  fluorescence plots (lower panel). (e), the same as (d), but in  $Ca_v1.2^{-/-}$  VSMC. (f), summary of the 10 mM caffeine-induced  $Ca^{2+}$  peaks in wild-type versus  $Ca_v1.2^{-/-}$  VSMCs.  $n = 7$  cells from 3 mice, 2–3 cells were recorded and analyzed from each mouse. \*,  $p < .05$ . n.s., not significant

treated VSMCs neither from young nor old mice. Next, we evaluated the ultrastructure of caveolae in young versus old VSMCs. Although caveolae were present in cells of both groups, the density of caveolae was reduced in old VSMCs compared to young VSMCs (Figure 3g–i). We next confirmed our results by using a novel *EHD2* genetic knockout (KO) mouse model. Since *EHD2* localizes to the caveolar neck region of all caveolae, genetic abolition of *EHD2* increases ubiquitously detachment of caveolae from the plasma

membrane (Matthaeus et al., 2019). In line with these findings, we found detachment of caveolae in *EHD2 del/del* VSMCs compared to control VSMCs (Figure 4a). These changes were accompanied by reduced expression of  $Ca_v3.2$  channels in *EHD2* KO (*del/del*) VSMCs compared to control cells. Furthermore,  $Ca^{2+}$  spark frequency and the percentage of cells firing  $Ca^{2+}$  sparks were diminished in VSMCs from *EHD2 del/del* mice (Figure 4). Together, ultrastructural alterations of caveolae, reduced expression of  $Ca_v3.2$  channels or both

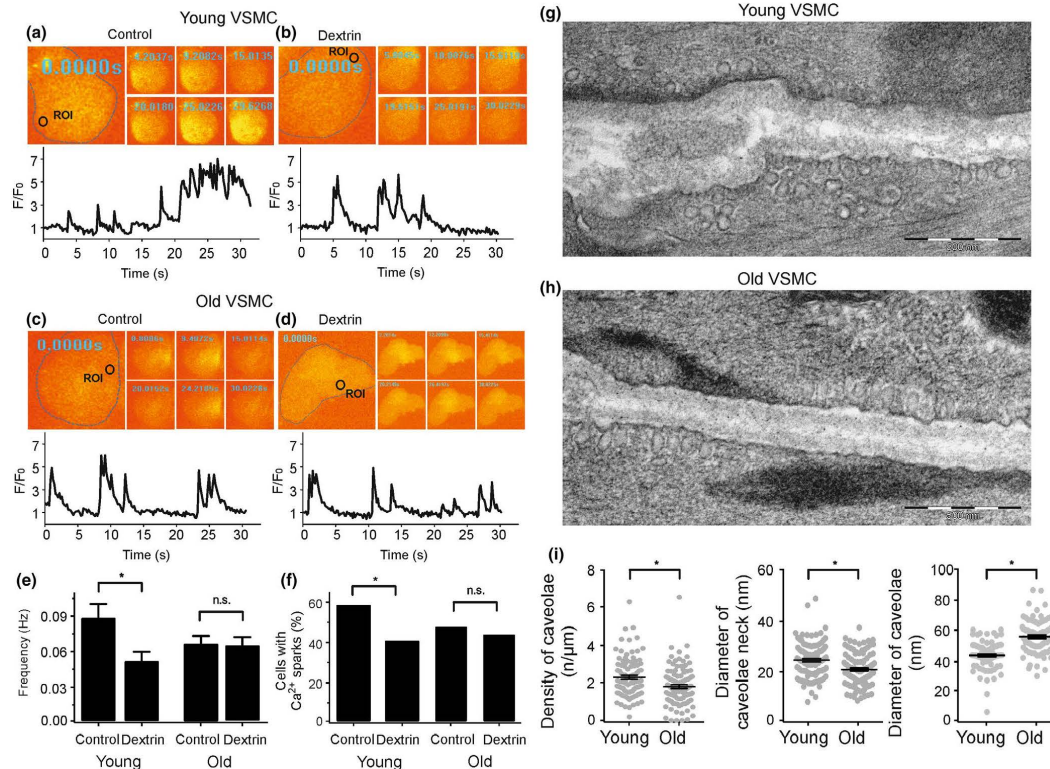


**FIGURE 3** Defective  $\text{Ca}_v3.2\text{-RyR}$  axis in aged VSMC result from alterations in the ultrastructure of caveolae. (a),  $\text{Ca}^{2+}$  fluorescence images of a Fluo-4-AM-loaded VSMC from a young mouse and time course of  $\text{Ca}^{2+}$  fluorescence changes in the cellular ROI (upper panel). Cell boundary is marked with dashed line. (b), same as (a) but with a cell incubated with methyl- $\beta$ -cyclodextrin (10 mM, 90 min at room temperature) to disrupt caveolae. (c), same as (a) but with VSMCs from old mice. (d), same as (c) but with a cell incubated with methyl- $\beta$ -cyclodextrin. (e, f), summary of the results.  $\text{Ca}^{2+}$  spark frequency (e) and fraction of cells producing  $\text{Ca}^{2+}$  sparks (f) in VSMCs from young mice ( $n = 98$ ), in VSMCs from young mice cells incubated with methyl- $\beta$ -cyclodextrin ( $n = 111$ ), in VSMCs from old mice ( $n = 121$ ), and in VSMCs from old mice cells incubated with methyl- $\beta$ -cyclodextrin ( $n = 128$ ). Cells were isolated from 4 mice in each group; 25–40 cells were recorded and analyzed from each mouse. (g), Electron microscopy image of a young VSMC. (h), same as (g) but from old VSMC. (i), summary of the results. Caveolae density, diameter of caveolae neck, caveolae size in VSMCs from young versus old mice (10–20 cells from each mouse, 4 mice in each group). \*,  $p < .05$ . n.s., not significant

could underlie the observed attenuation of the vascular T-type  $\text{Ca}_v3.2\text{-RyR}$  axis to generate  $\text{Ca}^{2+}$  sparks in aged vascular smooth muscle.

#### 2.4 | Residual $\text{Ca}^{2+}$ sparks in aged VSMCs

We noticed that there was a fraction of  $\text{Ca}^{2+}$  sparks in old VSMCs, which was insensitive to  $\text{Ca}_v1.2$  and  $\text{Ca}_v3.2$  channel blockade by  $\text{Cd}^{2+}$  and  $\text{Ni}^{2+}$ , respectively (Figure 5). Surprisingly,  $\text{Gd}^{3+}$ , a permissive TRP channel blocker, inhibited these remaining  $\text{Ca}^{2+}$  sparks (Figure 5). In contrast,  $\text{Gd}^{3+}$  (100  $\mu\text{M}$ ) had no effects on  $\text{Ca}^{2+}$  sparks in young VSMCs (Figure S11,m). Together, the data suggest that defective  $\text{Ca}_v3.2\text{-RyR}$  coupling in old VSMCs is counterbalanced by

putative  $\text{Gd}^{3+}$  sensitive (TRP) cation channels providing sufficient  $\text{Ca}^{2+}$  influx to generate  $\text{Ca}^{2+}$  sparks.

#### 2.5 | Age-dependent regulation of myogenic tone by $\text{Cav}3.2$ channels

To ascertain the importance of the  $\text{Ca}_v3.2\text{-RyR}$  relationship to regulate arterial tone, we performed video microscopic measurements on isolated arteries. In young wild-type mesenteric arteries, the  $\text{Ca}_v3.2$  blocker  $\text{Ni}^{2+}$  50  $\mu\text{M}$  increased myogenic tone from  $9.2\% \pm 1.2\%$  to  $13.04\% \pm 0.8\%$  at 60 mmHg, from  $11.6\% \pm 1.2\%$  to  $19.7\% \pm 0.5\%$  at 80 mmHg, and from  $17.7\% \pm 2\%$  to  $27.8\% \pm 1.3\%$  at 100 mmHg (Figure 6), whereas  $\text{Ni}^{2+}$  50  $\mu\text{M}$  did not affect myogenic constriction



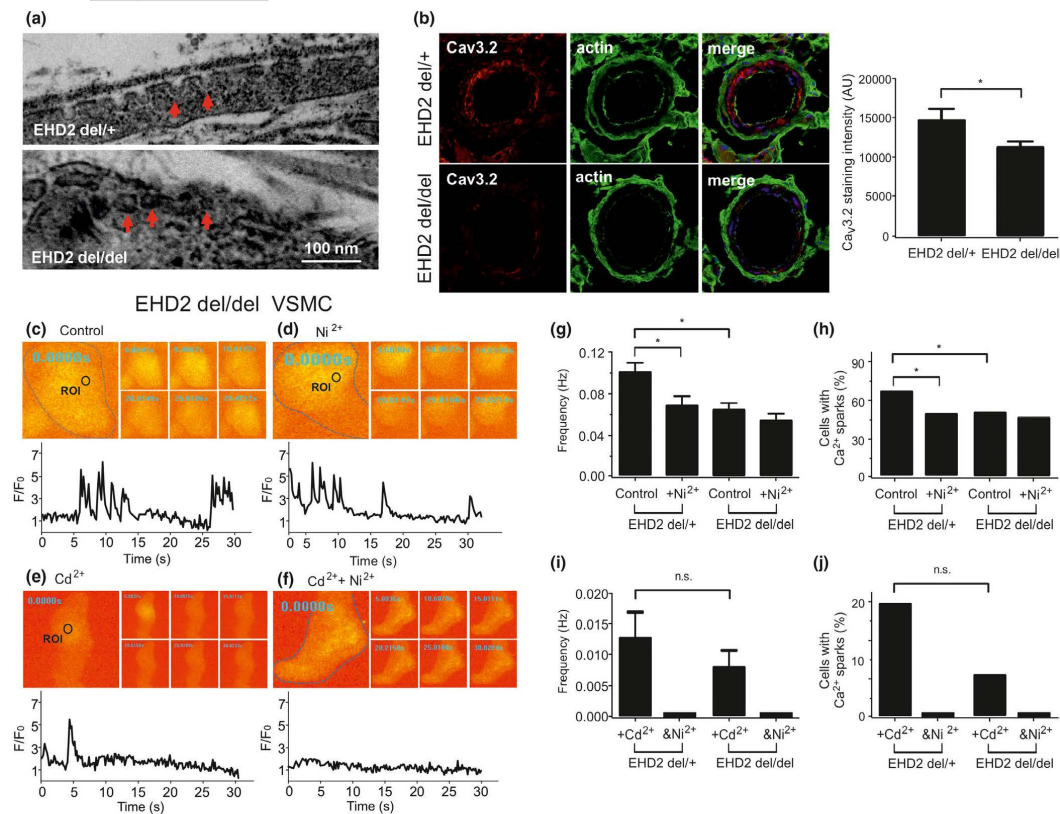


**FIGURE 4** *EHD2* knockout (*EHD2 del/del*) alters the ultrastructure of caveolae and decrease  $Ca_v3.2$  expression, resulting in  $Ca_v3.2$ -RyR axis malfunction. (a), Electron microscopy image of a *EHD2 del/+* VSMC and a *EHD2 del/del* VSMC. (b, left),  $Ca_v3.2$  immuno-staining in BAT cryostat sections from *EHD2 del/+* and *del/del* mice. (b, right), summary of the results,  $n$  (*del/+*)=46/5 mice and  $n$  (*del/del*)=53/5 mice. (c),  $Ca^{2+}$  fluorescence images of a Fluo-4-AM-loaded VSMC from *EHD2 del/del* mouse and time course of  $Ca^{2+}$  fluorescence changes in the cellular ROI (upper panel). Cell boundary is marked with dashed line. (d), same as (c) but in the presence of  $Ni^{2+}$  (50  $\mu$ M). (e), same as (c) but in the presence of  $Cd^{2+}$  (200  $\mu$ M). (f), same as (e) but in the presence of  $Ni^{2+}$  (50  $\mu$ M). (g, h), summary of the results.  $Ca^{2+}$  spark frequency (g) and fraction of cells producing  $Ca^{2+}$  sparks (h) in VSMCs from *EHD2 del/+* mice ( $n = 99$ ), in VSMCs from *EHD2 del/+* mice cells incubated with  $Ni^{2+}$  ( $n = 96$ ), in VSMCs from *EHD2 del/del* mice ( $n = 144$ ), and in VSMCs from *EHD2 del/del* mice cells incubated with  $Ni^{2+}$  ( $n = 125$ ). Cells were isolated from 4 mice in each group; 25–40 cells were recorded and analyzed from each mouse. (i, j), summary of the results.  $Ca^{2+}$  spark frequency (i) and fraction of cells producing  $Ca^{2+}$  sparks (j) in VSMCs from *EHD2 del/+* mice incubated with  $Cd^{2+}$  ( $n = 56$ ), in VSMCs from *EHD2 del/+* mice cells incubated with  $Ni^{2+}+Cd^{2+}$  ( $n = 56$ ), in VSMCs from *EHD2 del/del* mice incubated with  $Cd^{2+}$  ( $n = 75$ ), and in VSMCs from *EHD2 del/del* mice cells incubated with  $Ni^{2+}+Cd^{2+}$  ( $n = 68$ ). Cells were isolated from 4 mice in each group; 15–20 cells were recorded and analyzed from each mouse. \*,  $p < .05$ . n.s., not significant

in old vessels. Despite these differences, 60 mM  $K^+$ -induced vasoconstrictions were similar between young ( $54.2\% \pm 1.2\%$ ) and old ( $60.7\% \pm 2.1\%$ ) pressurized arteries (Figure 6c).

### 3 | DISCUSSION

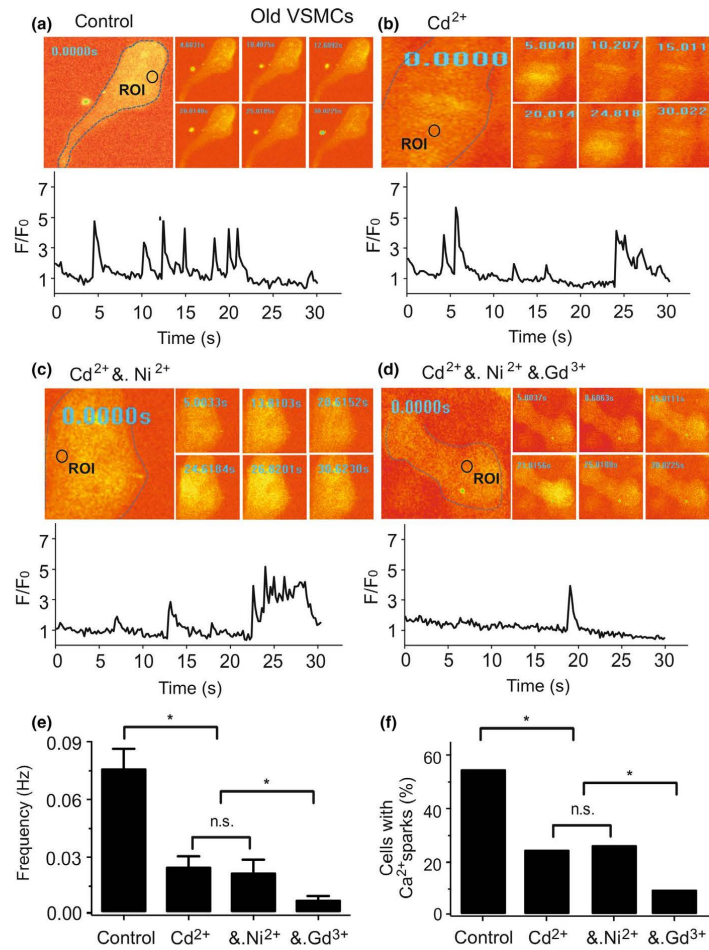
In this study, we analyzed the effects of aging on the  $Ca_v3.2$  channels-RyR axis on  $Ca^{2+}$  sparks generation in VSMCs. We employed pharmacological tools, smooth muscle-specific  $Ca_v1.2$  channel (SMAKO) and *EHD2* genetic knockout mice. Our studies demonstrate that caveolar

$Ca_v3.2$  channels-RyR axis is impaired in aged VSMCs. We observed age-related ultrastructural alterations of caveolae, which together with decreased  $Ca_v3.2$  expression, may underlie incomplete caveolae- $Ca_v3.2$ -RyR coupling for extracellular  $Ca^{2+}$  influx to trigger  $Ca^{2+}$  sparks and  $BK_{Ca}$  feedback in aged vascular smooth muscle.

#### 3.1 | Local and tight caveolar $Ca_v3.2$ -RyR coupling

L-type  $Ca_v1.2$  channels provide the predominant  $Ca^{2+}$  pathway for  $Ca^{2+}$  spark generation in VSMCs (Brenner et al., 2000; Filosa

**FIGURE 5**  $Gd^{3+}$  sensitive (TRP) cation channels generate  $Ca^{2+}$  sparks in old VSMCs. (a),  $Ca^{2+}$  fluorescence images of a Fluo-4-AM-loaded VSMC from an old mouse and time course of  $Ca^{2+}$  fluorescence changes in the cellular ROI (upper panel). Cell boundary is marked with dashed line. (b), same as (a) but with a cell incubated with  $Cd^{2+}$  (200  $\mu M$ ). (c), same as (a) but with  $Ni^{2+}$  (50  $\mu M$ ) following  $Cd^{2+}$  treatment. (d), same as (a) but with  $Gd^{3+}$  (100  $\mu M$ ) following  $Cd^{2+}$  &  $Ni^{2+}$  treatment. (e, f), summary of the results.  $Ca^{2+}$  spark frequency (e) and fraction of cells producing  $Ca^{2+}$  sparks (f) in cells ( $n = 66$ ), in cells incubated with  $Cd^{2+}$  ( $n = 69$ ), in cells incubated with  $Cd^{2+}$  &  $Ni^{2+}$  ( $n = 61$ ), and in cells incubated with  $Cd^{2+}$  &  $Ni^{2+}$  &  $Gd^{3+}$  ( $n = 86$ ). Cells were isolated from 4 old mice in each group; 15–30 cells were recorded and analyzed from each mouse. \*,  $p < .05$ . n.s., not significant



et al., 2006; Gollasch et al., 1998; Nelson et al., 1995; Pluger et al., 2000; Sausbier et al., 2005). This pathway increases  $Ca^{2+}$  load in the SR ( $[Ca^{2+}]_{SR}$ ) can activate RyRs from the SR luminal side of the receptor to produce  $Ca^{2+}$  sparks (Figure 6f) (Ching, Williams, & Sitsapesan, 2000; Essin et al., 2007). T-type  $Ca_v3.2$  channels, which are located in pits structures of caveolae, constitute an additional  $Ca^{2+}$  influx pathway to trigger  $Ca^{2+}$  sparks (Figure 6f) (Abd El-Rahman et al., 2013; Braunstein et al., 2009; Chen et al., 2003; Fan et al., 2018; Hashad et al., 2018). Our recent data show that RyR2 is the predominant RyR isoform responsible for  $Ca^{2+}$  sparks in VSMCs (Kassmann et al., 2019). The results from the present study are in line with these conceptual views. We first used low concentrations of the SR  $Ca^{2+}$ -ATPase inhibitor thapsigargin to decrease the SR calcium content (Janczewski & Lakatta, 1993; Lewartowski & Wolska, 1993; Nelson et al., 1995; Sagara, Fernandez-Belda, Meis, & Inesi, 1992) and found that  $[Ca^{2+}]_{SR}$  depletion reduced  $Ca^{2+}$  spark frequency. In contrast, thapsigargin did

not affect  $Ca^{2+}$  spark frequency in the absence of  $Ca_v1.2$  channels. These data indicate that SR calcium filling through SERCA is critical for  $Ca_v1.2$ -mediated  $Ca^{2+}$  sparks, but not for  $Ca_v3.2$ -RyR axis. They support that local and tight coupling between the  $Ca_v1.2$  channels and RyRs is not required to initiate  $Ca^{2+}$  sparks as previously suggested by our group (Essin et al., 2007). Indeed, the data indicate that  $Ca_v1.2$  channels contribute to global cytosolic  $[Ca^{2+}]$ , which in turn influences luminal SR calcium and thus  $Ca^{2+}$  sparks (Figure 6f) (Essin et al., 2007). We also found that  $Ca_v3.2$  channel blockade by  $Ni^{2+}$  had no effects on  $Ca^{2+}$  sparks and STOCs after treatment of cells with thapsigargin, that is, in conditions of suboptimal filled  $[Ca^{2+}]_{SR}$  stores. These data indicate that proper function of the caveolar T-type  $Ca_v3.2$ -RyR axis requires sufficient high  $[Ca^{2+}]_{SR}$  load. Second, we also explored the function of  $Ca_v1.2$  and  $Ca_v3.2$  channels for luminal SR  $Ca^{2+}$  load. We used high concentrations of caffeine (10 mM), a well-known activator RyRs, to induce SR calcium release. Caffeine evoked smaller  $Ca^{2+}$



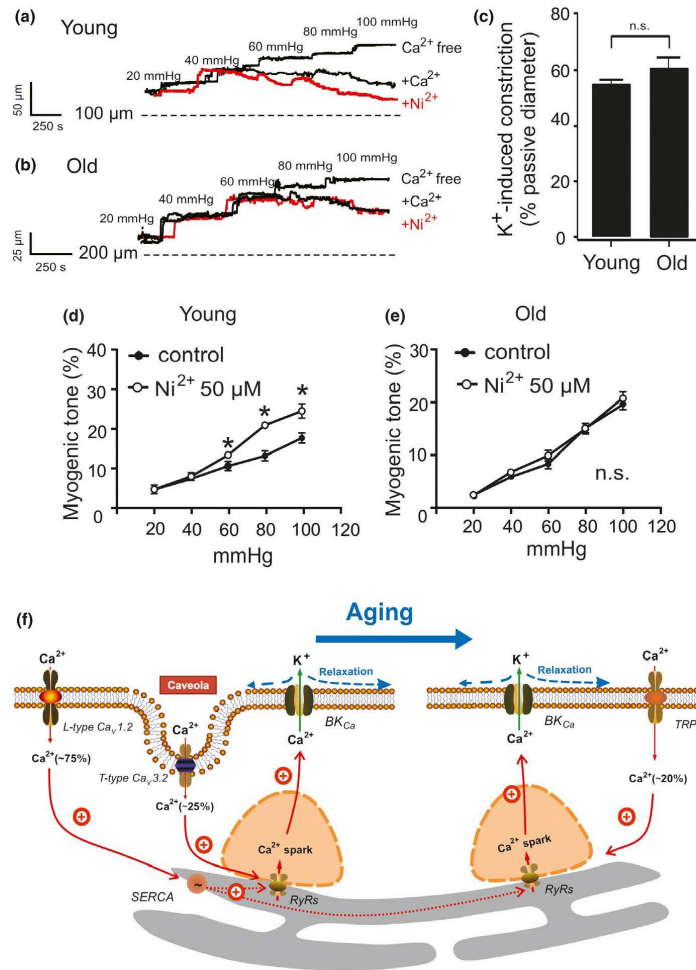


**FIGURE 6** T-type  $Ca_v3.2$  blockade does not constrict mesenteric arteries from old mice. (a, b), representative traces and summary data show the effect of  $Ni^{2+}$  (50  $\mu$ M) on mesenteric arteries pressurized to 60–100 mmHg from young and old mice, respectively. (c), vasoconstriction evoked by 60 mM  $K^+$  was similar in young and old pressurized (15 mmHg) arteries. (d, e), summary of myogenic tone measurements in pressurized mesenteric arteries from young and old mice ( $n = 5$  arteries from 5 mice, one artery was recorded and analyzed from each mouse). Experiments were performed in the absence and presence of 50  $\mu$ M  $Ni^{2+}$ . \*,  $p < .05$ . n.s., not significant. (f), schematic illustration of major  $Ca^{2+}$  influx pathways regulating  $Ca^{2+}$  sparks in VSMCs during aging.  $Ca^{2+}$  sparks, which result from opening of clustered RyRs in the SR, activate large-conductance  $Ca^{2+}$ -activated  $K^+$  ( $BK_{Ca}$ ) channels to produce a negative feedback effect on vasoconstriction. L-type  $Ca_v1.2$  channels contribute to global cytosolic  $[Ca^{2+}]_i$ , which in turn influences luminal SR calcium (via SERCA) and thus generates the majority (75%) of  $Ca^{2+}$  sparks. Caveolae position  $Ca_v3.2$  channels sufficiently close to RyRs for extracellular  $Ca^{2+}$  influx to trigger (~25%)  $Ca^{2+}$  sparks. In aged mice, this  $Ca_v3.2$ -RyR pathway loses importance. Instead, a gadolinium-sensitive  $Ca^{2+}$  influx pathway is upregulated to trigger (20%)  $Ca^{2+}$  sparks. This pathway may compromise nonselective TRP channels. RyRs, ryanodine receptors; SERCA, sarcoplasmic/endoplasmic calcium pump; SR, sarcoplasmic reticulum; VSMC, mesenteric artery vascular smooth muscle cell

transients through SR  $Ca^{2+}$  release in SMAKO  $Ca_v1.2^{-/-}$  VSMCs, in which T-type  $Ca_v3.2$  channels play a minor role in providing  $Ca^{2+}$  influx to induce  $Ca^{2+}$  sparks. These findings support the view that  $Ca^{2+}$  influx through L-type  $Ca_v1.2$  channels, but not T-type  $Ca_v3.2$  channels, represents the main source for luminal SR calcium load (Essin et al., 2007; Fan et al., 2018). To confirm this conclusion, we

studied  $Ca^{2+}$  uptake into luminal SR by 2 pulse-protocol of caffeine applications. We found that 10 mM caffeine evoked weak caffeine-induced peaks in SMAKO  $Ca_v1.2^{-/-}$  cells compared to control cells fifteen minutes after the 1st-pulse caffeine application. We failed to observe  $Ca^{2+}$  sparks in SMAKO  $Ca_v1.2^{-/-}$  cells before the 2nd-pulse caffeine application, whereas cells with functional

Ca<sub>v</sub>1.2 channels enabled generation of Ca<sup>2+</sup> sparks within the fifteen minutes interval. The poor recovery of the luminal SR calcium in SMAKO Ca<sub>v</sub>1.2<sup>-/-</sup> VSMCs suggests that T-type Ca<sub>v</sub>3.2 channels play a minor role in [Ca<sup>2+</sup>]<sub>SR</sub> filling. The results were also confirmed by our electrophysiological experiments.

### 3.2 | Effects of aging on T-type Ca<sub>v</sub>3.2-RyR axis

In order to explore the effects of aging on caveolar T-type Ca<sub>v</sub>3.2 channel-mediated Ca<sup>2+</sup> sparks, we treated VSMCs from young and old mice with Ni<sup>2+</sup> and methyl-β-cyclodextrin. Consistent with our previous findings (Fan et al., 2018; Hashad et al., 2018), both compounds inhibited Ca<sup>2+</sup> sparks in young VSMCs. In contrast, neither Ni<sup>2+</sup> nor methyl-β-cyclodextrin inhibited Ca<sup>2+</sup> sparks in old VSMCs. These results indicate that the T-type Ca<sub>v</sub>3.2-RyR axis loses its function to generate Ca<sup>2+</sup> sparks in aged VSMCs to drive negative feedback control of myogenic tone in resistance arteries (Figure 6a-e). The data are consistent with other data showing that Ca<sub>v</sub>3.2 channels lose their protective role against excess myogenic tone and the loss of Ca<sub>v</sub>3.2 channels induces a loss of flow-mediated vasodilation with advanced age (Mikkelsen et al., 2016). Since RyR2 is the predominant RyR isoform responsible for Ca<sup>2+</sup> sparks in VSMCs (Kassmann et al., 2019) and Ca<sub>v</sub>1.2-RyR2 axis works efficient in old VSMCs (Figure 5), RyRs reorganization should not be a key reason for altered calcium sparks in aged VSMCs. Thus, we propose that the observed malfunction of T-type Ca<sub>v</sub>3.2-RyR axis in aging results from reduced Ca<sub>v</sub>3.2 expression and ultrastructural alterations in caveolar microdomains responsible for Ca<sub>v</sub>3.2-RyR coupling. In accordance, we found that caveolae density was decreased and caveolae necks were narrowed in old VSMCs. T-type Ca<sub>v</sub>3.2-RyR axis provides an important vascular Ca<sup>2+</sup> influx pathway for triggering Ca<sup>2+</sup> sparks in young VSMCs that deserves further attention since Ca<sub>v</sub>3.2 T-type calcium channels contribute to cardiovascular diseases (Chiang et al., 2009; David et al., 2010). Defective T-type Ca<sub>v</sub>3.2-RyR axis may contribute to age-related cardiovascular complications involving increased myogenic tone and blood pressure with advanced age.

### 3.3 | Role of EHD2 on T-type Ca<sub>v</sub>3.2-RyR axis

EHD2 is a dynamin-related ATPase located at the neck of caveolae, which constitutes a structural component of caveolae involved in controlling the stability and turnover of this organelle (Ludwig et al., 2013; Morén et al., 2012; Stoeber et al., 2016). Knockout or down-regulation of EHD2 in vivo results in decreased surface association and increased mobility of caveolae, whereas EHD2 overexpression stabilizes caveolae at the plasma membrane (Matthaeus et al., 2019; Morén et al., 2012; Shvets, Bitsikas, Howard, Hansen, & Nichols, 2015; Stoeber et al., 2016). Here we used EHD del/del mice to disturb the stability of caveolae to explore the effect of caveolar microdomains on Ca<sub>v</sub>3.2-RyR axis. Loss of EHD2 decreased

the plasma membrane localization of caveolae and Ca<sub>v</sub>3.2 channel expression, thus impaired the ability of T-type Ca<sub>v</sub>3.2 on Ca<sup>2+</sup> sparks generation in the mesenteric SMC. It aligns with our above results and provides firm evidence that Ca<sub>v</sub>3.2 channels in caveolar microdomains contribute to Ca<sup>2+</sup> sparks in VSMCs of young but not old mice.

### 3.4 | Possible role of TRP channels

We found that complete blockade of both Ca<sub>v</sub>1.2 and Ca<sub>v</sub>3.2 channels (by Cd<sup>2+</sup> and Ni<sup>2+</sup>) abolished all Ca<sup>2+</sup> sparks in young VSMCs (see also Fan et al., 2018) but only ~70% of Ca<sup>2+</sup> sparks in old VSMCs. The findings suggest appearance of an additional Ca<sup>2+</sup> influx pathway evoking Ca<sup>2+</sup> sparks only in aged VSMCs. We found that gadolinium, a permissive TRP channel blocker (Hashad et al., 2017; Riehle et al., 2016), inhibited these remaining Ca<sup>2+</sup> sparks. In order to rule out possible effects of gadolinium on Ca<sub>v</sub>1.2 channel and/or Ca<sub>v</sub>3.2 channel-mediated Ca<sup>2+</sup> sparks, we tested the effects of gadolinium on Ca<sup>2+</sup> sparks in young VSMCs (in the absence of Cd<sup>2+</sup> and Ni<sup>2+</sup>) and found that gadolinium had no effects on these Ca<sup>2+</sup> sparks. Although gadolinium has been identified as nonspecific blocker (Berrier, Coulombe, Szabo, Zoratti, & Ghazi, 1992; Gottlieb, Suchyna, Ostrow, & Sachs, 2004; Trollinger, Rivkah Isseroff, & Nuccitelli, 2002), it is likely that a Ca<sup>2+</sup> permeable conductance (TRP channels) has been upregulated to compensate for loss of T-type Ca<sub>v</sub>3.2 channels driving Ca<sup>2+</sup> sparks in aged VSMCs (Figure 6f). Besides, TRP channels might trigger calcium sparks through reloading the SR with calcium since methyl-β-cyclodextrin treatment failed to alter calcium events in old VSMCs (Figure 3e,f). Further works are required to ascertain which TRP cation channel(s) or pathways are responsible for generation of these Ca<sup>2+</sup> sparks. Identification of the underlying pathways might be important for understanding age-dependent factors contributing to cardiovascular disease and providing novel therapeutic approaches.

### 3.5 | Summary

Our data provide further evidence that Ca<sub>v</sub>3.2 channels colocalize in microdomains with RyRs to initiate Ca<sup>2+</sup> sparks and activate BKCa channels to drive a feedback response on vascular tone. Here we demonstrate that caveolar Ca<sub>v</sub>3.2 channels are impaired in triggering Ca<sup>2+</sup> sparks in aged VSMCs. This defective caveolae-RyR coupling may be caused by age-related ultrastructural alterations of caveolae and reduced Ca<sub>v</sub>3.2 expression in VSMCs. Furthermore, we found that proper function of the T-type Ca<sub>v</sub>3.2-RyR axis requires sufficiently high SR Ca<sup>2+</sup> load, which is regulated via Ca<sup>2+</sup> influx through L-type Ca<sub>v</sub>1.2 channels. T-type Ca<sub>v</sub>3.2-RyR axis malfunction may provide a straightforward explanation on how aging affects blood pressure (Chiossi et al., 2016; Hilgers et al., 2017; Wirth et al., 2016). Targeting defective Ca<sub>v</sub>3.2-RyR coupling may provide new therapeutic avenues for treatment of cardiovascular disease in the elderly.

## 4 | EXPERIMENTAL PROCEDURES

### 4.1 | Mice

In this study, young (12–14 weeks) versus old (48–56 weeks) male mice were used. The generation and usage of mice deficient in the smooth muscle  $Ca_v1.2$   $Ca^{2+}$  channel (SMAKO, smooth muscle  $\alpha1c$ -subunit  $Ca^{2+}$  channel knockout) has been described previously (Moosmang et al., 2003). Briefly, a conditional lox P-flanked allele (L2) of the  $Ca_v1.2$  gene (i.e., exons 14 and 15) was generated by homologous recombination in R1 embryonic stem cells (Seisenberger et al., 2000). In addition, mice carried a knock-in allele (SM-CreER T2 (ki)) (Kuhbandner et al., 2000), which expresses the tamoxifen-dependent Cre recombinase, CreER T2, from the endogenous SM22  $\alpha$  gene locus, which is selectively expressed in smooth muscle of adult mice. Thus, tamoxifen treatment results in conversion of the lox P-flanked  $Ca_v1.2$  allele (L2) into a  $Ca_v1.2$  knockout allele (L1) specifically in SMCs (Moosmang et al., 2003) (Essin et al., 2007). Mice were maintained at the breeding facility of the Max Delbrück Center for Molecular Medicine Berlin (MDC) in individually ventilated cages under standardized conditions that included a 12-hr dark-light cycle and free access to standard chow (0.25% sodium; SSNIFF Spezialitäten, Soest, Germany) and drinking water. SMAKO mice ( $Ca_v1.2^{lox/flox}$ ; SM22 $\alpha$ -Cre<sup>T2</sup> or  $Ca_v1.2^{lox/flox}$ ; SM22 $\alpha$ -Cre<sup>T2/T2</sup>) and corresponding control mice ( $Ca_v1.2^{+/+}$ ; SM22 $\alpha$ -Cre<sup>T2/T2</sup>,  $Ca_v1.2^{+/+}$ ; SM22 $\alpha$ -Cre<sup>T2</sup>,  $Ca_v1.2^{+/+}$  or  $Ca_v1.2^{lox/flox}$ ) (12–14 weeks each) were i.p. injected with tamoxifen (30  $\mu$ g/g body weight/day) for five consecutive days and sacrificed within 2–4 days after the injections. *EHD2 del/del* or *EHD2 del/+* littermates (as control) mice (20–35 weeks each) were used as previously described (Matthaeus et al., 2019). All mice were deeply anesthetized by inhalation of isoflurane until cessation of breathing and then killed by cervical dislocation, and the mesenteric arteries were removed. Experiments were performed on the same day with arteries from litter-matched young versus aged mice, *EHD2* control versus *EHD2 del/del*, and control versus SMAKO mice. All animal protocols were approved by the local animal care committee (LAGeSo, Berlin, Germany) and the animal welfare officers of the MDC (No. X9011/16, G0154/14). There are no ethical concerns.

### 4.2 | Isolation of arterial vascular smooth muscle cells

Arterial VSMCs from mesenteric arteries were isolated as previously described (Gollasch et al., 1998; Kassmann et al., 2019; Plugger et al., 2000; Schleifenbaum et al., 2014). Briefly, arteries were removed and quickly transferred to cold (4°C) oxygenated (95% O<sub>2</sub>-5% CO<sub>2</sub>) physiological salt solution (PSS) of the following composition (mM): 119 NaCl, 4.7 KCl, 1.2 KH<sub>2</sub>PO<sub>4</sub>, 25 NaHCO<sub>3</sub>, 1.2 MgSO<sub>4</sub>, 1.6 CaCl<sub>2</sub>, and 11.1 glucose. The arteries were cleaned, cut into pieces, and placed into a Ca<sup>2+</sup>-free Hank's solution (mM): 55 NaCl, 80 sodium glutamate, 5.6 KCl, 2 MgCl<sub>2</sub>, 1 mg/ml bovine serum albumin (BSA,

Sigma, Taufkirchen), 10 glucose, and 10 HEPES (pH 7.4 with NaOH) containing 0.5 mg/ml papain (Sigma) and 1.0 mg/ml DTT for 37 min at 37°C. The segments were then placed in Hank's solution containing 1 mg/ml collagenase (Sigma, type F and H, ratio 30% and 70%) and 0.1 mM CaCl<sub>2</sub> for 17 min at 37°C. Following several washes in Ca<sup>2+</sup>-free Hank's solution (containing 1 mg/ml BSA), single cells were dispersed from artery segments by gentle triturating. Cells were then stored in the same solution at 4°C.

### 4.3 | Ca<sup>2+</sup> imaging measurements

Ca<sup>2+</sup> sparks were measured as previously described (Essin et al., 2007; Fan et al., 2018). Isolated VSMCs were placed onto glass coverslips and incubated with the Ca<sup>2+</sup> indicator fluo-4 a.m. (10  $\mu$ M) and pluronic acid (0.005%, w/v) for 60 min at room temperature in Ca<sup>2+</sup>-free Hanks' solution (Fan et al., 2018; Kassmann et al., 2019). After loading, cells were washed with bath solution for 10 min at room temperature. Isolated cells and intact arterial segments were imaged in a bath solution containing (mM): 134 NaCl, 6 KCl, 1 MgCl<sub>2</sub>, 2 CaCl<sub>2</sub>, 10 glucose and 10 HEPES (pH 7.4, NaOH). Images were recorded using a Nipkow disc-based UltraView LCI confocal scanner (Perkin Elmer, Waltham, MA, USA) linked to a fast digital camera (Hamamatsu Photonics Model C4742-95-12ERG, 1,344 × 1,024 active pixel resolution, 6.45  $\mu$ m square pixels). The confocal system was mounted on an inverted Nikon Eclipse Ti microscope with a x40 oil-immersion objective (NA 1.3, Nikon). Images were obtained by illumination with an argon laser at 488 nm and recording all emitted light above 515 nm. Ca<sup>2+</sup> spark analyses were performed off-line using the UltraView Imaging Suite software (Perkin Elmer). The entire area of each image was analyzed to detect Ca<sup>2+</sup> sparks. Ca<sup>2+</sup> sparks were defined as local fractional fluorescence increase ( $F/F_0$ ) above the noise level of 1.5. The frequency was calculated as the number of detected sparks divided by the total scan time. Caffeine-induced peak was measured as previously described (Fernandez-Sanz et al., 2014). After the VSMCs loaded with Ca<sup>2+</sup> indicator fluo-4 a.m. (10  $\mu$ M, 60 min at room temperature), images were obtained following a single pulse of 10 mM caffeine. Maximal amplitude of caffeine-induced peak fluorescence was normalized by the initial fluorescence value ( $F/F_0$ ) and considered as an index of total SR Ca<sup>2+</sup> load.

### 4.4 | Electrophysiology

Currents were measured in the whole-cell perforated-patch mode of the patch-clamp technique (Essin et al., 2007; Gollasch, Ried, Bychkov, Luft, & Haller, 1996; Kassmann et al., 2019). Patch pipettes (resistance, 1.5–3.5 M $\Omega$ ) were filled with a solution containing (in mM): 110 K-Asp, 30 KCl, 10 NaCl, 1 MgCl<sub>2</sub>, and 0.05 EGTA (pH 7.2). The patch pipette solution was supplemented with 200  $\mu$ g/ml Amphotericin B, dissolved in dimethyl sulfoxide (DMSO), to measure K<sup>+</sup> currents in the whole-cell perforated-patch mode. The external bath solution contained (in



mM): 134 NaCl, 6 KCl, 1 MgCl<sub>2</sub>, 2 CaCl<sub>2</sub>, 10 glucose, and 10 HEPES (pH 7.4); holding potential was -60 mV. Whole-cell currents were recorded using an Axopatch 200B amplifier (Axon Instruments/Molecular Devices) or an EPC 7 amplifier (List) at room temperature. Data were digitized at 5 kHz, using a Digidata 1440A digitizer (Axon CNS, Molecular Devices) and pClamp software versions 10.1 and 10.2. STOC analysis was performed off-line using IGOR Pro (WaveMetrics) and Microsoft Excel software (Microsoft Corporation). A STOC was identified as a signal with at least three times the BK<sub>Ca</sub> single-channel current amplitude (Kassmann et al., 2019).

#### 4.5 | Ultrastructure and quantitative assessment of caveolae

Quantitative assessment of caveolae was carried out as previously described (Lowalekar et al., 2012). Isolated VSMCs from mesenteric arteries were dehydrated in a graded series of ethanol and embedded in the PolyBed® 812 resin (Polysciences Europe GmbH), ultrathin sections (60–80 nm) were cut (Leica microsystems), and uranyl acetate and lead citrate staining was performed. Samples were examined at 80 kV with a Zeiss EM 910 electron microscope (Zeiss), and image acquisition was performed with a Quemesa CDD camera and the iTEM software (Emsis GmbH). The density of caveolae was calculated as number of caveolae per  $\mu\text{m}$ . The diameter of caveolae neck (nm) and caveolae size (nm) were determined by using the parallel dimension function of CorelDRAW. Values from all electron microscopy images ( $n = 18$  cells in each group) were averaged for each group.

#### 4.6 | Western blot analysis

Mesenteric arteries were isolated from mice and placed into cold physiological saline solution (PSS) previously oxygenated for 30 min (95% O<sub>2</sub>, 5% CO<sub>2</sub>). Vessels were cleaned of perivascular fat, and all tissues were immediately placed on dry ice and kept at -80°C until use. Samples were homogenized in RIPA buffer (Cell Signaling Technology) containing protease inhibitors (Sigma-Aldrich). Tubes containing homogenates were freeze-thawed three times at -80°C and 37°C, respectively, and then centrifuged at 11,200 *g* for 20 min at 4°C. After determining protein concentration, samples prepared in Laemmli buffer (50 mM Tris pH 6.8, 10% SDS, 10% glycerol, 5% mercaptoethanol, and 2 mg/ml bromophenol blue) were boiled for 2 min, separated by sodium dodecyl sulfate-polyacrylamide gel electrophoresis (SDS-PAGE) on 7% polyacrylamide gels and transferred onto polyvinylidene fluoride membranes. Membranes were blocked in 5% nonfat dry milk in phosphate-buffered saline (PBS) containing 0.1% Tween 20 and then incubated overnight at 4°C with primary anti-Cav3.2 antibody (Mouse. NBP1-22444, 1:1,000 final dilution; Novus Biologicals). After washing, membranes were incubated with anti-mouse IgG-peroxidase-linked secondary antibody (1:5,000 final dilution; GE Healthcare) for 1 hr at room temperature. Blots were washed and

incubated in enhanced chemiluminescence reagents (ECL Prime, Amersham Bioscience), after which bands were detected using a ChemiDoc XRS+ Imaging System (Bio-Rad). An anti-Actin antibody (Mouse. sc-8432, 1:500 final dilution; Santa Cruz) was used as a loading control, and Precision Plus Protein Prestained Standard (Bio-Rad) was used as a molecular weight marker.

#### 4.7 | Immunohistostaining of mesenteric arteries for confocal imaging

*EHD2 del/+* and *EHD2 del/del* mice were anesthetized with 2% ketamine/10% rompun, perfused by 30 ml PBS and 50 ml 4% PFA (Roth, diluted in PBS), and afterward, vessels were dissected, and tissue pieces were further fixed for 4 hr in 4% PFA, transferred to 15% sucrose (in PBS, Merck) for 4 hr and incubated in 30% sucrose overnight. After embedding in TissueTek (Sakura), the tissue is frozen at -80°C and 8- $\mu\text{m}$  sections were obtained in a Leica cryostat at -30°C. For immunostainings, the cryostat sections were incubated with blocking buffer (1% donkey serum/1% Triton X-100/PBS), the first antibody was applied overnight at 4°C, and after washing with PBS/1% Tween, the secondary antibody and DAPI were applied for 2 hr. Afterward, the sections were embedded in ImmoMount (Thermo Scientific #9990402). The stained sections were analyzed with Zeiss LSM700 microscope provided with Zeiss 40x objective, and images were analyzed by ImageJ/Fij. Antibodies: anti-beta-actin-mouse (Sigma #A2228), anti-Cav3.2-rabbit (Alomone Labs #ACC-025), anti-mouse-Alexa488 (Invitrogen #R37114), anti-rabbit-Cy3 (Dianova #711-165-152), and DAPI (Sigma #D9542).

#### 4.8 | Vessel myography

Vessel myography was performed as previously described (Schleifenbaum et al., 2014) (Kassmann et al., 2019). Mesenteric arteries (third or fourth order) were mounted on glass cannula and superfused continuously with physiological saline solution (95% O<sub>2</sub> -5% CO<sub>2</sub>; pH, 7.4; 37°C) containing (mM): 119 NaCl, 4.7 KCl, 25 NaHCO<sub>3</sub>, 1.2 KH<sub>2</sub>PO<sub>4</sub>, 1.6 CaCl<sub>2</sub>, 1.2 MgSO<sub>4</sub>, and 11.1 glucose. The intravascular pressure was incrementally elevated from 20 to 100 mmHg using a pressure servo control system (Living System Instrumentation), and the inner diameter of the vessel was measured (Nikon Diaphot). The recording system was connected to a personal computer for data acquisition and analysis (HaSoTec). Arteries were equilibrated at 15 mmHg for 60 min and contractile responsiveness assessed by applying 60 mM KCl before starting experiments.

#### 4.9 | Materials

Fluo-4-AM was purchased from Molecular Probes (Eugene). Thapsigargin was purchased from Alomone Laboratories. All salts

and other drugs were obtained from Sigma-Aldrich or Merck. In cases where DMSO was used as a solvent, the maximal DMSO concentration after application did not exceed 0.5% (Kassmann et al., 2019; Tsvetkov et al., 2016).

#### 4.10 | Statistics

Data are presented as means  $\pm$  SEM. Statistically significant differences in mean values were determined by Student's unpaired *t* test or one-way analysis of variance (ANOVA) or Mann-Whitney *U* test. *p*-values < .05 were considered statistically significant; "n" represents the number of cells.

#### ACKNOWLEDGMENTS

M.G. is supported by grants from the Deutsche Forschungsgemeinschaft (DFG) and Deutscher Akademischer Austauschdienst (DAAD). G.F. is supported by the CSC (China Scholarship Council). Y.X. is supported by the Health Commission of Hunan and by the Science and Technology Department of Hunan. We acknowledge support from the Open Access Publication Fund of Charité-Universitätsmedizin Berlin.

#### CONFLICT OF INTEREST

None declared.

#### AUTHOR CONTRIBUTIONS

G.F., M.K., Y.C., D.T., C.M., S.K., C.Z., S.Z., and Y.X. were responsible for data collection, analysis, and interpretation. M.K. and M.G. were responsible for the conception and design of the experiments. G.F. and M.G. drafted the manuscript. All authors were responsible for interpretation of the data, contributed to the drafting, and revised the manuscript critically for important intellectual content. All authors have approved the final version of the manuscript and agreed to be accountable for all aspects of the work. All persons designated as authors qualify for authorship, and all those who qualify for authorship are listed.

#### DATA AVAILABILITY STATEMENT

I confirm that my article contains a Data Availability Statement even if no new data was generated (list of sample statements) unless my article type does not require one.

#### ORCID

Gang Fan  <https://orcid.org/0000-0003-1894-3253>

#### REFERENCES

- Abd El-Rahman, R. R., Harraz, O. F., Brett, S. E., Anfinogenova, Y., Mufti, R. E., Goldman, D., & Welsh, D. G. (2013). Identification of L- and T-type Ca<sup>2+</sup> channels in rat cerebral arteries: Role in myogenic tone development. *American Journal of Physiology Heart and Circulatory Physiology*, 304, H58–H71.
- Bakircioglu, M. E., Sievert, K.-D., Nunes, L., Lau, A., Lin, C.-S., & Lue, T. F. (2001). Decreased trabecular smooth muscle and caveolin-1 expression in the penile tissue of aged rats. *The Journal of Urology*, 166, 734–738.
- Bergdahl, A., & Sward, K. (2004). Caveolae-associated signalling in smooth muscle. *Canadian Journal of Physiology and Pharmacology*, 82, 289–299.
- Berrier, C., Coulombe, A., Szabo, I., Zoratti, M., & Ghazi, A. (1992). Gadolinium ion inhibits loss of metabolites induced by osmotic shock and large stretch-activated channels in bacteria. *European Journal of Biochemistry*, 206, 559–565.
- Boersma, E., Poldermans, D., Bax, J. J., Steyerberg, E. W., Thomson, I. R., Banga, J. D., ... Group DS (2001). Predictors of cardiac events after major vascular surgery: Role of clinical characteristics, dobutamine echocardiography, and  $\beta$ -blocker therapy. *JAMA*, 285, 1865–1873.
- Braunstein, T. H., Inoue, R., Cribbs, L., Oike, M., Ito, Y., Holstein-Rathlou, N. H., & Jensen, L. J. (2009). The role of L- and T-type calcium channels in local and remote calcium responses in rat mesenteric terminal arterioles. *Journal of Vascular Research*, 46, 138–151.
- Brenner, R., Pérez, G. J., Bonev, A. D., Eckman, D. M., Kosek, J. C., Wiler, S. W., ... Aldrich, R. W. (2000). Vasoregulation by the  $\beta$ 1 subunit of the calcium-activated potassium channel. *Nature*, 407, 870.
- Chen, C. C., Lamping, K. G., Nuno, D. W., Barresi, R., Prouty, S. J., Lavoie, J. L., ... Campbell, K. P. (2003). Abnormal coronary function in mice deficient in  $\alpha$ 1H T-type Ca<sup>2+</sup> channels. *Science*, 302, 1416–1418.
- Cheng, X., & Jaggar, J. H. (2006). Genetic ablation of caveolin-1 modifies Ca<sup>2+</sup> spark coupling in murine arterial smooth muscle cells. *American Journal of Physiology. Heart and Circulatory Physiology*, 290, H2309–2319.
- Chiang, C. S., Huang, C. H., Chieng, H., Chang, Y. T., Chang, D., Chen, J. J., ... Chen, C. C. (2009). The Ca(v)3.2 T-type Ca(2+) channel is required for pressure overload-induced cardiac hypertrophy in mice. *Circulation Research*, 104, 522–530.
- Ching, L. L., Williams, A. J., & Sitsapesan, R. (2000). Evidence for Ca<sup>2+</sup> activation and inactivation sites on the luminal side of the cardiac ryanodine receptor complex. *Circulation Research*, 87, 201–206.
- Chiossi, G., Costantine, M. M., Tamayo, E., Hankins, G. D., Saade, G. R., & Longo, M. (2016). Fetal programming of blood pressure in a transgenic mouse model of altered intrauterine environment. *The Journal of Physiology*, 594, 7015–7025.
- David, L. S., Garcia, E., Cain, S. M., Thau, E., Tyson, J. R., & Snutch, T. P. (2010). Splice-variant changes of the Ca(V)3.2 T-type calcium channel mediate voltage-dependent facilitation and associate with cardiac hypertrophy and development. *Channels (Austin)*, 4, 375–389.
- del Corso, C., Ostrovskaya, O., McAllister, C. E., Murray, K., Hatton, W. J., Gurney, A. M., ... Wilson, S. M. (2006). Effects of aging on Ca<sup>2+</sup> signaling in murine mesenteric arterial smooth muscle cells. *Mechanisms of Ageing and Development*, 127, 315–323.
- Essin, K., Welling, A., Hofmann, F., Luft, F. C., Gollasch, M., & Moosmang, S. (2007). Indirect coupling between Cav1.2 channels and ryanodine receptors to generate Ca<sup>2+</sup> sparks in murine arterial smooth muscle cells. *The Journal of Physiology*, 584, 205–219.
- Fan, G., Kaßmann, M., Hashad, A. M., Welsh, D. G., & Gollasch, M. (2018). Differential targeting and signalling of voltage-gated T-type Cav3.2 and L-type Cav1.2 channels to ryanodine receptors in mesenteric arteries. *The Journal of Physiology*, 596:4863–4877.
- Fernandez-Sanz, C., Ruiz-Meana, M., Miro-Casas, E., Nuñez, E., Castellano, J., Loureiro, M., ... Garcia-Dorado, D. (2014). Defective sarcoplasmic reticulum-mitochondria calcium exchange in aged mouse myocardium. *Cell Death & Disease*, 5, e1573.
- Filosa, J. A., Bonev, A. D., Straub, S. V., Meredith, A. L., Wilkerson, M. K., Aldrich, R. W., & Nelson, M. T. (2006). Local potassium signaling couples neuronal activity to vasodilation in the brain. *Nature Neuroscience*, 9, 1397–1403.
- Gollasch, M., Ried, C., Bychkov, R., Luft, F. C., & Haller, H. (1996). K<sup>+</sup> currents in human coronary artery vascular smooth muscle cells. *Circulation Research*, 78, 676–688.



- Gollasch, M., Wellman, G. C., Knot, H. J., Jaggar, J. H., Damon, D. H., Bonev, A. D., & Nelson, M. T. (1998). Ontogeny of local sarcoplasmic reticulum Ca<sup>2+</sup> signals in cerebral arteries: Ca<sup>2+</sup> sparks as elementary physiological events. *Circulation Research*, *83*, 1104–1114.
- Gottlieb, P. A., Suchyna, T. M., Ostrow, L. W., & Sachs, F. (2004). Mechanosensitive ion channels as drug targets. *Current Drug Targets-CNS & Neurological Disorders*, *3*, 287–295.
- Harraz, O. F., Abd El-Rahman, R. R., Bigdely-Shamloo, K., Wilson, S. M., Brett, S. E., Romero, M., ... Welsh, D. G. (2014). Ca(V)<sub>3.2</sub> channels and the induction of negative feedback in cerebral arteries. *Circulation Research*, *115*, 650–661.
- Hashad, A. M., Harraz, O. F., Brett, S. E., Romero, M., Kassmann, M., Puglisi, J. L., ... Welsh, D. G. (2018). Caveolae link CaV3.2 channels to BKCa-mediated feedback in vascular smooth muscle. *Arteriosclerosis, Thrombosis, and Vascular Biology*, *38*:2371–2381.
- Hashad, A. M., Mazumdar, N., Romero, M., Nygren, A., Bigdely-Shamloo, K., Harraz, O. F., ... Welsh, D. G. (2017). Interplay among distinct Ca<sup>2+</sup> conductances drives Ca<sup>2+</sup> sparks/spontaneous transient outward currents in rat cerebral arteries. *The Journal of Physiology*, *595*, 1111–1126.
- Headrick, J. P., Willems, L., Ashton, K. J., Holmgren, K., Peart, J., & Matherne, G. P. (2003). Ischaemic tolerance in aged mouse myocardium: The role of adenosine and effects of A1 adenosine receptor overexpression. *The Journal of Physiology*, *549*, 823–833.
- Hilgers, R. H., Kundumani-Sridharan, V., Subramani, J., Chen, L. C., Cuello, L. G., Rusch, N. J., & Das, K. C. (2017). Thioredoxin reverses age-related hypertension by chronically improving vascular redox and restoring eNOS function. *Science Translational Medicine*, *9*:eaf6094.
- Jaggar, J. H., Wellman, G. C., Heppner, T. J., Porter, V. A., Perez, G. J., Gollasch, M., ... Nelson, M. T. (1998). Ca<sup>2+</sup> channels, ryanodine receptors and Ca(2+)-activated K<sup>+</sup> channels: A functional unit for regulating arterial tone. *Acta Physiologica Scandinavica*, *164*, 577–587.
- Janczewski, A. M., & Lakatta, E. G. (1993). Thapsigargin inhibits Ca<sup>2+</sup> uptake, and Ca<sup>2+</sup> depletes sarcoplasmic reticulum in intact cardiac myocytes. *American Journal of Physiology-Heart and Circulatory Physiology*, *265*, H517–H522.
- Kassmann, M., Szijarto, I. A., Garcia-Prieto, C. F., Fan, G., Schleifenbaum, J., Anistan, Y. M., ... Gollasch, M. (2019). Role of ryanodine type 2 receptors in elementary Ca<sup>2+</sup> signaling in arteries and vascular adaptive responses. *Journal of the American Heart Association*, *8*, e010090.
- Knot, H. J., Standen, N. B., & Nelson, M. T. (1998). Ryanodine receptors regulate arterial diameter and wall [Ca<sup>2+</sup>] in cerebral arteries of rat via Ca<sup>2+</sup>-dependent K<sup>+</sup> channels. *The Journal of Physiology*, *508*, 211–221.
- Kuhbandner, S., Brummer, S., Metzger, D., Chambon, P., Hofmann, F., & Feil, R. (2000). Temporally controlled somatic mutagenesis in smooth muscle. *Genesis*, *28*, 15–22.
- Lewartowski, B., & Wolska, B. M. (1993). The effect of thapsigargin on sarcoplasmic reticulum Ca<sup>2+</sup> content and contractions in single myocytes of guinea-pig heart. *Journal of Molecular and Cellular Cardiology*, *25*, 23–29.
- Lian, X., Matthaues, C., Kassmann, M., Daumke, O., & Gollasch, M. (2019). Pathophysiological Role of Caveolae in Hypertension. *Front Med (Lausanne)*, *6*, 153.
- Löhn, M., Fürstenau, M., Sagach, V., Elger, M., Schulze, W., Luft, F. C., ... Gollasch, M. (2000). Ignition of calcium sparks in arterial and cardiac muscle through caveolae. *Circulation Research*, *87*, 1034–1039.
- Löhn, M., Lauterbach, B., Haller, H., Pongs, O., Luft, F. C., & Gollasch, M. (2001).  $\beta$ 1-Subunit of BK channels regulates arterial wall [Ca<sup>2+</sup>] and diameter in mouse cerebral arteries. *Journal of Applied Physiology*, *91*, 1350–1354.
- Lowalekar, S. K., Cristofaro, V., Radisavljevic, Z. M., Yalla, S. V., & Sullivan, M. P. (2012). Loss of bladder smooth muscle caveolae in the aging bladder. *Neurobiology and Urodynamics*, *31*, 586–592.
- Ludwig, A., Howard, G., Mendoza-Topaz, C., Deerinck, T., Mackey, M., Sandin, S., ... Nichols, B. J. (2013). Molecular composition and ultrastructure of the caveolar coat complex. *PLoS Biology*, *11*, e1001640.
- Matthaues, C., Lahmann, I., Kunz, S., Jonas, W., Melo, A. A., Lehmann, M., ... Mueller, D. N. (2019). EHD2-mediated restriction of caveolar dynamics regulates cellular lipid uptake. *bioRxiv*, 511709.
- McEwen, D. P., Li, Q., Jackson, S., Jenkins, P. M., & Martens, J. R. (2008). Caveolin regulates kv1.5 trafficking to cholesterol-rich membrane microdomains. *Molecular Pharmacology*, *73*, 678–685.
- Mikkelsen, M. F., Björling, K., & Jensen, L. J. (2016). Age-dependent impact of CaV3.2 T-type calcium channel deletion on myogenic tone and flow-mediated vasodilatation in small arteries. *The Journal of Physiology*, *594*, 5881–5898.
- Moosmang, S., Schulla, V., Welling, A., Feil, R., Feil, S., Wegener, J. W., ... Klugbauer, N. (2003). Dominant role of smooth muscle L-type calcium channel Cav1.2 for blood pressure regulation. *The EMBO Journal*, *22*, 6027–6034.
- Morén, B., Shah, C., Howes, M. T., Schieber, N. L., McMahon, H. T., Parton, R. G., ... Lundmark, R. (2012). EHD2 regulates caveolar dynamics via ATP-driven targeting and oligomerization. *Molecular Biology of the Cell*, *23*, 1316–1329.
- Nelson, M. T., Cheng, H., Rubart, M., Santana, L. F., Bonev, A. D., Knot, H. J., & Lederer, W. J. (1995). Relaxation of arterial smooth muscle by calcium sparks. *Science*, *270*, 633–637.
- Ohno-Iwashita, Y., Shimada, Y., Hayashi, M., & Inomata, M. (2010). Plasma membrane microdomains in aging and disease. *Geriatrics & Gerontology International*, *10*, S41–S52.
- Parton, R. G., & Simons, K. (2007). The multiple faces of caveolae. *Nature Reviews Molecular Cell Biology*, *8*, 185–194.
- Pérez, G. J., Bonev, A. D., Patlak, J. B., & Nelson, M. T. (1999). Functional coupling of ryanodine receptors to KCa channels in smooth muscle cells from rat cerebral arteries. *The Journal of General Physiology*, *113*, 229–238.
- Plüger, S., Faulhaber, J., Furstenau, M., Lohn, M., Waldschutz, R., Gollasch, M., ... Pongs, O. (2000). Mice with disrupted BK channel beta 1 subunit gene feature abnormal Ca<sup>2+</sup> spark/STOC coupling and elevated blood pressure. *Circulation Research*, *87*, E53–E60.
- Ratajczak, P., Damy, T., Heymes, C., Oliviero, P., Marotte, F., Robidel, E., ... Samuel, J. L. (2003). Caveolin-1 and -3 dissociations from caveolae to cytosol in the heart during aging and after myocardial infarction in rat. *Cardiovascular Research*, *57*, 358–369.
- Riehle, M., Büscher, A. K., Gohlke, B.-O., Kaßmann, M., Kolatsi-Joannou, M., Bräsen, J. H., ... Hoyer, P. F. (2016). TRPC6 G757D loss-of-function mutation associates with FSGS. *Journal of the American Society of Nephrology*, *27*:2771–2783.
- Sagara, Y., Fernandez-Belda, F., De Meis, L., & Inesi, G. (1992). Characterization of the inhibition of intracellular Ca<sup>2+</sup> transport ATPases by thapsigargin. *Journal of Biological Chemistry*, *267*, 12606–12613.
- Sagara, Y., & Inesi, G. (1991). Inhibition of the sarcoplasmic-reticulum Ca<sup>2+</sup> transport ATPase by thapsigargin at subnanomolar concentrations. *Journal of Biological Chemistry*, *266*, 13503–13506.
- Sausbier, M., Arntz, C., Bucurenciu, I., Zhao, H., Zhou, X. B., Sausbier, U., ... Ruth, P. (2005). Elevated blood pressure linked to primary hyperaldosteronism and impaired vasodilation in BK channel-deficient mice. *Circulation*, *112*, 60–68.
- Schleifenbaum, J., Kassmann, M., Szijártó, I. A., Hercule, H. C., Tano, J.-Y., Weinert, S., ... Alenina, N. (2014). Stretch-activation of angiotensin II type 1a receptors contributes to the myogenic response of mouse mesenteric and renal arteries. *Circulation Research*, *115*, 263–272.
- Seisenberger, C., Specht, V., Welling, A., Platzer, J., Pfeifer, A., Kühbandner, S., ... Hofmann, F. (2000). Functional embryonic cardiomyocytes after disruption of the L-type  $\alpha$ 1C (Ca<sub>v</sub>1.2) calcium channel gene in the mouse. *Journal of Biological Chemistry*, *275*, 39193–39199.

- Shvets, E., Bitsikas, V., Howard, G., Hansen, C. G., & Nichols, B. J. (2015). Dynamic caveolae exclude bulk membrane proteins and are required for sorting of excess glycosphingolipids. *Nature Communications*, 6, 6867.
- Simons, K., & Ehehalt, R. (2002). Cholesterol, lipid rafts, and disease. *The Journal of Clinical Investigation*, 110, 597–603.
- Stoeber, M., Schellenberger, P., Siebert, C. A., Leyrat, C., Helenius, A., & Grünewald, K. (2016). Model for the architecture of caveolae based on a flexible, net-like assembly of Cavin1 and Caveolin discs. *Proceedings of the National Academy of Sciences of the United States of America*, 113, E8069–E8078.
- Thastrup, O. (1990). Role of Ca<sup>2+</sup>-ATPases in regulation of cellular Ca<sup>2+</sup> signaling, as studied with the selective microsomal Ca<sup>2+</sup>-ATPase inhibitor, thapsigargin. *Agents and Actions*, 29, 8–15.
- Trollinger, D. R., Rivkah Isseroff, R., & Nuccitelli, R. (2002). Calcium channel blockers inhibit galvanotaxis in human keratinocytes. *Journal of Cellular Physiology*, 193, 1–9.
- Tsvetkov, D., Shymanets, A., Huang, Y., Bucher, K., Piekorz, R., Hirsch, E., ... Nurnberg, B. (2016). Better understanding of phosphoinositide 3-kinase (PI3K) pathways in vasculature: Towards precision therapy targeting angiogenesis and tumor blood supply. *Biochemistry-Moscow+*, 81, 691–699.
- Wang, S.-Q., Wei, C., Zhao, G., Brochet, D. X. P., Shen, J., Song, L.-S., ... Cheng, H. (2004). Imaging microdomain Ca<sup>2+</sup> in muscle cells. *Circulation Research*, 94, 1011–1022.
- Wirth, A., Wang, S., Takefuji, M., Tang, C., Althoff, T. F., Schweda, F., ... Offermanns, S. (2016). Age-dependent blood pressure elevation is due to increased vascular smooth muscle tone mediated by G-protein signalling. *Cardiovascular Research*, 109, 131–140.

#### SUPPORTING INFORMATION

Additional supporting information may be found online in the Supporting Information section.

**How to cite this article:** Fan G, Kaßmann M, Cui Y, et al. Age attenuates the T-type Ca<sub>v</sub>3.2-RyR axis in vascular smooth muscle. *Aging Cell*. 2020;19:e13134. <https://doi.org/10.1111/accel.13134>

**Publication #3:****Phosphodiesterase 3A and Arterial Hypertension**

Ercu M, Markó L, Schächterle C, Tsvetkov D, **Cui Y**, Maghsodi S, Bartolomaeus TUP, Maass PG, Zühlke K, Gregersen N, Hübner N, Hodge R, Mühl A, Pohl B, Illas RM, Geelhaar A, Walter S, Napieczynska H, Schelenz S, Taube M, Heuser A, Anistan Y-M, Qadri F, Todiras M, Plehm R, Popova E, Langanki R, Eichhorst J, Lehmann M, Wiesner B, Russwurm M, Forslund SK, Kamer I, Müller DN, Gollasch M, Aydin A, Bähring S, Bader M, Luft FC and Klussmann E. Phosphodiesterase 3A and Arterial Hypertension. *Circulation*. 2020;142:133-149.

Accepted: 2020 May 01; Published online: 2020 Jun 11.



Journal Data Filtered By: **Selected JCR Year: 2018** Selected Editions: SCIE, SSCI  
 Selected Categories: **"CARDIAC and CARDIOVASCULAR SYSTEMS"** Selected  
 Category Scheme: WoS  
**Gesamtanzahl: 136 Journale**

Rank	Full Journal Title	Total Cites	Journal Impact Factor	Eigenfactor Score
1	EUROPEAN HEART JOURNAL	57,358	23.239	0.125920
2	CIRCULATION	166,484	23.054	0.211290
3	JOURNAL OF THE AMERICAN COLLEGE OF CARDIOLOGY	100,986	18.639	0.193290
4	Nature Reviews Cardiology	6,301	17.420	0.018820
5	CIRCULATION RESEARCH	52,988	15.862	0.072290
6	EUROPEAN JOURNAL OF HEART FAILURE	13,107	13.965	0.027620
7	JAMA Cardiology	3,280	11.866	0.019320
8	JACC-Cardiovascular Imaging	8,801	10.975	0.026160
9	JACC-Cardiovascular Interventions	11,555	9.544	0.033640
10	JACC-Heart Failure	3,537	8.910	0.016830
11	JOURNAL OF HEART AND LUNG TRANSPLANTATION	12,436	8.578	0.027310
12	CARDIOVASCULAR RESEARCH	21,828	7.014	0.021500
13	European Heart Journal-Cardiovascular Pharmacotherapy	442	6.723	0.001430
14	Circulation-Heart Failure	6,900	6.526	0.022830
15	BASIC RESEARCH IN CARDIOLOGY	4,137	6.470	0.005590
16	PROGRESS IN CARDIOVASCULAR DISEASES	4,055	6.162	0.008860
17	JOURNAL OF THE AMERICAN SOCIETY OF ECHOCARDIOGRAPHY	10,478	6.111	0.016060
18	EUROPACE	10,908	6.100	0.025320
19	Circulation-Cardiovascular Interventions	5,289	6.060	0.016640

# Phosphodiesterase 3A and Arterial Hypertension

**BACKGROUND:** High blood pressure is the primary risk factor for cardiovascular death worldwide. Autosomal dominant hypertension with brachydactyly clinically resembles salt-resistant essential hypertension and causes death by stroke before 50 years of age. We recently implicated the gene encoding phosphodiesterase 3A (*PDE3A*); however, in vivo modeling of the genetic defect and thus showing an involvement of mutant *PDE3A* is lacking.

**METHODS:** We used genetic mapping, sequencing, transgenic technology, CRISPR-Cas9 gene editing, immunoblotting, and fluorescence resonance energy transfer. We identified new patients, performed extensive animal phenotyping, and explored new signaling pathways.

**RESULTS:** We describe a novel mutation within a 15 base pair (bp) region of the *PDE3A* gene and define this segment as a mutational hotspot in hypertension with brachydactyly. The mutations cause an increase in enzyme activity. A CRISPR/Cas9-generated rat model, with a 9-bp deletion within the hotspot analogous to a human deletion, recapitulates hypertension with brachydactyly. In mice, mutant transgenic *PDE3A* overexpression in smooth muscle cells confirmed that mutant *PDE3A* causes hypertension. The mutant *PDE3A* enzymes display consistent changes in their phosphorylation and an increased interaction with the 14-3-3 $\theta$  adaptor protein. This aberrant signaling is associated with an increase in vascular smooth muscle cell proliferation and changes in vessel morphology and function.

**CONCLUSIONS:** The mutated *PDE3A* gene drives mechanisms that increase peripheral vascular resistance causing hypertension. We present 2 new animal models that will serve to elucidate the underlying mechanisms further. Our findings could facilitate the search for new antihypertensive treatments.

**Maria Ercu, MS\***  
**Lajos Markó, MD, PhD\***  
 :  
**Enno Klusmann<sup>1</sup>, PhD**

\*M. Ercu and Dr Markó contributed equally.

The full author list is available on page 147.

**Key Words:** blood pressure ■ genetics  
 ■ hypertension ■ phosphodiesterases

Sources of Funding, see page 148

© 2020 American Heart Association, Inc.

<https://www.ahajournals.org/journal/circ>

## Clinical Perspective

### What Is New?

- This study provides evidence that mutant, overactive phosphodiesterase 3A causes hypertension in a new family with hypertension with brachydactyly and in novel rodent models.
- The mechanism underlying the hypertension resides inside vascular smooth muscle.

### What Are the Clinical Implications?

- The findings direct attention to new potential therapeutic targets for lowering blood pressure, namely, phosphodiesterase 3A signaling and protein-protein interactions within the vascular wall.

**H**ypertension is the primary risk factor for cardiovascular disease.<sup>1</sup> Mendelian genetics has elucidated blood pressure-elevating mechanisms.<sup>2</sup> We reported earlier that hypertension with brachydactyly type E (HTNB) is an autosomal dominant, non-salt-sensitive, form of hypertension.<sup>3</sup> If untreated, patients die of stroke by the age of 50 years. We found mutations in 7 independent HTNB families within a 15 base pair (bp) region of the phosphodiesterase (*PDE3A*) gene (Figure 1).<sup>4,5</sup> Since our reports, other families have been described, suggesting that a mutant *PDE3A* enzyme causes HTNB. However, *in vivo* modeling of the genetic defect to test this hypothesis has been lacking.

PDEs comprise 11 enzyme families degrading cAMP and cyclic guanosine monophosphate. Some enzymes degrade both, cAMP and cGMP, such as *PDE3A*.<sup>6</sup> *PDE3A* exists in 3 isoforms that are derived from a single gene and the same transcript.<sup>7</sup> They all contain the same catalytic domain and are similar in activity and inhibitor sensitivity but differ at their N terminus (Figure 1). *PDE3A1* is the major form in human heart, *PDE3A2* is the dominant isoform in human vascular smooth muscle cells (VSMCs), and *PDE3A3* is predominantly expressed in placenta.<sup>7</sup>

The HTNB mutations cause amino acid substitutions in *PDE3A1* and *A2* enzymes N-terminally of the catalytic domain. This region is not present in *PDE3A3* (Figure 1). The mutant enzymes are hyperactive, and 2 serine residues, S428 and S438, are aberrantly phosphorylated by protein kinase A (PKA) and protein kinase C; alanine substitutions decreased *PDE3A* activity.<sup>4</sup> We now report about an additional family with HTNB, whose mutation lies within the 15-bp regulatory region of the *PDE3A* gene. We present 2 novel animal models that support the hypothesis that mutant *PDE3A* causes HTNB and increases peripheral vascular resistance.

## METHODS

All supporting data are available within the article and in the [Data Supplement](#), which also includes further details. The analytic methods will be made available to other researchers for purposes of reproducing the results in their own laboratories on request.

### Analysis of Patient Mutations

The Ethical Committee of the Charité and the local Internal Review Boards approved the studies. Written informed consent, including consent for publication of results with images, was obtained from all participants. Patient DNA was analyzed with conventional Sanger sequencing.<sup>4</sup>

### Rat Model

State of Berlin authorities approved the rat studies according to American Physiological Society guidelines (license No. G 0435/17). The rat model (Figure 2) was generated by pronuclear microinjection of Sprague-Dawley rat zygotes with a mixture of 25 ng/μL Cas9 mRNA, 30 ng/μL Cas9 protein (both from IDT), and 12.5 ng/μL *in vitro*-transcribed gRNA with the sequence 5'-AGGCAGTCCTGTGGCAGAGG (IDT) to target the region in the rat *Pde3a* gene homologous to the human T445N mutation. The injected zygotes were cultured to the 2-cell stage and transferred into foster mothers according to established methods.<sup>8</sup> The offspring were genotyped by polymerase chain reaction with primers flanking the gRNA target region (*PDE3a5*, 5'-CTTCCGCTCCTTGCTTACC; *PDE3a3*, 5'-GTAAGTCCTCTGAGGAGACC) and sequencing of the polymerase chain reaction fragment.

### Animal Phenotyping and Interventions

Male rats (500–600 g, ≈9 months) were used in all experiments. They were anesthetized with isoflurane (CuraMed Pharma GmbH). The pressure-sensing HD-S10 device (Data Science International) was placed into the abdominal aorta, and the transmitters were placed into a subcutaneous pocket along the right flank. Blood pressure and heart rate were recorded by using the DATAQUEST software (A.R.T. 2.1, Data Sciences International).

Telemetry measurements after at least 1 week after recovery from implantation were recorded continuously at 5-minute intervals for 10 s continuously day and night in freely moving animals. The data were analyzed by using mixed-effects modeling. Animal identity and time point within a day were included as random effects. Genotype, animal sex, and day/night status at the time of measurement were included as fixed effects, using the R *lme4* package. The scopes of effects were obtained from the model parameters (slope and intercept parameters). The significance of each factor was assessed by comparing each linear model with a simpler model omitting the genotype as a predictor; here, likelihood ratio tests were performed as implemented in the *lmerTest* R package. Data were visualized using loess regressions from the *ggplot2* R package.

Left front paws were scanned *ex vivo* in a micro-computed tomography scanner (SkyScan 1276, Bruker). The vendor's software was used for image acquisition (v.1.0.8). For imaging posterior inferior cerebellar artery loops, rats were anesthetized with isoflurane (4%–5%) and



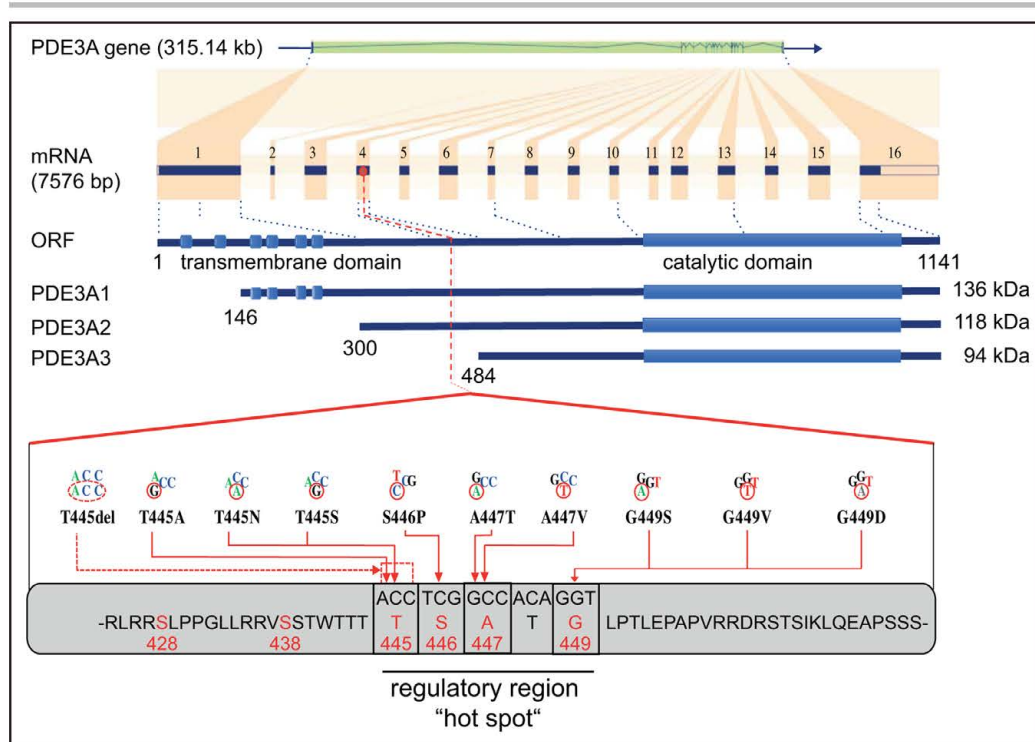


**Figure 1.** HTNB mutations are located in a 15-bp region of the *PDE3A* gene.

All the HTNB mutations known to date are shown. A conserved 15-bp regulatory hotspot region is invariably affected. The mutations in the 15-bp regulatory region alter the isoforms PDE3A1 and PDE3A2. HTNB indicates hypertension with brachydactyly, and ORF, open reading frame.

intracardially perfused with  $\approx 50$  mL of warm heparinized normal saline solution, followed by 8 mL of Microfil (Flow Tech, Inc) solution. The agent was allowed to harden (90 minutes); the brain was removed and kept in 4% paraformaldehyde solution overnight. Micro computed tomography was performed using a Skyscan 1276 scanner.

Echocardiography was performed (detector MS-250), and data were visualized and analyzed via the VEVO 2100 high-resolution imaging system (Visualsonics Fujifilm, VisualSonics).

Rats were treated with BAY 41-8543 (Cayman Chemical) in a formulation of Transcutol/Cremophor-EL/water (10%:20%:70%) per gavage to reach a dose of 3 mg/kg as described.<sup>9</sup>

Plasma and urine samples were measured at the Animal Phenotyping Platform of the Max Delbrück Center for Molecular Medicine (Berlin, Germany) using an AU480 Beckman Coulter chemistry analyzer. Circulating angiotensin levels and aldosterone and renin concentrations were measured by Attoquant Diagnostics GmbH (Vienna, Austria) as described earlier.<sup>10</sup>

### Vascular Isometric Contractions and Pressure Myography

Rat aortas were removed immediately after euthanizing the animals and dissected into 5-mm rings. In a Mulvany Small

Vessel Myograph (DMT 610 M; Danish Myo Technology), the rings were placed under a tension equivalent to that generated at 0.9 times the diameter of the vessel at 100 mmHg by stepwise distending vessels by using the LabChart DMT Normalization module. This normalization defined the passive diameter of the vessel at 100 mmHg. The basal tone of aortic rings was continuously monitored and adjusted to 1 g using the Organ Bath System (AD Instruments Ltd). The software Chart5 (AD Instruments) was used for data acquisition and display. After 60 minutes of equilibration, vessels were precontracted with phenylephrine until a stable resting tension was acquired and pharmacological agents were added into the bath. Tension is expressed as a percentage of the steady-state tension (100%) obtained with phenylephrine.

Pressure myography was performed as previously described.<sup>11</sup> Third-order mesenteric arteries were dissected from the rats and mounted on glass cannulas. They were perfused continuously with physiological saline solution containing (in mmol/L): 119 NaCl, 4.7 KCl, 25 NaHCO<sub>3</sub>, 1.2 KH<sub>2</sub>PO<sub>4</sub>, 1.6 CaCl<sub>2</sub>, 1.2 MgSO<sub>4</sub>, and 11.1 glucose, pH 7.4, under 95% O<sub>2</sub>-5% CO<sub>2</sub> at 37°C. The intravascular pressure was incrementally elevated from 20 to 100 mmHg using a pressure servo control system (Living System Instrumentation). We measured the vascular inner diameter with a video microscope (Nikon Diaphot) connected to a personal computer for data acquisition and analysis (HaSoTec). Arteries were equilibrated at

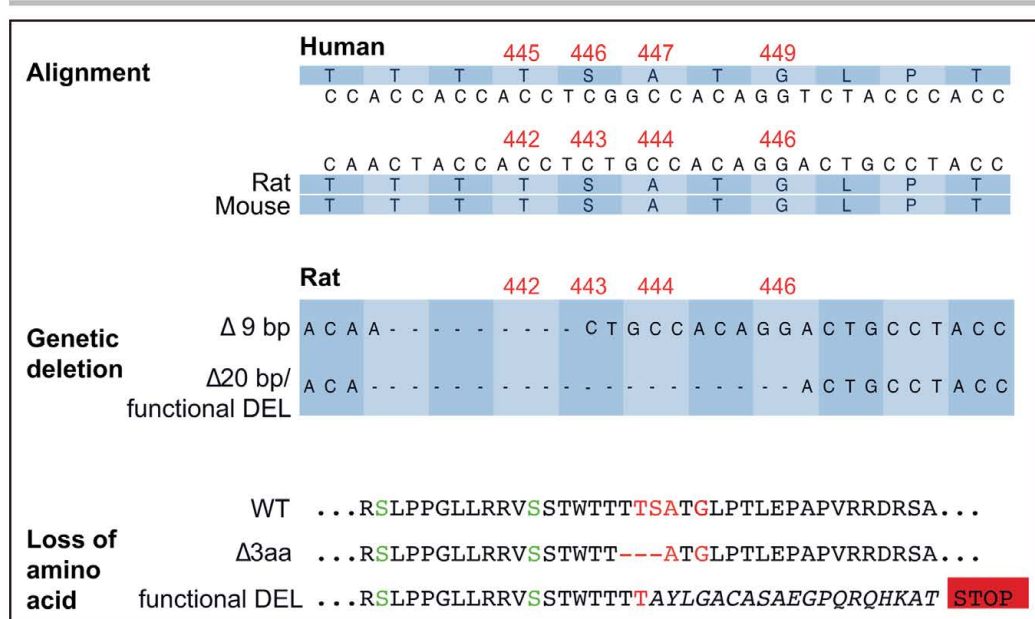


**Figure 2. A rat model of hypertension with brachydactyly**

A rat model harboring a 9-bp (3 amino acid) deletion ( $\Delta 3aa$ ) within the hotspot depicted in Figure 1 was generated with CRISPR/Cas9. A second model features a 20-bp deletion ( $\Delta 20$  bp) that results in a frameshift and thus in a truncated and functionally deleted protein (functional DEL). Sequences of human, mouse, and rat *PDE3A* genes and proteins are aligned. WT indicates wild-type.

15 mmHg for 60 minutes, and contractile responsiveness assessed by applying 60 mmol/L KCl.

### Histological Staining and cAMP Detection

Second-order rat mesenteric arteries were removed immediately after euthanizing the animals under isoflurane anesthesia. The vessels were dissected into 4-mm rings, and cAMP was measured using radioimmunoassays as described.<sup>12</sup> Alternatively, the second-order arteries were stained with hematoxylin-eosin (Sigma). Using an inverted microscope (Keyence BZ-9000) and imaging with Keyence BZ-9000 Analysis Software System, media-to-lumen area measurements were performed. Data were quantified by using Excel and GraphPad Prism.

### Cell Proliferation Assays

Thoracic aortas were obtained from male Sprague-Dawley rats, and VSMCs were isolated as previously described.<sup>13</sup> Primary VSMCs of passages 5 to 9 were counted using a sceptor device (Millipore Sceptor Handheld automated cell counter, No. PHCC00000).

### Plasmids and Antibodies

The vector encoding Flag-tagged PDE3A2<sup>3</sup> was modified by site-directed mutagenesis to encode the PDE3A2- $\Delta 3aa$  deletion. In addition, mCherry-tagged PDE3A2-T445N, PDE3A2-G449S, and PDE3A2- $\Delta 3aa$  were generated. The plasmid pcDNA3-ICUE3 was purchased from Addgene (Plasmid No.

61622). The following vectors were used as controls for the fluorescence resonance energy transfer (FRET) measurements: pcDNA3-cyan fluorescent protein (CFP; Plasmid No. 13030), mVenus-C1 (Plasmid No. 27794) and CFP-yellow fluorescent protein (YFP) tandem construct (kindly provide by Dr C. Rutz, Leibniz-Forschungsinstitut für Molekulare Pharmakologie [FMPI]).

Rats were immunized with peptides RR(pS428) LPPGLLRVSTW and RSLPPGLLRV(pS438)STW to generate antibodies against phosphoserine 428 and 438 (Eurogentec). The following antibodies were purchased: antiphospho-S312 antibody (University of Dundee), PDE3A (Bethyl; A302-740A), GAPDH (Cell Signaling; 14C10), the "anti-DDDDK tag coupled to Hrp" (Flag-Hrp) antibody (GeneTex; 77454), 14-3-3 $\theta$  (Santa Cruz; sc69720), smooth muscle actin (Cell Signaling; 14968), secondary antibodies antirabbit (No. 711-036-152), antimouse (No. 715-035-151), and antirat (No. 712-035-153) were from Jackson Immuno Research, and antisheep were from Invitrogen (No. 61-8620).

### FRET Measurements

HEK293 cells ( $3 \times 10^5$ ) were seeded on glass coverslips in 6-well plates and transfected to transiently express the sensor ICUE3<sup>14</sup> alone, to coexpress ICUE3 and PDE3A2-mCherry constructs, or the controls, CFP and Venus either alone or together, or a CFP-YFP tandem construct. FRET imaging was performed on an inverted confocal laser scanning microscope (CLSM510-META-NLO; Carl Zeiss) equipped with a Plan-Neofluar 40x/1.3 (Oil). CFP, excitation at 810 nm (Chameleon



diode-pumped laser; Coherent), emission 430 to 505 nm; Venus or YFP, excitation at 514 nm with an argon laser, emission 520 to 560 nm; mCherry, excitation at 543 nm, a LP 560-nm long-pass emission filter for fluorescence detection; FRET, excitation at 810 nm, emission at 430 to 655 nm. To calculate the FRET-based fluorescence, a  $\gamma$ -stack with a linear spectral unmixing mode was used to correct any YFP fluorescence cross talk into the FRET channel (523–532 nm). The  $\gamma$ -stack is an integral part of the confocal laser system software. YFP correction was performed to correct for direct excitation of the acceptor during donor excitation.

The effect of treatments with pharmacological agents on cAMP levels was expressed by changes in the FRET ratio, which is calculated by dividing the acceptor emission (Venus, 532 nm) by the donor emission (CFP, 458 nm).  $\Delta$ FRET (%) was calculated by subtracting the FRET ratio obtained on stimulation from the FRET ratio of the control condition and normalization of the value to the FRET ratio of the control condition and multiplying by 100 to yield percentage.

### Biochemical and Molecular Biological Methods

Immunoprecipitation, Western blotting, and quantitative reverse transcription polymerase chain reaction were performed as previously described.<sup>4,15,16</sup>

### Statistics

Statistically significant differences were determined by 1-way and 2-way ANOVA and Bonferroni multicomparison, Student *t* test, or log-rank (Mantel-Cox) test. *P* < 0.05 was accepted as significant. Telemetry data were analyzed by likelihood ratio comparisons of nested mixed-effects models assessing whether genotype adds predictive power to a model already containing animal identity and time as random effects, and day-night stage as fixed effect, using the R lme4 and lmer packages.

## RESULTS

### Mutation in a Hot Spot Region of the PDE3A Gene Causes HTNB

A woman aged 54 years (Figure 3; I/2; [Data Supplement Material, Table I in the Data Supplement](#)) with a 17-year history of hypertension was admitted to hospital with a blood pressure of 190/100 mmHg. The short fingers and toes are documented in the photograph and the roentgenogram (Figure 3). Our analysis of the patient and her 23-year-old daughter revealed a mutation in exon 4 of the *PDE3A* gene causing a G449S (glycine-to-serine) substitution in the enzyme. Earlier, others and we had reported a G449D substitution.<sup>5,17</sup> In addition, a S446P substitution<sup>18</sup> and a 3-bp T445del was discovered in HTNB families.<sup>19</sup> Thus, all HTNB mutations affect a region of 15 bp in exon 4 of the *PDE3A* gene encoding a 5-amino-acid segment (amino acids 445–449) N-terminally of the catalytic domain (Figure 1).

### Pde3a Mutation Recapitulates HTNB in a Rat Model

To prove that mutations in the mutational hotspot of the *PDE3A* gene cause HTNB, we generated animal models. The rat model exhibits a 9-bp deletion within the hotspot that leads to the loss of 3 amino acids (aa 441–443 analogous to human PDE3A aa 444–446; Figure 2). The  $\Delta$ 3aa deletion corresponds to the human deletion, T445del.<sup>19</sup> Because HTNB is autosomal dominant, the heterozygous condition matches the situation in the patients. We also generated a rat strain with a frame-shift mutation ( $\Delta$ 20 bp) that produces a truncated protein and, when homozygous, a functional deletion (DEL) of PDE3A.

In aortas of the wild-type (WT) and the heterozygous (HET)  $\Delta$ 3aa rats, 2 PDE3A isoforms were detected, corresponding in size to PDE3A1 and A2. The expression of both isoforms was reduced in the  $\Delta$ 3aa HET rats, which may be attributable to altered phosphorylation and protein-protein interactions of the mutant enzyme (see later in this article) and thus altered detection by our antibody. The remaining wild-type allele encoding the PDE3A isoforms apparently did not compensate the reduction in expression. Both proteins were undetectable in the homozygous functional DEL animals (Figure 4A). Micro computed tomography imaging of the left front paws confirmed short fingers typical for HTNB; metacarpal bone III was significantly shorter (Figure 4B) and its volume was significantly smaller ([Figure IA in the Data Supplement](#)) in the  $\Delta$ 3aa HET rats than in the WT rats. Also, the  $\Delta$ 3aa HET animals were  $\approx$ 20% lighter than the WT rats ([Figure IB in the Data Supplement](#)).

Radiotelemetry was performed at age >9 months. The data show mean systolic and diastolic blood pressure values of 148/105 mmHg in  $\Delta$ 3aa HET rats, whereas the functional DEL rats had systolic and diastolic blood pressure values of 115/84 mmHg. WT rats had systolic and diastolic blood pressure values at 125/88 mmHg. We have encountered no homozygous patients in our PDE3A families; however, we crossed the  $\Delta$ 3aa HET rats to produce a homozygous  $\Delta$ 3aa/ $\Delta$ 3aa strain (HOM). Their blood pressure was 155/120 mmHg (Figure 4C). The WT, the  $\Delta$ 3aa HET, and HOM rats had similar heart rates (WT, 297 beats/min;  $\Delta$ 3aa HET, 293 beats/min; and  $\Delta$ 3aa HOM, 294 beats/min) that were all lower than those of the PDE3A functional DEL animals (330 beats/min; for statistical analysis; [Table II in the Data Supplement](#)). The echocardiographic estimates of cardiac output, ejection fraction, and further cardiac parameters in the  $\Delta$ 3aa HET and HOM rats were not significantly altered in comparison with WT animals (Figure 4D, [Figure IC in the Data Supplement](#)). We described possible neurovascular aberrations in 15 patients with HTNB. The patients all had left-side posterior inferior cerebellar artery or vertebral artery loops.<sup>20</sup>

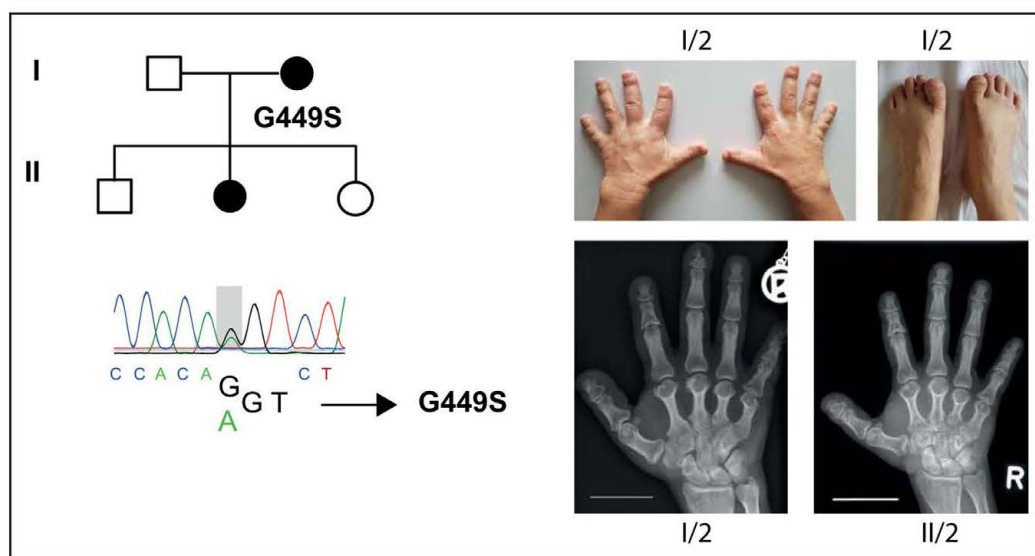


**Figure 3. A G449S substitution in PDE3A is associated with hypertension with brachydactyly.**

A novel amino acid substitution, G449S, encoded in the mutational hotspot region of the *PDE3A* gene was identified (see also Figure 1). Shown are photographs and roentgenograms of the mother's hands and feet (age 54 years; I/2). The hypertension and skeletal phenotypes are similar to those described earlier.<sup>4</sup>

Micro computed tomography imaging of brain vessels revealed that the  $\Delta 3aa$  HET rats also exhibited posterior inferior cerebellar artery loops. Loops were not detected in any WT animal (Figure 4E).

The aortas of WT,  $\Delta 3aa$  HET, and PDE3A functional DEL rats did not exhibit an increased size of the media (Figure 4D in the Data Supplement). To test their function, aortic rings from the rats were precontracted with phenylephrine. Adenylyl cyclase stimulation with forskolin triggered about a 40% reduced relaxation of rings from  $\Delta 3aa$  HET rats (relatively resistant) and an increased relaxation of rings from PDE3A functional DEL rats in comparison with the WT controls (Figure 4F). In patients with HTNB, an increased peripheral resistance and hyperplasia of peripheral arterial *Tunica media* are the only hypertension-relevant features. Similar to the human situation, the median-to-lumen ratio of second-order mesenteric arteries of the  $\Delta 3aa$  HET rats was increased in comparison with the WT animals. In the functional DEL animals, the ratio was decreased in comparison with WT animals (Figure 4G). Moreover, because of the hyperactivity of the  $\Delta 3aa$  PDE3A variant (see later in this article), the cAMP values were lower in such vessels derived from  $\Delta 3aa$  HET than in those from WT animals (Figure 4H).

Next, we pressurized third-order rat mesenteric arteries isolated from WT and  $\Delta 3aa$  HET rats (Figure 4I). Myogenic tone was assessed over a range of intraluminal pressures between 20 and 100 mmHg. The myogenic tone of the vessels was similar at all pressures. However, the pressurized (100 mmHg) vessels from

$\Delta 3aa$  HET rats showed weaker vasodilation in response to forskolin than those from WT animals. The diameter of vessel from the  $\Delta 3aa$  HET rats changed by  $\approx 5\%$  in comparison with the 10% change in the WT animals (Figure 4I). The data indicate that the basal myogenic tone is not affected by mutant PDE3A (see later in this article), but that, on stimulation of the adenylyl cyclase/cAMP system, the hyperactivity of PDE3A (see later in this article) limits the ability of small arteries to dilate. The data confirm our findings obtained by wire myography (Figure 4F).

We had previously observed that patient-derived stem cells differentiated into VSMC grew at a faster rate than those of unaffected family members.<sup>4</sup> The proliferation rate of VSMC from the  $\Delta 3aa$  HET rats was increased similarly to those of VSMC from WT or functional DEL animals. The cell number after 120 hours in culture was 50% higher than the number of WT cells (Figure 4J). As in mouse VSMC where *Pde3a* was deleted,<sup>21</sup> the VSMC from our PDE3A functional DEL rats grew at a rate similar to the those from the WT animals. Transient expression of the  $\Delta 3aa$  PDE3A2 version in HEK293 cells also led to higher proliferation rates than expression of the WT (data not shown).

PDE3A is inhibited by cGMP.<sup>22</sup> To stimulate cGMP synthesis in our WT and  $\Delta 3aa$  HET rats, we treated the animals with a single-gavage dose (3 mg/kg) of a soluble guanylyl cyclase (sGC) stimulator, BAY 41-8543, as previously described.<sup>9</sup> The compound is a derivative of the drug, riociguat, which is approved for the treatment of pulmonary hypertension in similar doses (maximal daily



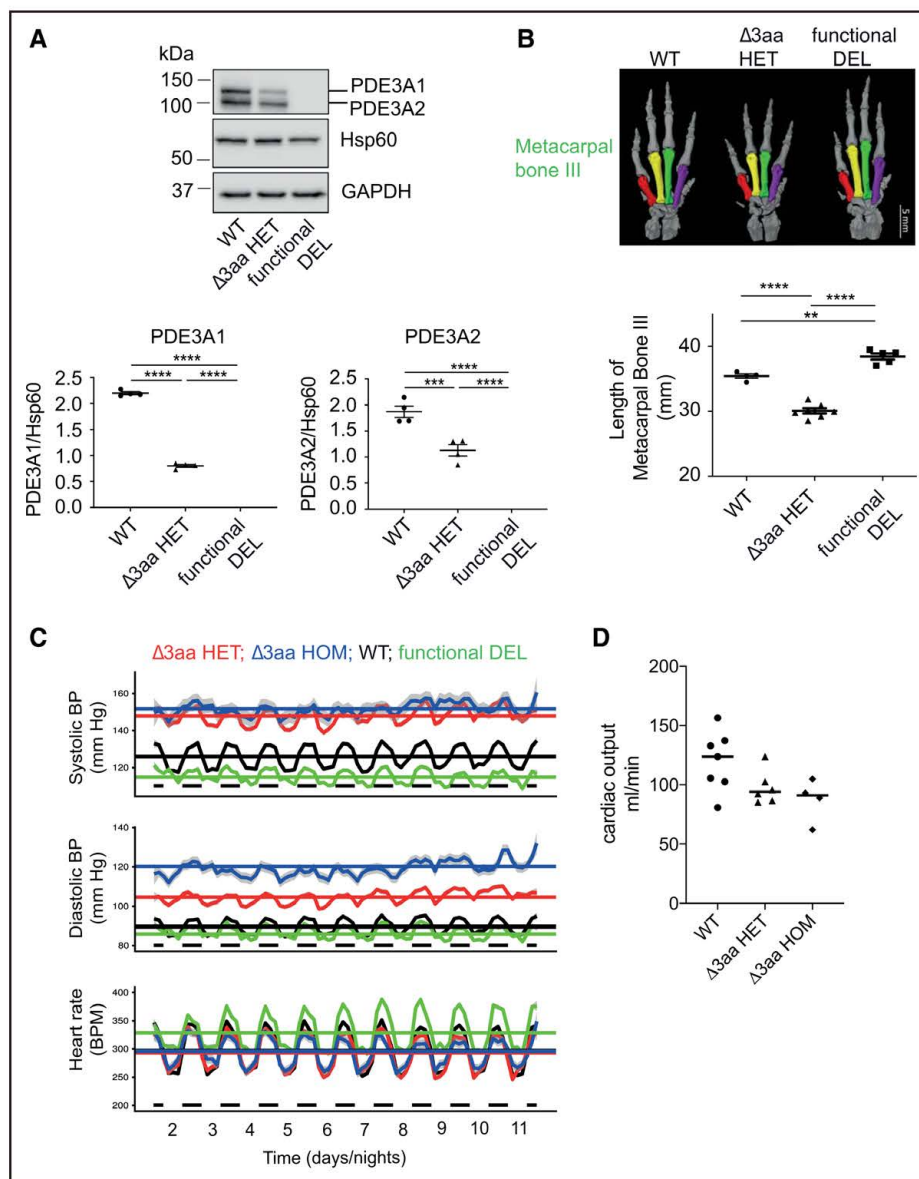


**Figure 4. A rat model expressing mutant *PDE3A* recapitulates hypertension with brachydactyly.**

**A**, Detection of PDE3A1 and PDE3A2 in the aortas of WT,  $\Delta 3aa$  HET, and the rat model without expression of PDE3A (functional DEL) by Western blotting. The expression of the PDE3A isoforms was not detectable in the functional DEL animals. **Lower**, Semiquantitative analysis of the expression of the 2 isoforms by densitometry of the signals.  $n=4$  independent experiments; data are mean $\pm$ SEM, \*\*\*\* $P<0.0001$ , \*\*\*\* $P<0.0001$ . **B**, The affected  $\Delta 3aa$  HET rats had shorter forepaw metacarpal bones III than WT and the functionally deleted (functional DEL) PDE3A rats (WT=4,  $\Delta 3aa$  HET=7, PDE3A functionally deleted=5). The images were obtained by microCT measurements of the left forepaw. Quantitation is from the metacarpal bone III; data are mean $\pm$ SEM, \*\* $P<0.01$ , \*\*\*\* $P<0.0001$ . **C**, Heterozygous  $\Delta 3aa$  (red), homozygous  $\Delta 3aa$  (blue), WT (black), PDE3A functionally deleted (DEL; green) rats were monitored for >10 days with radiotelemetry. The plots show blood pressure (systolic/diastolic mmHg), and heart rate (beats per minute, BPM) over time (horizontal axis, night phases marked in black). Curves show loess fits made using R package ggplot2 with gray intervals indicating 95% CIs for loess parameters. Horizontal lines represent model expectation value for WT and the mutant rats. Lower black bars depict night periods. The systolic blood pressure between all groups is significantly different. Only the systolic blood pressures of  $\Delta 3aa$  HET and HOM rats were not significantly different. The diastolic blood pressure differs significantly between all groups. The heart rate is only significantly different between the functional DEL and  $\Delta 3aa$  HET and the functional DEL and the  $\Delta 3aa$  HOM. All  $P$  values are listed in Table II in the Data Supplement. Significance (nested model likelihood ratio test  $P$  value) and effect size (model fit parameter, same unit as vertical axis) is noted. (Continued)



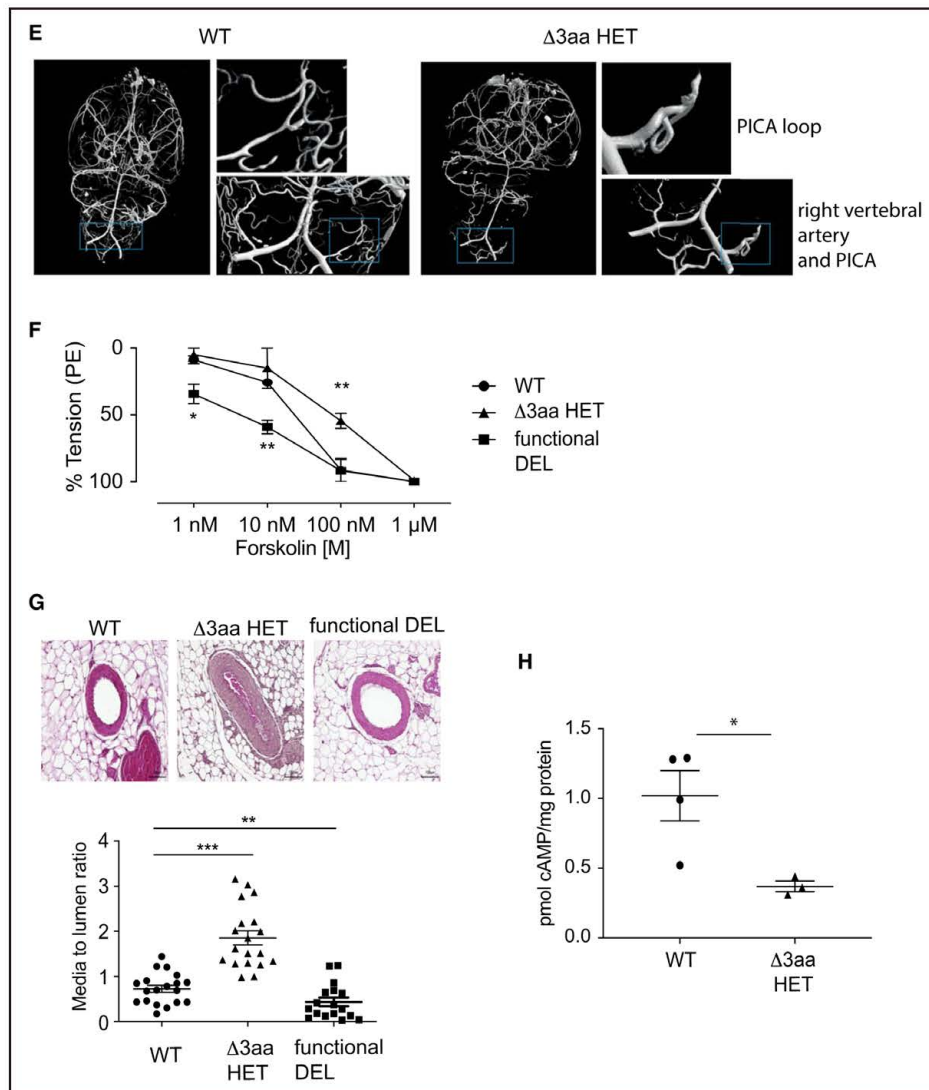


**Figure 4 Continued.** **D**, Cardiac output of WT, heterozygous  $\Delta 3aa$ , and homozygous  $\Delta 3aa$  PDE3A rats was estimated by echocardiography. Cardiac output was measured by tracing the endocardium in systole and diastole of a parasternal long axis view of the left ventricle. The differences were statistically not significant. **E**, Heterozygous  $\Delta 3aa$  PDE3A rats show loops in the posterior inferior cerebellar arteries (PICA). Brain vessels were perfused with Microfil and visualized using microCT. Shown are representative images from  $n=2$   $\Delta 3aa$  HET and  $n=5$  WT rats. **F**, Myograph experiments using aortic rings document that the  $\Delta 3aa$  HET rats have lower relaxation capacity in response to forskolin (adenylate cyclase stimulator) than WT aortic rings and rings from the PDE3A functionally deleted (DEL) rats (WT,  $n=3$ ;  $\Delta 3aa$  HET,  $n=4$ ; PDE3A functional DEL,  $n=4$ ); data are mean $\pm$ SEM, \* $P<0.05$ , \*\* $P<0.01$ . **G**, The media to lumen ratio of second-order mesenteric arteries in  $\Delta 3aa$  HET rats is increased in comparison with WT animals. Presented are representative images from 3 to 5 mesenteric arteries per rat.  $n=3$  WT,  $n=3$   $\Delta 3aa$  HET, and  $n=2$  functional DEL rats. The quantification shows mean $\pm$ SEM. \*\* $P<0.01$ , \*\*\* $P<0.001$ . **H**, The concentration of cAMP in resting second-order mesenteric arteries is lower in  $\Delta 3aa$  HET rats than in WT animals. The cAMP levels were determined by radioimmunoassay. Second-order mesenteric arteries were obtained from 2 animals per group, cAMP was measured in  $n=4$  arteries from WT and  $n=3$  arteries from  $\Delta 3aa$  HET rats, mean $\pm$ SEM, \* $P<0.05$ . **I**, The myogenic tone of rat third-order mesenteric arteries from WT and  $\Delta 3aa$  HET rats was determined. **Upper**, Diameter of mesenteric arteries recorded during pressure steps incrementally elevated from 20 to 100 mmHg. Vessels were incubated in physiological salt solution (PSS, +Ca<sup>2+</sup>) or Ca<sup>2+</sup>-free PSS (-Ca<sup>2+</sup>). **Lower left**, Myogenic tone expressed as dilation of vessels induced by Ca<sup>2+</sup>-free PSS. **Lower middle and right**, Pressurized (100 mmHg) mesenteric arteries ( $n=4$  vessels from 4 rats) from  $\Delta 3aa$  HET showed weaker dilation in response to forskolin than vessels from WT rats ( $n=3$  from 3 rats). Dotted line shows the diameter of a WT vessel (320  $\mu$ m) and of a  $\Delta 3aa$  HET vessel (500  $\mu$ m). \* $P<0.05$ . **J**, Primary VSMC derived from aorta of  $\Delta 3aa$  HET rats proliferate faster than those from WT and PDE3A functionally deleted (DEL) rats. VSMC from  $n=6$  animals per group were counted every 24 hours. Shown are mean $\pm$ SEM, \* $P<0.05$ . (Continued)

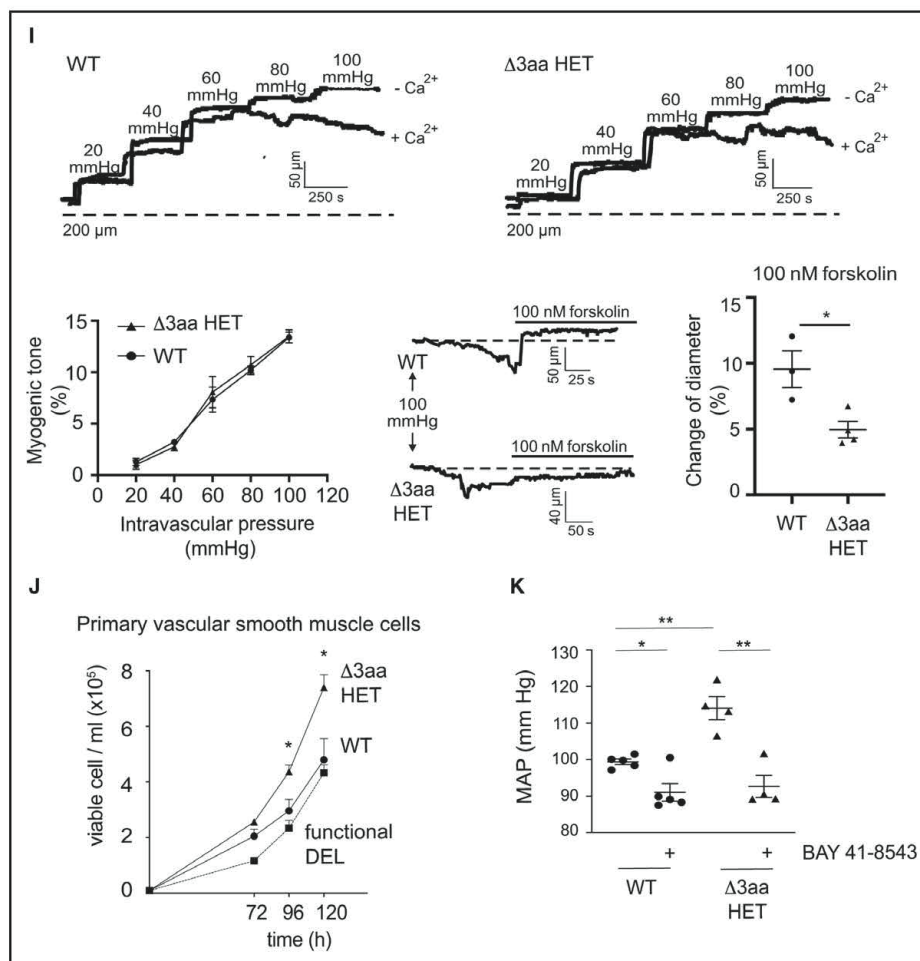


**Figure 4 Continued.** **K**, WT and  $\Delta 3aa$  HET rats were submitted to blood pressure–lowering treatments and found that a single gavage dose (3 mg/kg) of the soluble guanylyl cyclase stimulator BAY 41-8543 lowered the mean arterial pressure (MAP) within 3 hours in  $\Delta 3aa$  HET to a level similar to WT rats,  $n=5$  WT and  $n=4$   $\Delta 3aa$  HET rats, mean $\pm$ SEM, \* $P<0.05$ , \*\* $P<0.01$ . HET indicates heterozygous; HOM, homozygous; microCT indicates micro computed tomography; PE, phenylephrine VSMC, vascular smooth muscle cells; and WT, wild-type.

dose of 7.5 mg). HEK293 cells express sGC, and BAY 41-8543 raised the cGMP level and caused inhibition of WT PDE3A2 and stronger of the  $\Delta 3aa$  version (Figure IE in the Data Supplement, see later in this article). Within 3 hours, BAY 41-8543 reduced the mean arterial blood pressure in the  $\Delta 3aa$  HET to levels lower than in the WT animals (ie, from 114 to 92 mmHg in the  $\Delta 3aa$  HET rats and from 99 to 91 mmHg in the WT animals). The levels that were reached were similar (Figure 4K). The lower levels were stable for  $\approx 12$  hours; blood pressure reached original levels after  $\approx 24$  hours. A further single-gavage dose treatment of the same animals, 24 hours after the initial administration, had effects similar to those of the first treatment (Figure IF in the Data Supplement).

We also generated a conditional mouse model that expresses the T445N-encoding mutation as a human PDE3A2 transgene in smooth muscle cells (Figure IIA in the Data Supplement). Hemizygous transgenic mice were used for the analysis (MyhCre+/PDE3A2-T445N+). As controls, littermate mice not expressing the transgene were used. Mice overexpressing WT PDE3A2 were not available. The transgenes were reduced in body weight and lived for a shorter time than the control animals (Figure IIB in the Data Supplement). The reason for the smaller litter sizes and shorter survival rates of the mutants is unclear. The protein and human transgene PDE3A2 mRNA were detected in bladders, aortas, and first- and second-order

mesenteric arteries of the mutant animals, but not in the controls. However, leaky expression of the transgene in skeletal muscle was observed. mRNA expression of the endogenous mouse *Pde3a* was detected in all tissues to similar degrees in transgenic and control animals (Figure IIC and IID in the Data Supplement). The transgenic mice were hypertensive with systolic blood pressure of  $\approx 126$  mmHg, diastolic blood pressure of  $\approx 85$  mmHg, whereas controls were 115/84 mmHg, and their heart rate was decreased (Figure IIE in the Data Supplement). The blood pressure data of 2 mice, not included in the analysis because they did not survive the 10-day radiotelemetry observation, are documented in Figure IIF in the Data Supplement. One mouse had a blood pressure of 155/125 mmHg for 5 days before it died. Another mouse was fairly normotensive for 5 days and then developed a massive increase in blood pressure to 270/200 mmHg before it died. The media of aorta from the transgenes was not different from the control animals (Figure IIG in the Data Supplement). Mesenteric arteries from the transgene-expressing mice, precontracted with the adrenergic agent phenylephrine, reached  $\approx 25\%$  less dilation than the arteries from control animals in response to stimulation with forskolin (Figure IIH in the Data Supplement), suggesting an enhanced level of cAMP

degradation. Thus, the mouse model underscores that hyperactive PDE3A2 in VSMC results in hypertension.

### Serum and Urine Parameters in HTNB Models Are in the Physiological Range

We next evaluated serum and urine parameters in our animal models. All parameters (Table) were similar in WT and  $\Delta 3aa$  HET rats. Chloride in urine, the fractional sodium and chloride excretion in the functional DEL rats were significantly greater than in WT animals. The reason for the differences is unknown. Serum and urine parameters of the transgenic mice were not different from the control animals (Table III in the Data Supplement). Furthermore, we found no proteinuria or perturbed renal function in the mutant animals. Albumin, creatinine, and urine/albumin creatinine ratios were not different in comparison with WT animals (Table, Table III in the Data Supplement).

Angiotensin-II levels, angiotensinogen, aldosterone, and plasma renin concentrations were also not significantly different between the control and mutant rats (Figure 5 and Table). The mRNA expression of the renal damage markers *Lcn2* and *Havcr1* was not altered in the  $\Delta 3aa$  HET rats in comparison with WT; however, in the functional DEL rats, *Lcn2* was upregulated (Figure

**Table. Plasma and Urine Parameters Determined of Wild-Type (WT), Heterozygous ( $\Delta 3aa$  HET), and Functional Deletion (DEL) Rats**

Parameters	WT	$\Delta 3aa$ HET	Functional DEL
Serum or plasma			
Sodium, mmol/L	141.68 $\pm$ 1.57	140.88 $\pm$ 0.90	141.14 $\pm$ 1.8
Potassium, mmol/L	5.97 $\pm$ 0.24	5.33 $\pm$ 0.59	4.76 $\pm$ 0.42
Chloride, mmol/L	101.74 $\pm$ 0.46	102.40 $\pm$ 1.67	100.68 $\pm$ 2.13
Urea nitrogen, mg/dL	35.42 $\pm$ 3.99	39.40 $\pm$ 3.86	33.34 $\pm$ 0.37
Creatinine, mg/dL	0.35 $\pm$ 0.04	0.32 $\pm$ 0.02	0.38 $\pm$ 0.06
Cystatin, mg/L	0.23 $\pm$ 0.04	0.23 $\pm$ 0.02	0.21 $\pm$ 0.03
Angiotensinogen, $\mu$ g/mL	22.07 $\pm$ 2.73	21.56 $\pm$ 3.51	21.40 $\pm$ 1.52
Renin, ng angiotensin I·mL <sup>-1</sup> ·h <sup>-1</sup>	6.14 $\pm$ 6.04	2.37 $\pm$ 1.44	9.43 $\pm$ 10.63
Urine			
Sodium, mmol/L	57.95 $\pm$ 30.88	54.22 $\pm$ 28.17	96.11 $\pm$ 39.79
Potassium, mmol/L	88.74 $\pm$ 46.75	106.63 $\pm$ 24.55	109.58 $\pm$ 21.70
Chloride, mmol/L	78.52 $\pm$ 33.83	78.74 $\pm$ 15.96	125.14 $\pm$ 29.41 #( <i>P</i> =0.03)
Urea nitrogen, mg/dL	1621.70 $\pm$ 650.72	1732.11 $\pm$ 195.83	1859.35 $\pm$ 423.59
Creatinine, mg/dL	34.60 $\pm$ 15.59	32.38 $\pm$ 5.07	34.10 $\pm$ 7.49
Albumin, mg/dL	0.13 $\pm$ 0.10	0.15 $\pm$ 0.12	0.51 $\pm$ 0.36
Calculated			
FENa, %	0.46 $\pm$ 0.21	0.37 $\pm$ 0.15	0.75 $\pm$ 0.25 *( <i>P</i> =0.03)
FEK, %	18.04 $\pm$ 5.72	19.95 $\pm$ 5.40	25.94 $\pm$ 5.11
FECl, %	0.79 $\pm$ 0.06	0.75 $\pm$ 0.05	1.38 $\pm$ 0.20 #( <i>P</i> <0.001)
Urine/albumin creatinine, mg/mmol	0.49 $\pm$ 0.54	0.58 $\pm$ 0.49	1.60 $\pm$ 0.85

Shown are plasma, urine, and calculated values. Statistical comparison was performed by 1-way analysis of variance. *n*=4 to 5 animals per group. \**P*<0.05 vs  $\Delta 3aa$  HET and #*P*<0.05 vs WT and  $\Delta 3aa$  HET, Tukey post hoc test. Values are mean $\pm$ SD. FE indicates fractional excretion.



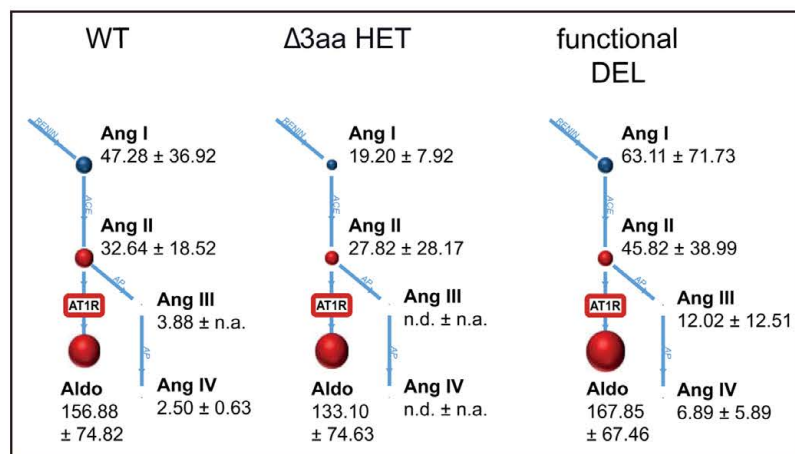


**Figure 5.** Schematic representation of the renin-angiotensin-aldosterone system in wild-type and mutant rats

The indicated parameters of the renin-angiotensin-aldosterone system were investigated in wild-type (WT), heterozygous  $\Delta 3aa$  (HET), and PDE3A functionally deleted (DEL) rats. Similar sizes of spheres indicate similar relative concentrations (all in pmol/L).  $n=5$  animals per group. Values are means $\pm$ SD. ALDO indicates aldosterone; Ang, angiotensin; n.a., not available; and n.d., not determinable.

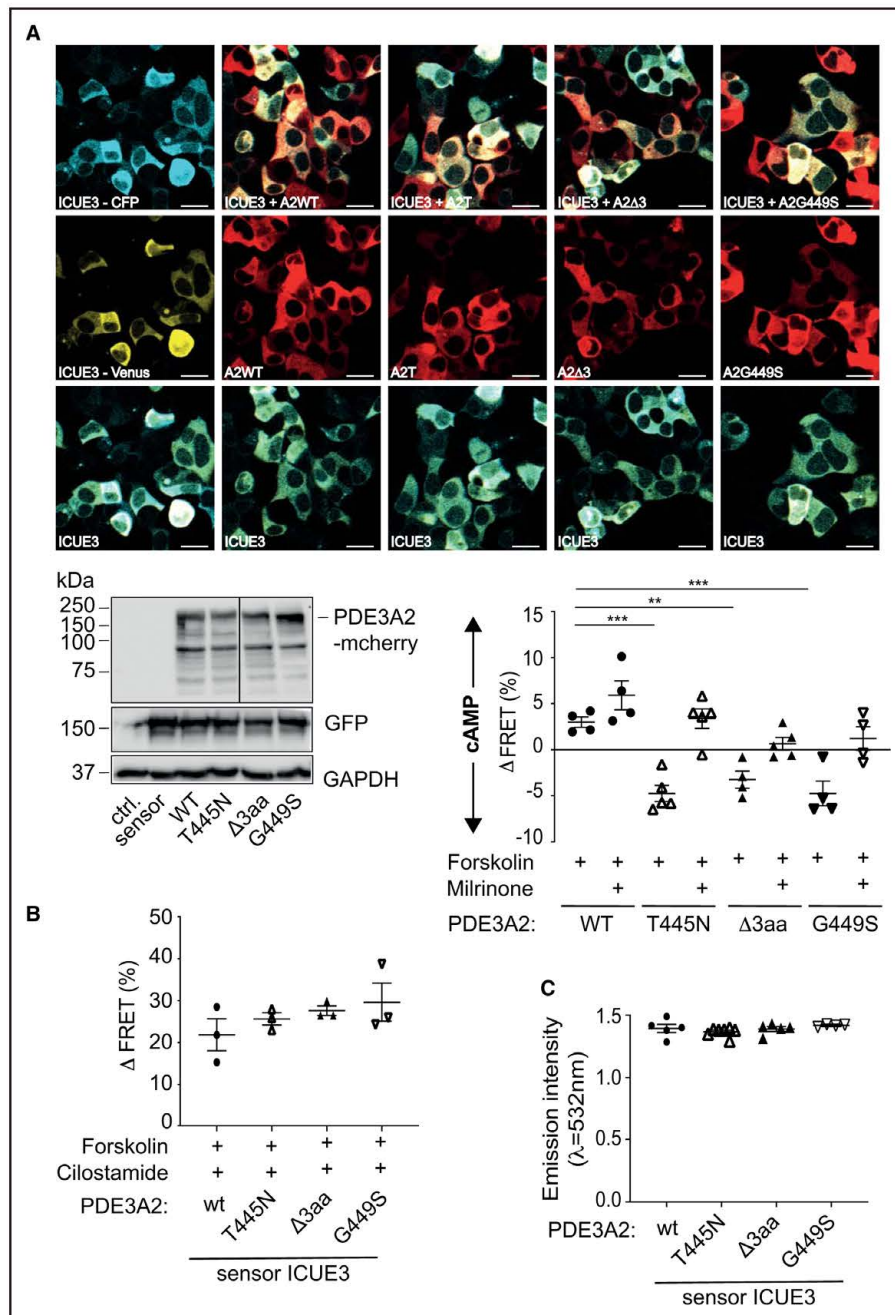
IG in the Data Supplement). Similarly, in our transgenic mice, angiotensin-II levels, angiotensinogen, aldosterone, and plasma renin concentrations or *Lcn2* and *Havcr1* were not altered in comparison with control animals (Figure III and IIJ in the Data Supplement, Table III in the Data Supplement). Thus, our  $\Delta 3aa$  HET rat and the transgenic mouse models resemble our patients, who, aside from stroke, also had little evidence of target-organ damage, and hardly deviate from values observed in patients with essential hypertension.<sup>23</sup>

### Aberrant Signaling of HTNB PDE3A2 Mutants

To obtain insight into the molecular mechanisms underlying the HTNB phenotype, we measured the activity of our new mutant G449S and the  $\Delta 3aa$  variants using FRET in HEK293 cells. The cytosolic cAMP sensor, ICUE3,<sup>14</sup> consists of a cAMP binding domain of exchange protein directly activated by cAMP (Epac) flanked by cyan fluorescent protein (CFP) and Venus, a variant of YFP. On cAMP binding, the sensor undergoes a conformational change that increases the distance between CFP and Venus and thereby decreases FRET (Figure IIIA in the Data Supplement). The sensor was co-expressed with WT or mutant (T445N, G449S, or  $\Delta 3aa$ ) PDE3A2-mCherry in HEK293 cells. The PDE3A2 versions were expressed at similar levels and were mainly located in the cytosol (Figure 6A). The emission intensity of the sensor was determined in the absence or presence of forskolin and the PDE3A inhibitor milrinone. Changes in FRET and thus activity of the PDE3A2 versions are shown as  $\Delta$ FRET, which reflects the difference in emission intensity. An increase in  $\Delta$ FRET indicates

increased cAMP, consistent with decreased PDE3A activity. In cells expressing the T445N, G449S, or the  $\Delta 3aa$  mutant, forskolin led to a reduction in the  $\Delta$ FRET in comparison with the WT, reflecting less cAMP in the mutant-expressing cells than in WT-expressing ones. The data indicate that mutations in the hotspot region of the *PDE3A* gene cause an increase in PDE3A2-mediated cAMP hydrolysis. The differences were abolished by the PDE3A inhibitor, cilostamide, indicating similar sensitivity of the WT and the mutant enzymes to this agent (Figure 6B). Based on the observation, that BAY 41-8543 lowered blood pressure in the  $\Delta 3aa$  HET and WT rats, we tested whether the compound affects mutant PDE3A activity. sGC is expressed in HEK293 cells and inhibition of PDE3A through sGC activation, and cGMP elevation induced by BAY 41-8543 changed the  $\Delta$ FRET and thus caused inhibition of PDE3A (see earlier in this article; Figure IE in the Data Supplement). Under resting conditions, enzyme activities of WT and mutant PDE3A2 variants were similar because there were no differences in emission intensities (Figure 6C).

We had demonstrated increased phosphorylation at S428 and S438 of mutant HTNB PDE3A enzymes in HeLa cells (T445N, T445S, T445A, A447T, A447V, and G449V).<sup>4</sup> We verified these results for the T445N variant using HEK293 cells, which do not express PDE3A endogenously. Figure 6D and 6E shows that, when expressed in HEK293 cells, protein kinase C stimulation via phorbol-12-myristate-13-acetate (PMA) consistently increased the phosphorylation at S428 of the T445N and the  $\Delta 3aa$  mutants in comparison with the WT. Forskolin stimulation caused a reduction of the phosphorylation at another serine, S312, for both mutants in comparison with the WT, most likely



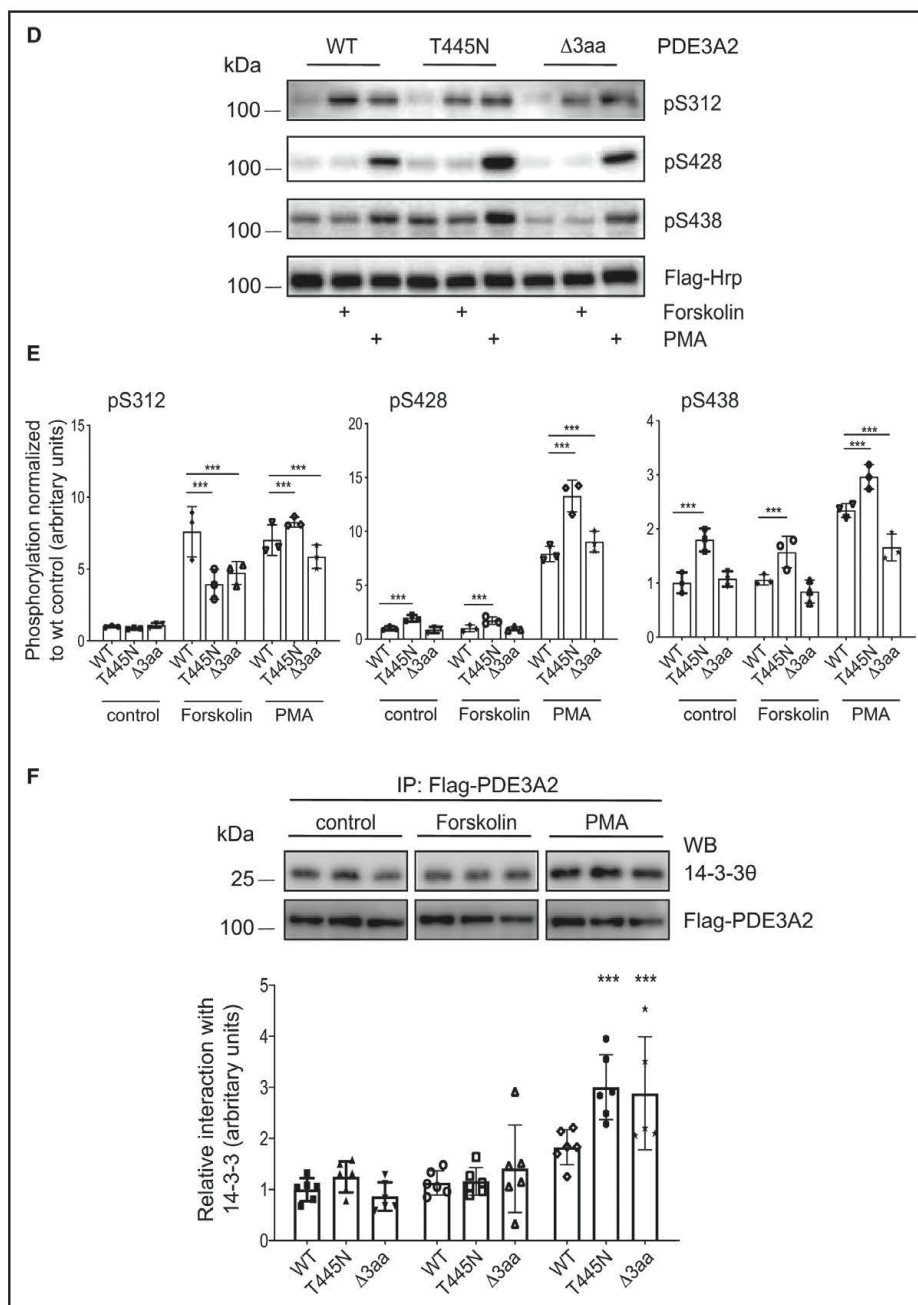


**Figure 6 Continued.** the T445N mutant, the  $\Delta 3aa$  deletion, and the G449S mutation revealed significantly increased PDE3A activity, indicated by the negative  $\Delta$ FRET values, which in turn indicate lower cAMP levels in those conditions in comparison with the WT. When the effect of forskolin alone (30  $\mu$ mol/L) was examined, the substance was added and the measurement immediately started. When the effect of milrinone was investigated, the cells were incubated with the agent (30  $\mu$ mol/L) for 30 minutes before the addition of forskolin (30  $\mu$ mol/L) and subsequent measurement. Statistical analysis was performed using 2-way ANOVA and Bonferroni multicomparison,  $n \geq 4$  independent experiments and analysis of 24 to 65 individual cells per PDE3A2 variant and condition. Shown are mean  $\pm$  SEM, \*\* $P < 0.01$ ; \*\*\* $P < 0.001$ . Further controls including measurements of independent CFP and Venus, noninteracting (Continued)



because PKA activates phosphatases.<sup>24</sup> Thus, there are consistently altered phosphorylation patterns for both mutants. In addition, mutant-specific alterations of the phosphorylation occur, which may account for the differences in activity between the mutants (Figure 6A through 6C).

Phosphorylation of S292/S293 by PKA recruits PDE3A1 into AKAP (A-kinase-anchoring protein)18-based signalosome at the sarcoplasmic reticulum of cardiac myocytes.<sup>16</sup> To test whether *PDE3A* mutations that cause HTNB also alter protein-protein interactions, we expressed WT, the T445N, and the  $\Delta$ 3aa mutants in HEK293 cells and coimmunoprecipitated them with a known interaction partner of WT PDE3A, namely, a scaffolding protein from the adaptor-protein family 14-3-3 (Figure 6F). The 14-3-3 proteins comprise a family of conserved regulatory molecules expressed in all eukaryotic cells. They can bind phosphorylated serine residues of a multitude of functionally diverse signaling proteins including kinases, phosphatases, and transmembrane receptors. An association between 14-3-3 $\theta$  and PMA-induced pS428 was described earlier.<sup>25</sup> On challenge with PMA, we observed an increase of pS428 (see earlier in this article) and of the interactions of 14-3-3 $\theta$  with the mutants in comparison with the WT. Forskolin did not affect the interaction. The findings demonstrate that the HTNB phenotype is associated with altered phosphorylation and altered protein-protein interactions of PDE3A mutants.

## DISCUSSION

We present a new human *PDE3A* mutation that causes an amino acid substitution within a 5-amino-acid-long PDE3A region N-terminally of the enzyme's catalytic domain. Diverse mutations in the encoding 15-bp gene segment are now known, and only 3 bp to date are not yet involved. We introduce 2 new animal models, a hypertensive rat model that recapitulates the phenotypes of HTNB and a PDE3A2 smooth muscle-specific overexpressing transgenic mouse model with hypertension. These animals underscore the role of increased

peripheral vascular resistance as a driving mechanism for increasing blood pressure.

We suggest that our findings are relevant to essential hypertension as found in the general population. This point of view is supported by the robust linkage we found in a subfamily of Chinese subjects with essential hypertension that coincided with our *PDE3A* locus.<sup>26</sup> In addition, 4 independent genome-wide association studies identified the *PDE3A* locus, and a fifth genome-wide association study discusses its relevance.<sup>27–31</sup> Mendelian genetic evidence implicates sodium-(chloride) reabsorption in the distal nephron as responsible for hypertension.<sup>32</sup> We previously tested the salt sensitivity of our HTNB subjects and determined that this form of hypertension is relatively salt resistant.<sup>23</sup> We measured serum electrolytes, sodium handling, and components of the renin-angiotensin-aldosterone axis in patient with HTNB,<sup>23</sup> and in our rat and mouse models as reported here, as well, and found no aberrancy in comparison with WT. We identified an increased VSMC proliferation rate, compromised vascular relaxation, and aberrant intracellular signaling suggesting such factors as contributors to hypertension, and as potential therapeutic targets.

Our data suggest that sGC activation could be suitable for the treatment of patients with HTNB. The sGC stimulator BAY 41-8543 normalized the blood pressure in our  $\Delta$ 3aa HET rat model. sGC activation caused elevation of cGMP, and we showed that both BAY 41-8543 and cGMP could inhibit PDE3A. BAY 41-8543 and cGMP mediated the inhibition of the WT and the hyperactive T445N mutant enzymes when expressed in HeLa cells<sup>4,33</sup>; our FRET experiments using HEK293 cells also point to an inhibitory effect of BAY 41-8543 on the hyperactive  $\Delta$ 3aa PDE3A2 mutant. The inhibition is most likely attributable to the binding of cGMP to PDE3A and is probably operative in the rats. The apparently stronger inhibitory effect of BAY 41-8543 on the  $\Delta$ 3aa mutant than on the WT is in line with the stronger blood pressure-lowering effect in the  $\Delta$ 3aa HET rats than in the WT animals. However, the mechanism underlying the lowering of blood pressure in the

**Figure 6 Continued.** coexpressed CFP and Venus or of a CFP-YFP tandem construct are shown in Figure III B and III C in the Data Supplement. **B.** The PDE3A inhibitor cilostamide (10  $\mu$ mol/L) inhibits WT and the indicated PDE3A2 mutant versions to a similar extent. Cilostamide (10  $\mu$ mol/L) and forskolin (30  $\mu$ mol/L) were added simultaneously and the measurement immediately started. n=3 independent experiments per PDE3A2 version. **C.** Under resting conditions, the cAMP hydrolytic activity of WT and the indicated PDE3A2 mutants is similar as indicated by the similar emission intensities. **D.** To compare the effect of forskolin and the protein kinase C stimulator, phorbol-12-myristate-13-acetate (PMA), on the phosphorylation of S312, S428, and S438 of the WT, the T445N mutant, and the rat PDE3A2- $\Delta$ 3aa deletion, these proteins were expressed in HEK293 cells. The cells were stimulated with the agents and phosphorylation was detected by Western blotting with phosphate site-specific antibodies. Representative blots from n=3 independent experiments are shown. **E.** The semiquantitative analysis of Western blots from Figure 6D by densitometry. Ordinate shows ratios of signals for mutant relative to control WT PDE3A2. On PMA stimulation, the S428 phosphorylation consistently increased in both mutants in comparison with WT. Forskolin stimulation consistently decreased S312 phosphorylation of the mutants in comparison with WT. n=3; shown are mean $\pm$ SEM, \*\*\*P<0.001. **F.** The stimulation with PMA increased the interaction of the mutant T445N and the  $\Delta$ 3aa deletion with the adapter protein, 14-3-3 $\theta$ , in comparison with WT. WT and the PDE3A2 mutants T445N and PDE3A2- $\Delta$ 3aa were transiently expressed in HEK293 cells and immunoprecipitated via their Flag tags. Similar precipitation efficiencies were confirmed by detection of PDE3A2 with an anti-Flag tag antibody by Western blotting. Coimmunoprecipitated 14-3-3 $\theta$  was also detected by Western blotting. Relative interaction of 14-3-3 $\theta$  with the mutant PDE3A2 versions in comparison with control PDE3A2-WT-Flag is shown. Semiquantitative analysis was performed by densitometry. n=6, shown are mean $\pm$ SEM, \*\*\*P<0.001. CFP indicates cyan fluorescent protein; ctrl., control; FRET, fluorescence resonance energy transfer; GFP, green fluorescent protein; IP, immunoprecipitation; WT, wild type; and YFP, yellow fluorescent protein.



rats may also involve the cGMP-mediated activation of protein kinase G, which leads to vasodilation.<sup>34</sup>

Compartmentalization of cAMP signaling in nanodomains is a common mechanism used by all cells to ensure the interaction of this second messenger within localized pools of appropriate effector proteins.<sup>35</sup> In this way, the cell can elicit differential responses by using a single, diffusible, molecular species.<sup>36,37</sup> PDE enzymes are not haphazardly distributed but instead engage in protein-protein interactions, for example, with AKAPs to establish cAMP signaling compartments.<sup>38</sup> In cardiac myocytes, PDE3A is part of an AKAP18-based signalosome consisting of PKA, phospholamban, and sarco/endoplasmic reticulum Ca<sup>2+</sup>-dependent ATPase 2a, which regulates Ca<sup>2+</sup> reuptake into the sarcoplasmic reticulum and thereby relaxation of the heart.<sup>16,39</sup> PDE3A is recruited into the complex on PKA phosphorylation of S292/S293 and hydrolyzes the local cAMP establishing a negative feedback loop.<sup>16</sup> Thus, the phosphorylation of PDE3A changes its localization.

We found that the S428 phosphorylation was consistently higher in the mutants than in WT, after activation of protein kinase C, and we had previously shown that hyperactive PDE3A mutants that are aberrantly phosphorylated, such as the T445N version, are enriched in microsomal fractions when transiently expressed in HeLa cells.<sup>33</sup> We show here increased interactions of 14-3-3 $\theta$  with the PDE3A mutants T445N and  $\Delta$ 3aa. In analogy to the recruitment of PKA-phosphorylated PDE3A1, the increased phosphorylation-dependent interaction could change the localization of the mutants, and, as a consequence, local cAMP would be reduced by the hyperactive enzymes. PKA phosphorylation of PDE3B promotes 14-3-3 $\theta$  binding and inhibits protein phosphatase-mediated inactivation.<sup>40</sup> Thus, binding of 14-3-3 $\theta$  may participate in the regulation of local activity of the mutant PDE3A versions at their cognate cellular location.

Collectively, the data in this study and our previous analysis of patients with HTNB<sup>23</sup> indicate that PDE3A controls the blood pressure independent of the renin-angiotensin-aldosterone system and salt reabsorption by the kidney, but rather by influencing signaling in VSMCs and their proliferation. Our findings suggest that, by modulating PDE3A downstream signaling, in particular, its protein-protein interactions, new approaches to reduce blood pressure could be developed. Even the skeletal phenotype of patients with HTNB might have therapeutic implications beyond cardiovascular medicine. Parathyroid hormone-related peptide is responsible for the brachydactyly we describe.<sup>41</sup> This protein plays a role in the hypercalcemia of malignancy, and is involved in metastases of solid tumors.<sup>42</sup> Our previous findings that PDE3A can regulate the PTHLH gene, which encodes parathyroid hormone-related peptide,<sup>4</sup> suggests that HTNB may find use as a model

for conditions unrelated to cardiovascular disease. Our vision is the development of precise intracellular pharmacological treatments that target PDE3A-directed nanodomains and thereby specifically influence intracellular signaling.

## ARTICLE INFORMATION

Received August 5, 2019; accepted May 1, 2020.

The Data Supplement is available with this article at <https://www.ahajournals.org/doi/suppl/10.1161/CIRCULATIONAHA.119.043061>.

## Authors

Maria Ercu, MS\*; Lajos Markó, MD, PhD\*; Carolin Schächterle, PhD; Dmitry Tsvetkov, MD; Yingqiu Cui, MD; Sara Maghsodi, MS; Theda U.P. Bartolomaeus, MS; Philipp G. Maass, PhD; Kerstin Zühlke, PhD; Nerine Gregersen, MD; Norbert Hübner, MD; Russell Hodge, MA; Astrid Mühl, BS; Bärbel Pohl, BS; Rosana Molé Illas, MD; Andrea Geelhaar, BS; Stephan Walter, MD; Hanna Napieczynska, PhD; Stefanie Schelenz, Martin Taube, Arnd Heuser, MD; Yolanda Marie Anistan, MD; Fatimunnisa Qadri, PhD; Mihail Todiras, MD; Ralph Plehm, MS; Elena Popova, PhD; Reika Langanki, BS; Jenny Eichhorst, Dipl-Ing (FH); Martin Lehmann, PhD; Burkhard Wiesner, PhD; Michael Russwurm, MD; Sofia K. Forslund, PhD; Ilona Kamer, BS; Dominik N. Müller, PhD; Maik Gollasch, MD, PhD; Atakan Aydin, PhD; Sylvia Bähring, PhD; Michael Bader, MD; Friedrich C. Luft, MD; Enno Klussmann, PhD

## Correspondence

Friedrich C. Luft, MD, Experimental and Clinical Research Center (ECRC), Lindenbergerweg 80, 13125 Berlin, Germany; or Enno Klussmann, PhD, Max-Delbrück-Center for Molecular Medicine (MDC) in the Helmholtz Association, Robert Rossle-Strasse 10, 13125 Berlin, Germany. Email Friedrich.Luft@charite.de or enno.klussmann@mdc-berlin.de

## Affiliations

Max-Delbrück-Center for Molecular Medicine (MDC) in the Helmholtz Association, Berlin, Germany (M.E., C.S., S.M., K.Z., N.H., R.H., A.M., B.P., A.G., H.N., S.S., M. Taube, A.H., F.Q., M. Todiras, R.P., E.P., R.L., S.K.F., D.N.M., A.A., M.B., F.C.L., E.K.). German Center for Cardiovascular Research (DZHK), Partner Site Berlin, Germany (M.E., L.M., C.S., T.U.P.B., N.H., S.K.F., D.N.M., M.B., E.K.). Charité-Universitätsmedizin Berlin, Germany (L.M., T.U.P.B., N.H., Y.-M.A., S.K.F.). Experimental and Clinical Research Center, a joint cooperation between the Charité Medical Faculty and the Max-Delbrück Center for Molecular Medicine, Berlin, Germany (L.M., C.S., D.T., Y.C., T.U.P.B., R.M.I., S.K.F., I.K., D.N.M., M.G., S.B., F.C.L.). Genetics and Genome Biology Program, SickKids Research Institute and Department of Molecular Genetics, University of Toronto, ON, Canada (P.G.M.). Auckland District Health Board (ADHB), Genetic Health Service New Zealand – Northern Hub (N.G.). Abteilung für Nephrologie/Hypertensiologie, St. Vincenz Krankenhaus, Limburg, Germany (S.W.). Division of Nephrology and Intensive Care Medicine, Medical Department, Charité-Universitätsmedizin, Berlin, Germany (Y.-M.A., M.G.). Leibniz-Forschungsinstitut für Molekulare Pharmakologie (FMP), Berlin, Germany (J.E., M.L., B.W.). Institut für Pharmakologie und Toxikologie, Medizinische Fakultät MA N1, Ruhr-Universität Bochum, Germany (M.R.). Berlin Institute of Health (BIH), Germany (S.K.F.). Department of Internal Medicine and Geriatrics, University Medicine Greifswald, Germany (M.G.). European Molecular Biology Laboratory, Structural and Computational Biology Unit, Heidelberg, Germany (S.K.F.). Institute for Biology, University of Lübeck, Germany (M.B.).

## Acknowledgments

We thank our patients for their participation in these studies. Drs Luft and Klussmann, designed the study and wrote the manuscript. Drs Bader, Müller, and Popova designed and supported the generation of animal models. M. Ercu performed fluorescence resonance energy transfer experiments and Western blotting. Dr Schächterle, and M. Ercu performed Western blotting and cell proliferation measurements. Drs Markó, Forslund, and Todiras, and R. Plehm performed and evaluated telemetric blood pressure measurements. S. Maghsodi, Drs Cui, Tsvetkov, and Gollasch measured and evaluated contractility parameters of isolated vessels. Dr Zühlke and A. Geelhaar measured cell



proliferation of vascular smooth muscle cells. Drs Napieczynska and Heuser did micro computed tomography experiments. S. Schelenz, M. Taube, and Dr Heuser performed echocardiography. Dr Qadri, T.U.P. Bartolomaeus, and Dr Markó, performed histological stainings and quantitative polymerase chain reaction. Drs Maass, Gregersen, and Hübner were involved in genetic analysis. A. Mühl, B. Pohl, Dr Aydın, and Dr Illas cloned. J. Eichhorst and Drs Lehmann and Wiesner were involved in fluorescence resonance energy transfer experiments. Dr Russwurm performed radioimmunoassays. J. Eichhorst and R. Langanki supported animal studies. Dr Anistan discovered the novel German mutation. R. Hodge assisted in phenotyping in Turkey and conducted clinical protocols, in addition to chronicizing our events. Dr Walter recruited and phenotyped the German family with the G449S substitution. Dr Bähring contributed to conceptualizing the study, genetic analyses, and coordination of animal studies.

### Sources of Funding

The Deutsche Forschungsgemeinschaft (DFG) supported the study to Drs Bähring, Klusmann and Gollasch, (BA 1773/10-1, KL1415/7-1, GO766/12-3, GO766/15-2, and the program-project grant, 394046635 – SFB 1365), and grants to Dr Klusmann from the Bundesministerium für Bildung und Forschung (BMBF, 16GW0179K), the German Center for Cardiovascular Research (DZHK) partner site Berlin (81X2100146), and the German Israeli Foundation (GIF, I-1452-203/13–2018).

### Disclosures

None.

### Supplemental Materials

German family with HTNB, substitution G449S  
Expanded Methods  
Overexpression of hyperactive PDE3A2 causes hypertension in mice  
Data Supplement Figures I–IV  
Data Supplement Tables I–III

### REFERENCES

- Olsen MH, Angell SY, Asma S, Boutouyrie P, Bürger D, Chirinos JA, Damasceno A, Delles C, Gimenez-Roqueplo AP, Hering D, et al. A call to action and a lifecourse strategy to address the global burden of raised blood pressure on current and future generations: the Lancet Commission on hypertension. *Lancet*. 2016;388:2665–2712. doi: 10.1016/S0140-6736(16)31134-5
- Seidel E, Scholl UI. Genetic mechanisms of human hypertension and their implications for blood pressure physiology. *Physiol Genomics*. 2017;49:630–652. doi: 10.1152/physiolgenomics.00032.2017
- Schuster H, Wienker TE, Bähring S, Bilginturan N, Toka HR, Neitzel H, Jeschke E, Toka O, Gilbert D, Lowe A, et al. Severe autosomal dominant hypertension and brachydactyly in a unique Turkish kindred maps to human chromosome 12. *Nat Genet*. 1996;13:98–100. doi: 10.1038/ng0596-98
- Maass PG, Aydın A, Luft FC, Schächterle C, Weise A, Stricker S, Lindschau C, Vaegler M, Qadri F, Toka HR, et al. PDE3A mutations cause autosomal dominant hypertension with brachydactyly. *Nat Genet*. 2015;47:647–653. doi: 10.1038/ng.3302
- van den Born BJ, Oskam LC, Zidane M, Schächterle C, Klusmann E, Bähring S, Luft FC. The case! A handful of hypertension. *Kidney Int*. 2016;90:911–913. doi: 10.1016/j.kint.2016.03.037
- Ercu M, Klusmann E. Roles of A-kinase anchoring proteins and phosphodiesterases in the cardiovascular system. *J Cardiovasc Dev Dis*. 2018;5:14. doi: 10.3390/jcdd5010014
- Choi YH, Ekholm D, Krall J, Ahmad F, Degerman E, Manganiello VC, Movsesian MA. Identification of a novel isoform of the cyclic-nucleotide phosphodiesterase PDE3A expressed in vascular smooth-muscle myocytes. *Biochem J*. 2001;353(pt 1):41–50.
- Popova E, Krivokharchenko A, Ganten D, Bader M. Efficiency of transgenic rat production is independent of transgene-construct and overnight embryo culture. *Theriogenology*. 2004;61:1441–1453. doi: 10.1016/j.theriogenology.2003.08.006
- Wick N, Marko L, Balogh A, Kraker K, Herse F, Bartolomaeus H, Szijarto IA, Gollasch M, Reichhart N, Strauss O, et al. Nitric oxide-sensitive guanylyl cyclase stimulation improves experimental heart failure with preserved ejection fraction. *JCI Insight*. 2018;3:e96006. doi: 10.1172/jci.insight.96006
- Basu R, Poglitsch M, Yogasundaram H, Thomas J, Rowe BH, Oudit GY. Roles of angiotensin peptides and recombinant human ACE2 in heart failure. *J Am Coll Cardiol*. 2017;69:805–819. doi: 10.1016/j.jacc.2016.11.064
- Schleifenbaum J, Kassmann M, Szjártó IA, Hercule HC, Tano JY, Weinert S, Heidenreich M, Pathan AR, Anistan YM, Alenina N, et al. Stretch-activation of angiotensin II type 1a receptors contributes to the myogenic response of mouse mesenteric and renal arteries. *Circ Res*. 2014;115:263–272. doi: 10.1161/CIRCRESAHA.115.302882
- Brooker G, Harper JF, Terasaki WL, Moylan RD. Radioimmunoassay of cyclic AMP and cyclic GMP. *Adv Cyclic Nucleotide Res*. 1979;10:1–33.
- Chi J, Meng L, Pan S, Lin H, Zhai X, Liu L, Zhou C, Jiang C, Guo H. Primary culture of rat aortic vascular smooth muscle cells: a new method. *Med Sci Monit*. 2017;23:4014–4020. doi: 10.12659/msm.902816
- DiPilato LM, Zhang J. The role of membrane microdomains in shaping  $\beta_2$ -adrenergic receptor-mediated cAMP dynamics. *Mol Biosyst*. 2009;5:832–837. doi: 10.1039/b823243a
- Vukičević T, Hinze C, Baltzer S, Himmerkus N, Quintanova C, Zühlke K, Compton F, Ahlborn R, Dema A, Eichhorst J, et al. Flucanazole increases osmotic water transport in renal collecting duct through effects on aquaporin-2 trafficking. *J Am Soc Nephrol*. 2019;30:795–810. doi: 10.1681/ASN.2018060668
- Ahmad F, Shen W, Vandeput F, Szabo-Fresnais N, Krall J, Degerman E, Goetz F, Klusmann E, Movsesian M, Manganiello V. Regulation of sarcoplasmic reticulum Ca<sup>2+</sup> ATPase 2 (SERCA2) activity by phosphodiesterase 3A (PDE3A) in human myocardium: phosphorylation-dependent interaction of PDE3A1 with SERCA2. *J Biol Chem*. 2015;290:6763–6776. doi: 10.1074/jbc.M115.638585
- Fan P, Zhang D, Yang KQ, Zhang QY, Luo F, Lou Y, Liu YX, Zhang HM, Song L, Cai J, et al. Hypertension and brachydactyly syndrome associated with vertebral artery malformation caused by a PDE3A missense mutation. *Am J Hypertens*. 2020;33:190–197. doi: 10.1093/ajh/hpz151
- Boda H, Uchida H, Takaiso N, Ouchi Y, Fujita N, Kuno A, Hata T, Nagatani A, Funamoto Y, Miyata M, et al. A PDE3A mutation in familial hypertension and brachydactyly syndrome. *J Hum Genet*. 2016;61:701–703. doi: 10.1038/jhg.2016.32
- Renkema KY, Westermann JM, Nivelstein RAJ, Lo-A-Njoe SM, van der Zwaag B, Manshande ME, van Haelst MM. PDE3A gene screening improves diagnostics for patients with Bilginturan syndrome (hypertension and brachydactyly syndrome). *Hypertens Res*. 2018;41:981–988. doi: 10.1038/s41440-018-0094-5
- Naraghi R, Schuster H, Toka HR, Bähring S, Toka O, Oztekin O, Bilginturan N, Knoblauch H, Wienker TF, Busjahn A, et al. Neurovascular compression at the ventrolateral medulla in autosomal dominant hypertension and brachydactyly. *Stroke*. 1997;28:1749–1754. doi: 10.1161/01.str.28.9.1749
- Begum N, Hockman S, Manganiello VC. Phosphodiesterase 3A (PDE3A) deletion suppresses proliferation of cultured murine vascular smooth muscle cells (VSMCs) via inhibition of mitogen-activated protein kinase (MAPK) signaling and alterations in critical cell cycle regulatory proteins. *J Biol Chem*. 2011;286:26238–26249. doi: 10.1074/jbc.M110.214155
- Movsesian M. Novel approaches to targeting PDE3 in cardiovascular disease. *Pharmacol Ther*. 2016;163:74–81. doi: 10.1016/j.pharmthera.2016.03.014
- Schuster H, Wienker TF, Toka HR, Bähring S, Jeschke E, Toka O, Busjahn A, Hempel A, Tahlhammer C, Oelkers W, et al. Autosomal dominant hypertension and brachydactyly in a Turkish kindred resembles essential hypertension. *Hypertension*. 1996;28:1085–1092. doi: 10.1161/01.hyp.28.6.1085
- Zolnierowicz S. Type 2A protein phosphatase, the complex regulator of numerous signaling pathways. *Biochem Pharmacol*. 2000;60:1225–1235. doi: 10.1016/S0006-2952(00)00424-X
- Pozuelo Rubio M, Campbell DG, Morrice NA, Mackintosh C. Phosphodiesterase 3A binds to 14-3-3 proteins in response to PMA-induced phosphorylation of Ser428. *Biochem J*. 2005;392(pt 1):163–172. doi: 10.1042/BJ20051103
- Gong M, Zhang H, Schulz H, Lee YA, Sun K, Bähring S, Luft FC, Nürnberg P, Reis A, Rohde K, et al. Genome-wide linkage reveals a locus for human essential (primary) hypertension on chromosome 12p. *Hum Mol Genet*. 2003;12:1273–1277. doi: 10.1093/hmg/ddg135
- Ehret GB, Ferreira T, Chasman DI, Jackson AU, Schmidt EM, Johnson T, Thorleifsson G, Luan J, Donnelly LA, Kanoni S, et al. CHARGE-EchoGen consortium; CHARGE-HF consortium; Wellcome Trust Case Control Consortium. The genetics of blood pressure regulation and its target organs from association studies in 342,415 individuals. *Nat Genet*. 2016;48:1171–1184. doi: 10.1038/ng.3667

28. Kato N, Loh M, Takeuchi F, Verweij N, Wang X, Zhang W, Kelly TN, Saleheen D, Lehne B, Leach IM, et al; BIOS-consortium; CARDIoGRAM-plusCD; Lifelines Cohort Study; InterAct Consortium. Trans-ancestry genome-wide association study identifies 12 genetic loci influencing blood pressure and implicates a role for DNA methylation. *Nat Genet*. 2015;47:1282–1293. doi: 10.1038/ng.3405
29. Simino J, Sung YJ, Kume R, Schwander K, Rao DC. Gene-alcohol interactions identify several novel blood pressure loci including a promising locus near SLC16A9. *Front Genet*. 2013;4:277. doi: 10.3389/fgene.2013.00277
30. Warren HR, Evangelou E, Cabrera CP, Gao H, Ren M, Mifsud B, Ntalla I, Surendran P, Liu C, Cook JP, et al; International Consortium of Blood Pressure (ICBP) 1000G Analyses; BIOS Consortium; Lifelines Cohort Study; Understanding Society Scientific group; CHD Exome+ Consortium; ExomeBP Consortium; T2D-GENES Consortium; GoT2DGenes Consortium; Cohorts for Heart and Ageing Research in Genome Epidemiology (CHARGE) BP Exome Consortium; International Genomics of Blood Pressure (iGEN-BP) Consortium; UK Biobank CardioMetabolic Consortium BP working group. Genome-wide association analysis identifies novel blood pressure loci and offers biological insights into cardiovascular risk. *Nat Genet*. 2017;49:403–415. doi: 10.1038/ng.3768
31. Evangelou E, Warren HR, Mosen-Ansorena D, Mifsud B, Pazoki R, Gao H, Ntritsos G, Dimou N, Cabrera CP, Karaman I, et al; Million Veteran Program. Genetic analysis of over 1 million people identifies 535 new loci associated with blood pressure traits. *Nat Genet*. 2018;50:1412–1425. doi: 10.1038/s41588-018-0205-x
32. Lifton RP, Gharavi AG, Geller DS. Molecular mechanisms of human hypertension. *Cell*. 2001;104:545–556. doi: 10.1016/s0092-8674(01)00241-0
33. Toka O, Tank J, Schächterle C, Aydin A, Maass PG, Elitok S, Bartels-Klein E, Hollfinger I, Lindschau C, Mai K, et al. Clinical effects of phosphodiesterase 3A mutations in inherited hypertension with brachydactyly. *Hypertension*. 2015;66:800–808. doi: 10.1161/HYPERTENSIONAHA.115.06000
34. Hofmann F, Bernhard D, Lukowski R, Weinmeister P. cGMP regulated protein kinases (cGK). *Handb Exp Pharmacol*. 2009;137–162. doi: 10.1007/978-3-540-68964-5\_8
35. Musheshe N, Schmidt M, Zaccolo M. cAMP: from long-range second messenger to nanodomain signalling. *Trends Pharmacol Sci*. 2018;39:209–222. doi: 10.1016/j.tips.2017.11.006
36. McCormick K, Baillie GS. Compartmentalisation of second messenger signalling pathways. *Curr Opin Genet Dev*. 2014;27:20–25. doi: 10.1016/j.gde.2014.02.001
37. Dema A, Perets E, Schulz MS, Deák VA, Klussmann E. Pharmacological targeting of AKAP-directed compartmentalized cAMP signalling. *Cell Signal*. 2015;27:2474–2487. doi: 10.1016/j.celsig.2015.09.008
38. Klussmann E. Protein-protein interactions of PDE4 family members – functions, interactions and therapeutic value. *Cell Signal*. 2016;28:713–718. doi: 10.1016/j.celsig.2015.10.005
39. Lygren B, Carlson CR, Santamaria K, Lissandron V, McSorley T, Litzenberg J, Lorenz D, Wiesner B, Rosenthal W, Zaccolo M, et al. AKAP complex regulates Ca<sup>2+</sup> re-uptake into heart sarcoplasmic reticulum. *EMBO Rep*. 2007;8:1061–1067. doi: 10.1038/sj.embor.7401081
40. Palmer D, Jimmo SL, Raymond DR, Wilson LS, Carter RL, Maurice DH. Protein kinase A phosphorylation of human phosphodiesterase 3B promotes 14-3-3 protein binding and inhibits phosphatase-catalyzed inactivation. *J Biol Chem*. 2007;282:9411–9419. doi: 10.1074/jbc.M606936200
41. Maass PG, Wirth J, Aydin A, Rump A, Stricker S, Tinschert S, Otero M, Tsuchimochi K, Goldring MB, Luft FC, et al. A cis-regulatory site downregulates PTHLH in translocation t(8;12)(q13;p11.2) and leads to Brachydactyly Type E. *Hum Mol Genet*. 2010;19:848–860. doi: 10.1093/hmg/ddp553
42. Roodman GD. Genes associate with abnormal bone cell activity in bone metastasis. *Cancer Metastasis Rev*. 2012;31:569–578. doi: 10.1007/s10555-012-9372-x

## **Curriculum Vitae**

My curriculum vitae does not appear in the electronic version of my paper for reasons of data protection.



---

## Complete list of publications

1. **Cui Y**, Kassmann M, Nickel S, Zhang C, Alenina N, Anistan YM, Schleifenbaum J, Bader M, Welsh DG, Huang Y and Gollasch M. Myogenic Vasoconstriction Requires Canonical  $G_{q/11}$  Signaling of the Angiotensin II Type 1 Receptor. *J Am Heart Assoc.* 2022:e022070.
2. Fan G, Kaßmann M, **Cui Y**, Matthaeus C, Kunz S, Zhong C, Zhu S, Xie Y, Tsvetkov D, Daumke O, Huang Y and Gollasch M. Age attenuates the T-type Ca 3.2-RyR axis in vascular smooth muscle. *Aging Cell.* 2020;19:e13134.
3. Ercu M, Markó L, Schächterle C, Tsvetkov D, **Cui Y**, Maghsodi S, Bartolomaeus TUP, Maass PG, Zühlke K, Gregersen N, Hübner N, Hodge R, Mühl A, Pohl B, Illas RM, Geelhaar A, Walter S, Napieczynska H, Schelenz S, Taube M, Heuser A, Anistan Y-M, Qadri F, Todiras M, Plehm R, Popova E, Langanki R, Eichhorst J, Lehmann M, Wiesner B, Russwurm M, Forslund SK, Kamer I, Müller DN, Gollasch M, Aydin A, Bähring S, Bader M, Luft FC and Klussmann E. Phosphodiesterase 3A and Arterial Hypertension. *Circulation.* 2020;142:133-149.
4. Fan G, **Cui Y**, Gollasch M and Kassmann M. Elementary calcium signaling in arterial smooth muscle. *Channels (Austin).* 2019;13:505-519.

## Acknowledgments

I would like to extend my deep gratitude to all those who have offered me support and assistance during the preparation of my thesis.

My sincere gratitude is given to my supervisor Prof. Dr. med. Dr. rer. nat. Maik Gollasch for the valuable guidance throughout the study. Your patience, motivation and passion for knowledge are beneficial to me consistently on research, which would help me go further professionally. What's more, I would like to present my thanks to Prof. Yu Huang and all the group members at Chinese University of Hong Kong for the warm welcome and wonderful collaboration.

Special acknowledgment to Dmitry Tsvetkov for the effort to support me in the data collection and the contribution to the studies. I'm delighted to have worked with you. I am profoundly grateful for Yoland-Marie Anistan, Johanna Schleifenbaum, Mario Kassmann for introducing me the lab instruction and teaching me useful methods. Particular thanks to all members of AG Gollasch group who provided me with a friendly and inspiring environment to work. Wish you all the best.

I am also grateful for the hard work of all my co-authors and their contribution to the studies presented in this thesis.

Finally, I'd like to express the gratitude to my lovely family and friends. Without your support, this work would not have been possible to be completed.